2018-04-01

Effect of Inclined Loading on Passive Force-Deflection Curves and Skew Adjustment Factors

Joshua Rex Curtis
Brigham Young University

Effect of Inclined Loading on Passive Force Deflection Curves and Skew Adjustment Factors

Joshua Rex Curtis

A thesis submitted to the faculty of
Brigham Young University
In partial fulfillment of the requirements for the degree of

Master of Science

Kyle M. Rollins, Chair
Kevin W. Franke
Norman L. Jones

Department of Civil and Environmental Engineering

Brigham Young University

ABSTRACT

Effect of Inclined Loading on Passive Force Deflection Curves and Skew Adjustment Factors

Joshua Rex Curtis
Department of Civil and Environmental Engineering, BYU
Master of Science

Skewed bridges have exhibited poorer performance during lateral earthquake loading in comparison to non-skewed bridges (Apirakvorapinit et al. 2012; Elnashai et al. 2010). Results from numerical modeling by Shamsabadi et al. (2006), small-scale laboratory tests by Rollins and Jessee (2012), and several large-scale tests performed by Rollins et al. at Brigham Young University (Franke 2013; Marsh 2013; Palmer 2013; Smith 2014; Frederickson 2015) led to the proposal of a reduction curve used to determine a passive force skew reduction factor depending on abutment skew angle (Shamsabadi and Rollins 2014). In all previous tests, a uniform longitudinal load has been applied to the simulated bridge abutment. During seismic events, however, it is unlikely that bridge abutments would experience pure longitudinal loading. Rather, an inclined loading situation would be expected, causing rotation of the abutment backwall into the backfill.

In this study, a large-scale test was performed where inclined loading was applied to a 30° skewed bridge abutment with sand backfill and compared to a baseline test with uniform loading and a non-skewed abutment. The impact of rotational force on the passive resistance of the backfill and the skew adjust factor was then evaluated. It was determined that inclined loading does not have a significant effect on the passive force skew reduction factor. However, the reduction factor was somewhat higher than predicted by the proposed reduction curve from Shamsabadi and Rollins 2014. This can be explained by a reduction in the effective skew angle caused by the friction between the side walls and the back wall.

The inclined loading did not change the amount of movement required to mobilize passive resistance with ultimate passive force developing for displacements equal to 3 to 6% of the wall height. The rotation of the pile cap due to inclined loading produced higher earth pressure on the obtuse side of the skew wedge, as was expected.

These findings largely resolve the concern that inclined loading situations during an earthquake may render the proposed passive force skew reduction curve invalid. We suggest that the proposed reduction curve remains accurate during inclined loading and should be implemented in current codes and practices to properly account for skew angle in bridge design.

Keywords: bridge abutment, skew, passive force, bridge rotation, inclined loading, seismic design, large-scale, pile cap

ACKNOWLEDGEMENTS

I would like to thank Dr. Kyle M. Rollins, my graduate advisor, for providing me the opportunity to be involved in this research. I was in a unique position as I was asked to take on this research project after all of the field testing had already been performed. I appreciate Dr. Rollins efforts to help me understand the testing methods and assist me in analyzing and reducing the raw data. It was an honor to work with him and I learned a lot from his expertise and humble leadership. I would also like to thank the members of my graduate committee, Dr. Kevin W. Franke and Dr. Norman L. Jones, for their time and efforts in assisting me.

I thank Tyler Remund, Clay Hansen, and Kirk Kauer for spending long hours at the Salt Lake Airport performing the tests described in this thesis. I am also grateful to Daniel Schwict and Rebecca Black for allowing me to help them perform tests for their research at the same test site, thus getting first-hand experience of how the data I was working with had been produced.

I am especially grateful to my wife, Jessica, for allowing me to spend long hours away from her as I completed this research. She was very supportive and provided encouragement when stress levels were high.

Funding for this study was provided by FHWA pooled fund TPF-5(264) supported by the Departments of Transportation from the states of California, Minnesota, Montana, New York, Oregon, Utah, and Wisconsin. Utah served as the lead agency with David Stevens as the project manager. This support is gratefully acknowledged. BYU Department Technicians David Anderson and Rodney Mayo provided invaluable service in performing these tests which is much appreciated. We also express appreciation to the Salt Lake City Department of Airports for allowing us to use a test site at the Salt Lake International Airport for the testing.

TABLE OF CONTENTS

LIST OF TABLES

LIST OF FIGURES

1 INTRODUCTION

The purpose of this research is to determine the influence of inclined loading on passive force displacement curves and skew adjustment factors.

1.1 Background

Tests have shown that skewed bridges do not perform as well as non-skewed bridges during seismic events. Laboratory tests performed by Rollins and Jessee (2012) and numerical analyses performed by Shamsabadi et al. (2006) both found that there is a significant reduction in passive force as skew angle increases. Recent large-scale tests (Franke 2013, Marsh 2013, Palmer 2013, Smith 2014, and Frederickson 2015) have been conducted to determine the passive force-deflection relationships for skewed bridge abutments.

Recently, questions have been raised concerning the loading mechanism in these tests. In all previous tests, a longitudinal load has been applied to the simulated bridge abutment with minimal rotation. During seismic events, however, it is unlikely that bridge abutments would experience pure longitudinal loading. Rather, an inclined loading situation would be expected, causing rotation of the abutment backwall into the backfill. For this thesis, the focus was on determining the impacts of inclined loading on passive force displacement curves and skew adjustment factors. Two large-scale field tests were performed with skew angles of 0° and 30° using an existing pile cap and skew wedge apparatus. Inclined loading was applied to the 30° skew

test. No skewed abutments with inclined loading have been tested previously. Therefore, this test provides the first results for an inclined loading situation.

1.2 Research Objectives

The research objectives for this study were:

1. Determine the influence of inclined loading on ultimate passive force.
2. Investigate the influence of inclined loading on skew adjustment factors for passive force.
3. Measure the influence of inclined loading on the soil pressure distribution on the backwall.

1.3 Order of Presentation

This thesis will begin with a literature review that will describe the current state of knowledge and the need for new research pertaining to the effects of inclined loading on passive force displacement curves and adjustment factors for skewed bridge abutments. Next, the field site layout and test setup will be described in detail. The geotechnical properties of the backfill used in the tests will then be characterized. The testing procedure will be explained next. Field test results will then be described in the following order: Force-deflection relationships, surface heave, failure surface, lateral surface movement, skew reduction factor and effective skew, surface displacement and strain, pile cap rotation, backfill soil pressure distribution. Lastly, a PYCAP analysis of the field results will be presented.

2 LITERATURE REVIEW

2.1 Passive Earth Pressure Theories

Three widely used passive earth pressure theories have been developed to estimate the ultimate lateral compressive strength of a soil. They are known as the Coulomb (1776), Rankine (1857), and Logarithmic Spiral (Log Spiral) theories. The theories differ in the method used to approximate the shear plane of the soil. Shear plane geometry defines the boundaries of a soil mass that is mobilized from a lateral load, which is directly related to the ultimate passive resistance (P_p) of the soil using a passive earth pressure coefficient *(K_p)*, as shown in Equation (2-1).

$$P_P = \frac{1}{2} K_P \gamma H^2 + 2\sqrt{K_P} c' H \tag{2-1}$$

where,

$P_P = Ultimate\ passive\ force\ per\ unit\ width$

$K_p = Passive\ earth\ pressure\ coefficient$

$\gamma = Moist\ unit\ weight\ of\ the\ soil$

$H = Wall\ height$

$c' = Soil\ cohesion$

The form of Equation (2-1) is approximated using a uniform pressure distribution attributed to cohesion and triangular pressure distribution attributed to the weight and friction angle of the soil, as shown in Figure 2-1. Methods for calculating K_p according to the Rankine, Coulomb, and Log Spiral theories will be described below.

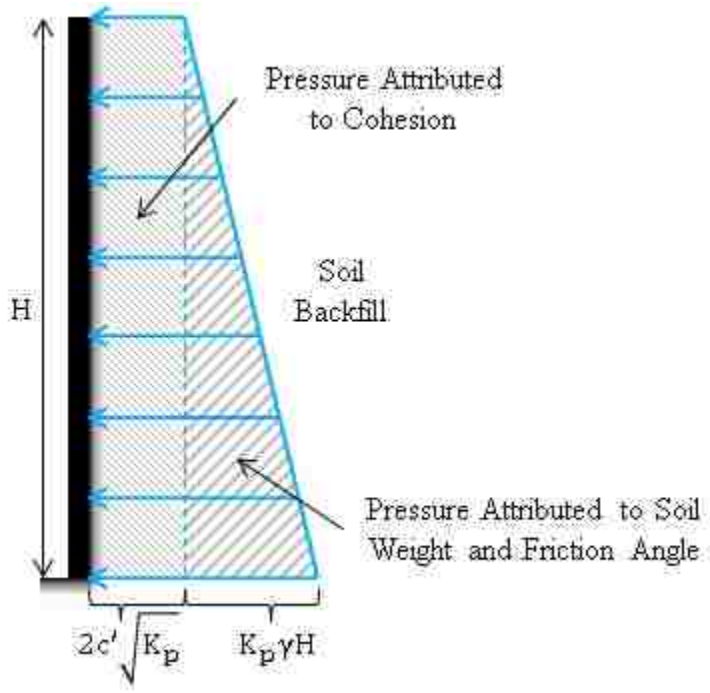

Figure 2-1: Lateral pressure distribution for soil

2.1.1 Coulomb (1776)

The earliest recorded analytical method of estimating passive earth pressures was developed by Charles-Augustin de Coulomb in 1776. Coulomb mathematically defined the geometry of the mobilized soil mass using the friction angle of the soil (ϕ), the slope of the wall being pushed into the soil (θ), the backfill inclination (α), and the friction angle at the interface between the wall and the soil (δ). The geometry of the mobilized soil mass is shown in Figure 2-2.

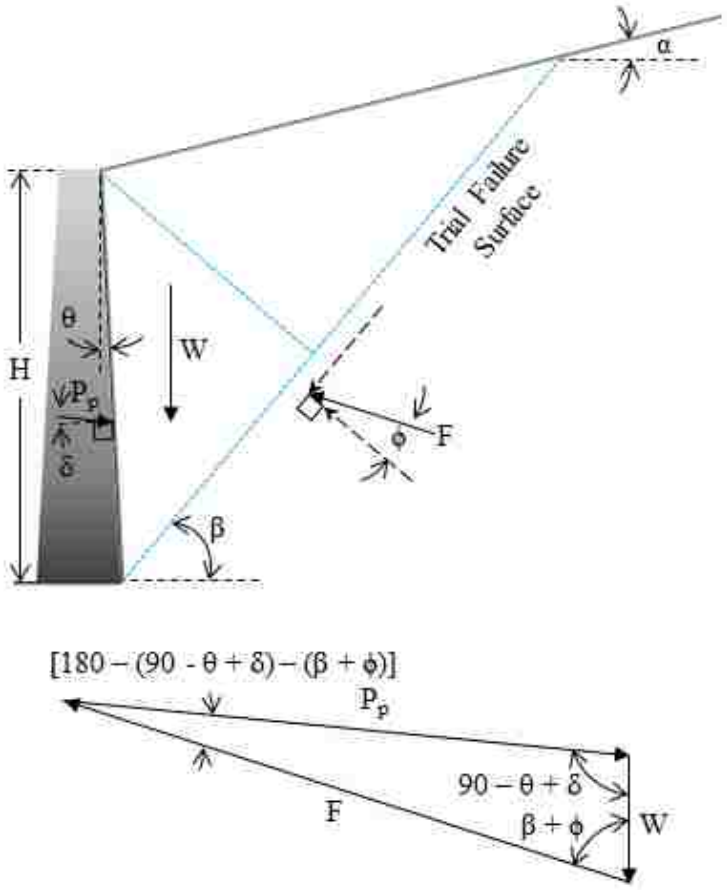

Figure 2-2: Shear failure surface geometry and direction of resultant force

Coulomb approximated the mobilized soil mass using a linear shear plane and also considered wall friction at the soil-wall interface. The value for K_p is calculated based on the geometry of the mobilized soil mass predicted by ϕ, θ, α, and δ. A solution is obtained by using a series of trial failure wedges and finding the critical wedge which provides the lowest passive force. Although Coulomb's theory gives a closed form solution for ultimate passive force, experimental and field observations indicate that his theory predicts erroneously high values for K_p when $\delta > 0.4\phi$, which would lead to an unconservative design in most cases. Engineers are discouraged from using Coulomb's theory for predicting ultimate passive force because typical construction materials that induce passive forces in soil have a $\delta > 0.4\phi$, as shown in Table 2-1.

Table 2-1: Typical Values for δ_{max}/ϕ, adapted from Potyondy (1961)

Soil Type	δ_{max}/ϕ		
	Steel	Concrete	Wood
Sand	0.54	0.76	0.76
Silt and Clay	0.54	0.5	0.55

2.1.2 Rankine (1857)

William Rankine developed a mathematical theory to describe the stability of a loose granular mass based only on the mutual friction of the soil grains (Rankine 1857). Rankine used the Mohr-Coulomb failure criterion to develop and publish equations for passive and active earth pressure coefficients. His equations do not account for wall friction, but the error associated with assuming no wall friction is usually on the conservative side because wall friction typically increases passive and decreases active pressures (Terzaghi et al. 1996). Equation (2-2) defines the passive earth pressure coefficient as published by Rankine.

$$K_P = \tan^2\left(45 + \frac{\phi'}{2}\right) \tag{2-2}$$

where

$\phi' =$ effective soil friction angle

The Rankine method assumes a linear failure surface that begins at the bottom of the wall and rises to the surface at an angle of inclination equal to 45° - ϕ/2, where ϕ = the angle of internal friction for the soil. This Rankine failure geometry is shown in Figure 2-3. Similar to the Coulomb method, the Rankine method will not produce accurate results for situations where the wall friction is greater than approximately 40% of the soil friction angle (Duncan and Mokwa 2001). In these cases, the predicted ultimate passive resistance may only be one-third of the actual resistance.

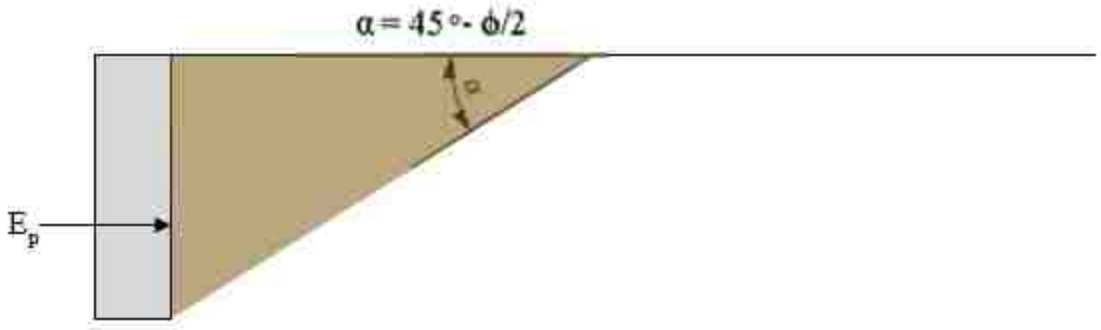

Figure 2-3: Rankine failure geometry

2.1.3 Log Spiral

The log spiral method was developed by Terzaghi (1943) and is widely considered to be the most accurate method for determining the passive earth pressure coefficient (K_p) when large wall friction angles are present. The log spiral method also provides the best agreement between the geometries of the predicted and actual mobilized soil mass (Duncan and Mokwa 2001; Rollins and Cole 2006). The shear plane is modeled using an initial curved log spiral segment followed by a linear Rankine portion, as shown in Figure 2-4. The non-linear shear plane leads to more accurate estimates of K_p when $\delta > 0.4\phi$, which makes the log spiral method more appropriate for predicting passive forces induced by concrete, steel, or wooden walls (Duncan and Mokwa 2001). Passive force can be computed by the log spiral theory either graphically, numerically, or with charts and tables.

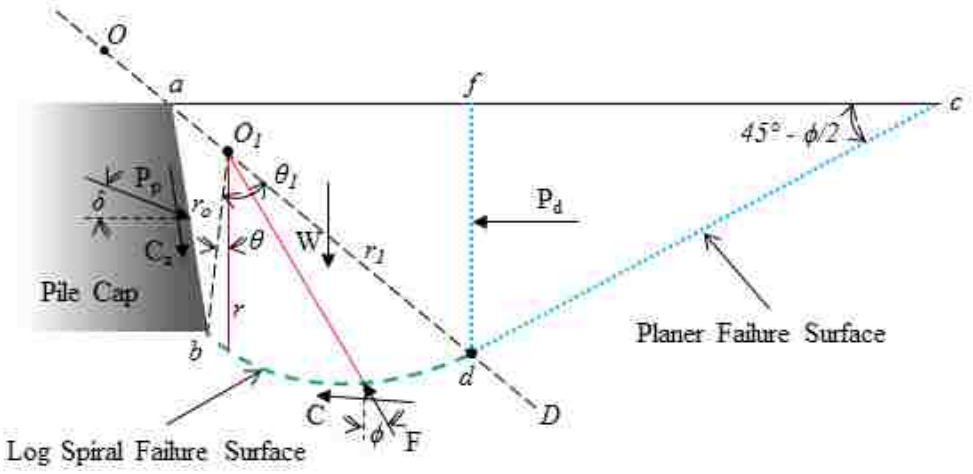

Figure 2-4: Log spiral shear failure surface geometry

A general comparison of the failure surface geometries predicted using the three different passive earth pressure theories is shown in Figure 2-5. A wall friction angle (δ) of approximately 0.75ϕ for concrete was used to compute the geometries. The volume of the failure mass for each method helps explain why the Rankine method underestimates resistance while the Coulomb method overestimates passive resistance relative to the log spiral method and large-scale test results.

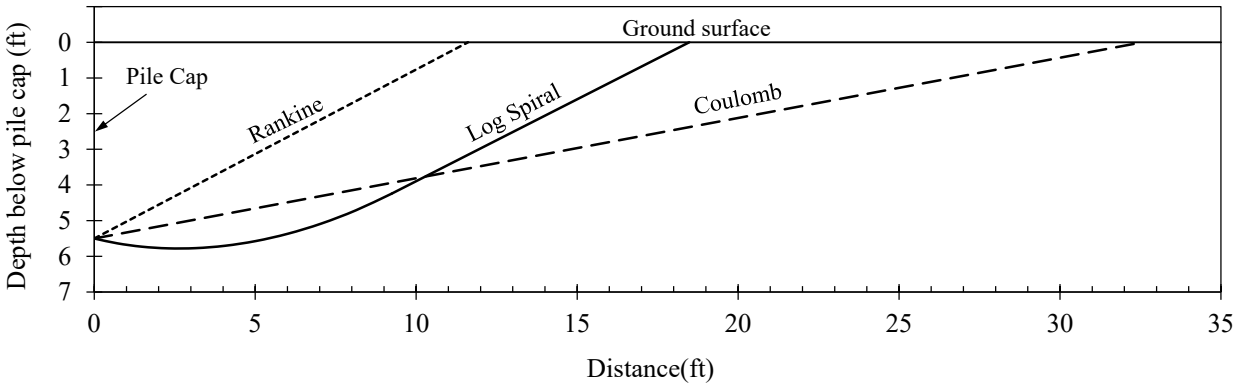

Figure 2-5: Comparison of Coulomb, Rankine, and Log Spiral failure surfaces

2.2 Passive Force-Deflection Relationships

Ultimate passive force is not developed until a certain amount of displacement of the backwall occurs. Large-scale laboratory and field testing has been performed to develop passive force-deflection curves by approximating intermediate values of passive force before the peak force is reached. Passive force-deflection relationships are especially useful in bridge abutment design, where the passive resistance of the abutment backfill is considered in the total lateral resistance of the abutment. The amount of displacement required to mobilize full passive resistance is typically normalized to abutment backwall height (H) and expressed as Δ_{max}/H. Table 2-2 shows values of Δ_{max}/H for different types of backfill as determined by Cole and Rollins (2006), Canadian Geotechnical Society (1992), Clough and Duncan (1991), and Sowers and Sowers (1961).

Table 2-2: Values of Δ_{max}/H for Different Backfill Types, adapted from Cole and Rollins (2006)

	Values of Δ_{max}/H			
Type of backill	Cole and Rollins (2006)	Canadian Geotechnical Society (1992)	Clough and Duncan (1991)	Sowers and Sowers (1961)
Coarse gravel	0.04	-	-	-
Fine gravel	0.03	-	-	-
Dense sand	0.03	0.02	0.01	0.002
Medium-dense sand	-	-	0.02	-
Loose sand	-	0.06	0.04	0.006
Silty sand	0.052	-	-	-
Stiff cohesive	-	0.02	-	-
Soft cohesive	-	0.04	-	-
Compacted silt	-	-	0.02	-
Compacted lean clay	-	-	0.05	-
Compacted fat clay	-	-	0.05	-

In general, more movement is required to achieve peak passive resistance in loose soils than in dense soils. The effect of a soil's relative density (loose or dense) on the passive force-deflection curve is addressed by assigning a stiffness value (K) to the soil. There are two main approaches currently used to predict soil passive resistance at displacements below Δ_{max}: bilinear and hyperbolic relationships. The Caltrans method is a common bilinear approximation, while the Duncan and Mokwa (2001) and Shamabadi et al. (2007) methods are more accurate hyperbolic approximations. All three methods will be described in detail below. The skew angle of the bridge is currently not considered in any of these approaches.

2.2.1 Caltrans Method

The Caltrans Seismic Design Criteria v1.6 (2010) approximates non-linear passive force-deflection behavior using a bilinear model illustrated in Figure 2-6. The approximation is based on large-scale abutment testing performed at BYU, UC Davis, and UCLA.

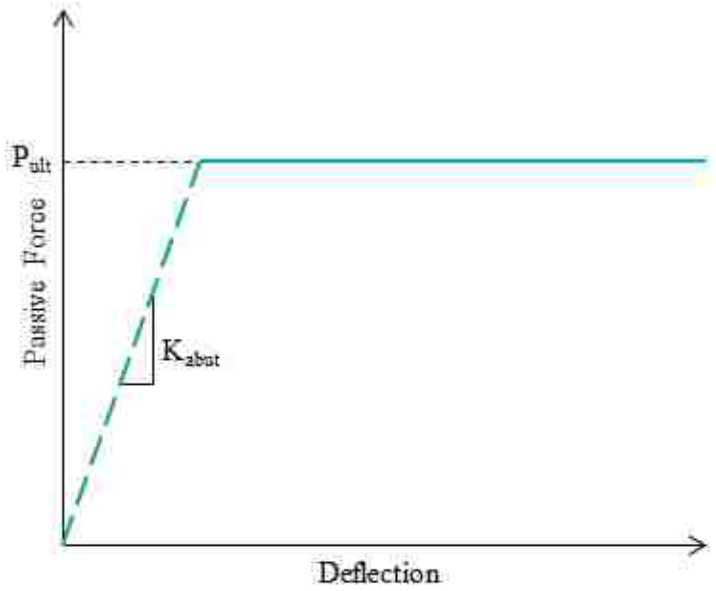

Figure 2-6: Caltrans bilinear passive force-deflection design curve

The initial stiffness of backfill material that meets the Caltrans Standard Specifications for fine-grained material is estimated according to Equation (2-3). If the backfill material does not meet specification, the initial stiffness is estimated according to Equation (2-4). Caltrans Standard Specifications typically include (Caltrans 2010):

- Standard penetration, upper layer [0 to 10 ft (0 to 3 m)] N = 20 (Granular soils)
- Standard penetration, lower layer [10 to 30 ft (3 to 9 m)] N = 30 (Granular soils)
- Undrained shear strength, s_u > 1500 psf (72 kPa) (Cohesive soils)
- Shear wave velocity, v_s > 600 ft/sec (180 m/sec)
- Low potential for liquefaction, lateral spreading, or scour

NOTE: N = The uncorrected blow count from the Standard Penetration Test (SPT)

Initial stiffness is adjusted proportional to the abutment backwall height in Equation (2-5) and used to construct the passive force-deflection curve.

$$K_i = \frac{50\ kip/in}{ft} \quad \left(\frac{28.70\ kN/mm}{m}\right) \tag{2-3}$$

$$K_i = \frac{25\ kip/in}{ft} \quad \left(\frac{14.35\ kN/mm}{m}\right) \tag{2-4}$$

$$K_{abut} = \begin{cases} K_i \times w \times \left(\frac{h}{5.5ft}\right) & \text{U.S. Units} \\ K_i \times w \times \left(\frac{h}{1.7m}\right) & \text{S.I. Units} \end{cases} \tag{2-5}$$

where,

$K_i = Initial\ soil\ stiffness$

$w = Abutment\ width$

$h = Abutment\ height$

The ultimate passive resistance (P_{ult}) is calculated using Equation (2-6) and is used as a constant value in the second segment of the bilinear curve.

$$P_{ult} = \begin{cases} A_e \times 5.0ksf \times \left(\frac{h}{5.5}\right) & (ft, kip) \quad \text{U.S. Units} \\ A_e \times 239kPa \times \left(\frac{h}{1.7}\right) & (m, kN) \quad \text{S.I. Units} \end{cases} \tag{2-6}$$

where,

$A_e = Effective\ abutment\ area\ (h \times w)$

$h = Abutment\ height$

There are several limitations to the Caltrans bilinear model. First, it does not capture the continuous reduction in soil stiffness with deflection. It also is limited by only dividing the soil types into two categories: those that meet the Caltrans Standard Specifications and those that do not. Lastly, this model does not allow the flexibility to accurately predict passive forces for soils outside of Caltrans Standard Specifications.

2.2.2 Duncan and Mokwa (2001) Method

In the Duncan and Mokwa (2001) method, the variation in passive resistance with deflection is approximated using a hyperbola based on the hyperbolic stress-strain relationship determined by Duncan and Chang (1970), as shown in Figure 2-7. An initial stiffness (K_{max}) is used to define the initial slope of the curve and the ultimate passive resistance (P_{ult}) is computed using the log spiral method. The hyperbolic curve in Figure 2-7 is defined by Equation (2-7).

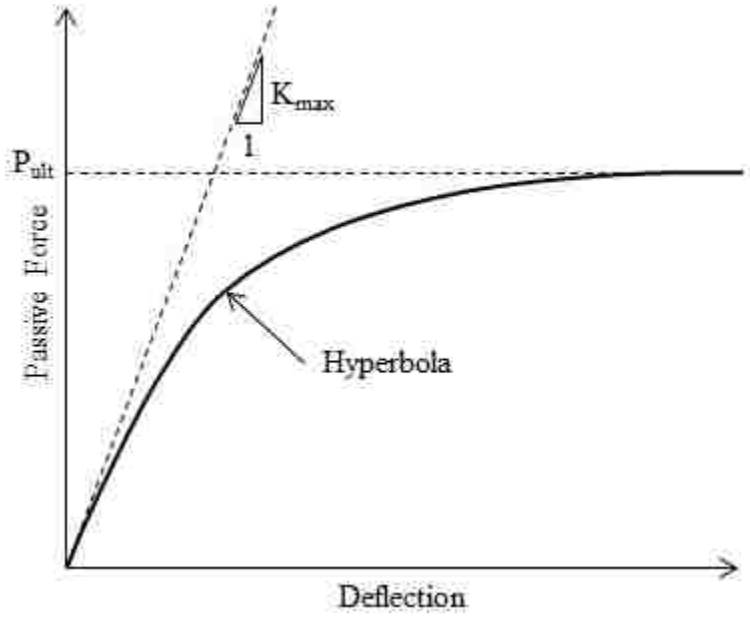

Figure 2-7: Duncan and Mokwa (2001) hyperbolic passive force-deflection curve

$$P = \frac{y}{\left[\frac{1}{K_{max}} + R_f \frac{y}{P_{ult}}\right]} \tag{2-1}$$

where,

$y = Pile\ cap\ deflection$

$K_{max} = Maximum\ soil\ stiffness$

$R_f = Failure\ ratio = 0.75\ to\ 0.95$

$P_{ult} = Maximum\ passive\ soil\ resistance$

K_{max} is estimated using the approach developed by Douglas and Davis (1964), which is based on elastic theory and depends on the soil's Young's modulus (E) and Poisson's ratio (ν). The values of E and ν are combined with the applied force (P), backwall dimensions, and influence factors to approximate the average deflection (y_{avg}). Maximum soil stiffness (K_{max}) is computed as

P/y_{avg}. The failure ratio (R_f) is the ratio of ultimate passive pressure to the asymptotic value of passive resistance. If no test data is available, values of R_f are estimated based on observations and experience. Duncan and Chang (1970) suggested values of $0.75 < R_f < 0.95$ for hyperbolic stress-strain curves. These values can produce reasonable results for load-deflection curves as well. The P_{ult} value defines the maximum value, or asymptote, of the hyperbola and is computed using the log spiral method. The equation for P_{ult} can be written as Equation (2-7).

$$P_{ult} = E_p bM \tag{2-7}$$

where,

$E_p = Passive\ resistance\ per\ unit\ width$

$b = Pile\ cap\ width$

$M = Brinch\ Hansen\ 3D\ correction\ factor$

The Brinch-Hansen 3D correction factor (M) ranges from 1 to 2 and essentially increases the effective width of the soil failure mass that provides passive resistance against the structure. This factor is appropriate for unconfined soils that allow the shear plane to extend beyond the width of the structure that applies the force.

In conjunction with their study, Duncan and Mokwa (2001) developed a spreadsheet program called PYCAP that computes the passive force-deflection hyperbola. The PYCAP spreadsheet generates force-deflection curves based on 12 input parameters: cap width (b), cap height (H), embedment depth (z), surcharge (q_s), cohesion (c), soil friction angle (ϕ), wall friction

angle (δ), initial soil modulus (E_i), Poisson's ratio (ν), soil unit weight (γ), adhesion factor (α), and Δ_{max}/H.

The hyperbolic force-deflection relationship by Duncan and Mokwa (2001) is more accurate than the Caltrans method in estimating the continuous increase in passive resistance with increasing deflection. Because a 3D correction factor and the log spiral method are used to compute P_{ult}, the ultimate passive resistance can be predicted more accurately for confined and unconfined backfills with a wide variety of soil types.

2.2.3 Shamsabadi et al. (2007) Method

Similar to the Caltrans method, the method developed by Shamsabadi et al. (2007) uses the hyperbolic stress-strain relationship by Duncan and Chang (1970) to approximate the variation in passive resistance with deflection. The approximated hyperbolic passive force-deflection curve is shown in Figure 2-8. The hyperbolic curves are generated by a numerical model and have accurately modeled passive force-deflection relationships of several large-scale tests to date.

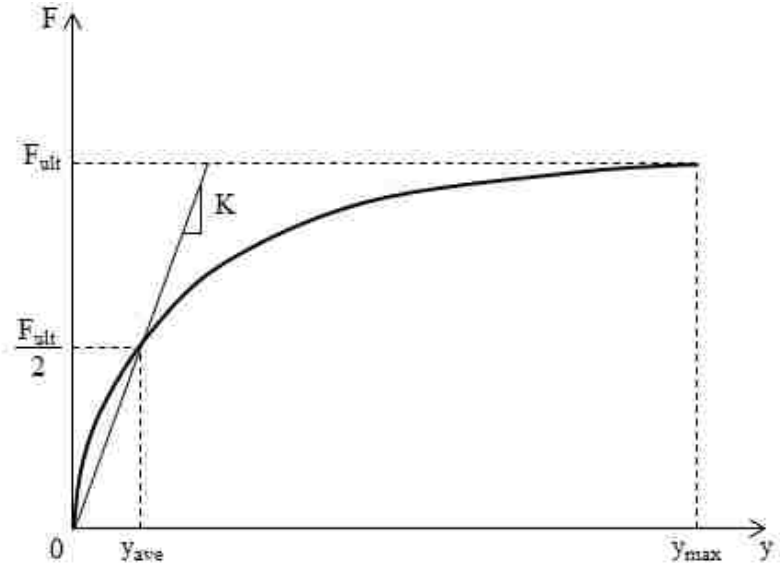

Figure 2-8: Shamsabadi et al. (2007) hyperbolic passive force-deflection curve

The hyperbolic curve in Figure 2-8 is expressed by Equation (2-8).

$$F(y) = \frac{y}{\frac{y_{max}}{2Ky_{max} - F_{ult}} + \frac{2(Ky_{max} - F_{ult})}{F_{ult}(2Ky_{max} - F_{ult})}y} \quad (2\text{-}8)$$

where,

$y = Abutment\ displacement$

$y_{max} = Maximum\ displacement$

$K = Average\ soil\ stiffness$

$F_{ult} = Maximum\ abutment\ force$

The parameters used in Equation (2-8) (K, F_{ult}, and y_{max}) are typically the three parameters provided by the geotechnical engineer for seismic bridge design. The force-deflection relationship by Shamsabadi et al. (2007) has the same hyperbolic form $\left[F(y) = \frac{y}{A+By}, where\ A\ and\ B\ are\ constants\right]$ as the Duncan and Mokwa (2001) method [Compare Equation (2-6) and Equation (2-8)]. However, the Shamsabadi et al. (2007) method uses the average stiffness instead of the maximum stiffness. Also, Condition II of the three boundary conditions listed below gives the general hyperbolic curve a different shape compared to the general hyperbola by Duncan and Mokwa (2001). The three boundary conditions used by Shamsabadi et al. (2007) are as follows:

- Condition I $F(y) = 0\ at\ y = 0$
- Condition II $F(y) = \frac{F_{ult}}{2}\ at\ y = y_{avg}$

- Condition III $F(y) = F_{ult}\ at\ y = y_{max}$

The average stiffness is not based on elastic theory but rather computed as $K = \frac{1}{2}F_{ult}/y_{ave}$.

Table 2.3 provides suggested values for K and y_{max}/H for granular and cohesive soils.

Table 2-3: Suggested Values for K and y_{max}/H (Shamsabadi et al. 2007)

Abutment backfill type	K kN/cm/m (kip/in/ft)	y_{max}/H
Granular	290 (50)	0.05
Cohesive	145 (25)	0.1

The hyperbolic method developed by Shamsabadi et al. (2007) has similar advantages to the Duncan and Mokwa (2001) method. It accurately estimates the continuous nonlinear increase in passive resistance with increasing deflection and the model can be used for a wide variety of soil types. However, there are also significant differences between the two approaches. Duncan and Mokwa's (2001) approach for computing initial soil stiffness is more fundamentally based on soil mechanics theory than the approach of estimating an average soil stiffness. Shamsabadi et al. (2007) provides a suggested value of y_{max}/H for cohesive soils (0.10) which is more than twice the value of Duncan and Mokwa's (2001) recommended value of 0.04 for all soil types.

2.3 Skewed Bridges vs. Non-skewed Bridges

It has been observed that skewed bridges exhibit a greater damage from lateral loads in comparison with non-skewed bridges. Inspection following large seismic events in Northridge, California (1994), Chi Chi, Taiwan (1999), and Maule, Chile (2010) report significantly more damage to skewed bridges compared to non-skewed bridges (Apirakvorapinit et al. 2012; Elnashai

et al. 2010; Shamsabadi et al. 2006). Significant damage was experienced by the Pico Lyons Bridge (40° skew) in the 1994 California Northridge earthquake. Apirakvorapinit et al. (2012) performed a finite element analysis which suggested that end girders on a 40° skewed bridge can experience a 50% stress increase compared with non-skewed bridges. During the 1999 Chi Chi earthquake in Taiwan, the skewed Wushi highway bridge was severely damaged (Shamsabadi et al. 2006). The magnitude 8.8 Maule, Chile (2010) earthquake had damage rate nearly twice as high for skewed bridges compared to non-skewed bridges (Toro et al. 2013).

During the field reconnaissance following the 2010 Maule, Chile earthquake, it was observed that many of the bridge-decks were unseated from the abutment, especially on skewed bridges. Significant damage was reported for the Las Mercedes Bridge (10° skew), the Paso Cladio Arrau Bridge (50° skew), and the Route 5 overpass near Chillan (highly skewed). In general, it was observed that rotation of the bridge deck caused the shear keys to fail, resulting in the unseating of the bridge deck from the abutment. However, rotation was often associated with significant deformation of the backwall suggesting significant mobilization of passive force.

In addition to seismic events, concern has been expressed regarding poor performance of skewed bridges due to rotation from thermal expansion. To address these concerns, pressures behind a skewed abutment in Maine were monitored for 33 months and a non-uniform lateral pressure distribution was measured as the superstructure expanded due to temperature increases in the soil backfill (Sandford and Elgaaly 1993). Pressures near the obtuse corner of the abutment increased 4 to 6 times the cold weather value compared to pressures near the acute corner which only increased 2 to 3 times. A design lateral pressure distribution was developed that assigned the Rankine active pressure to the acute corner of the abutment and the Rankine passive pressure to the obtuse corner, as shown in Figure 2-9. The higher pressure at the obtuse end indicates that the

obtuse end of the abutment rotated into the backfill while the acute corner rotated away from the backfill. The rotation mechanism for skewed bridges during seismic events or thermal expansion is explained in the next section.

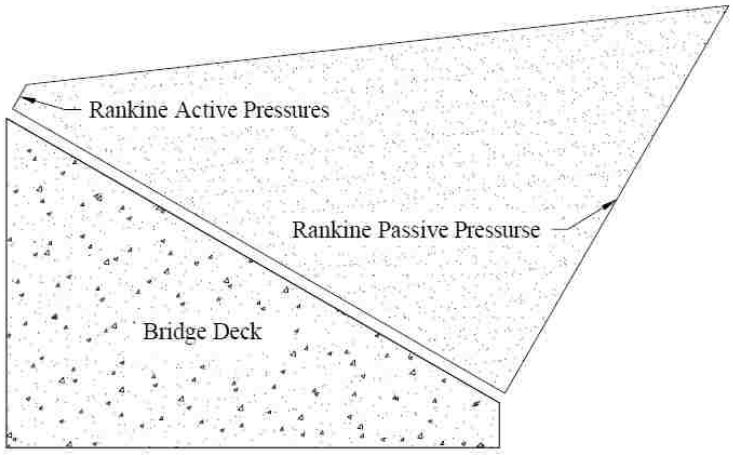

Figure 2-9: Nonuniform lateral pressure distribution, adapted from Sandford and Elgaaly (1993)

2.3.1 Skewed Bridge Geometry

For non-skewed bridges, the total soil passive force is composed of the ultimate horizontal force as the bridge displaces into the backfill and a vertical force resulting from wall friction. For skewed bridges, however, there is an additional rotational force that develops as a result of the skewed geometry. Figure 2-10 illustrates the forces that are present in a skewed bridge configuration. The longitudinal force, P_L, acts at an angle, θ, from perpendicular to the face of the abutment wall (the skew angle). This causes a horizontal component of wall friction, P_R, to develop. A moment is also developed resulting in tendency for bridge rotation. This rotation is the

cause of significant failures of skewed bridges during seismic events or as a result of thermal expansion.

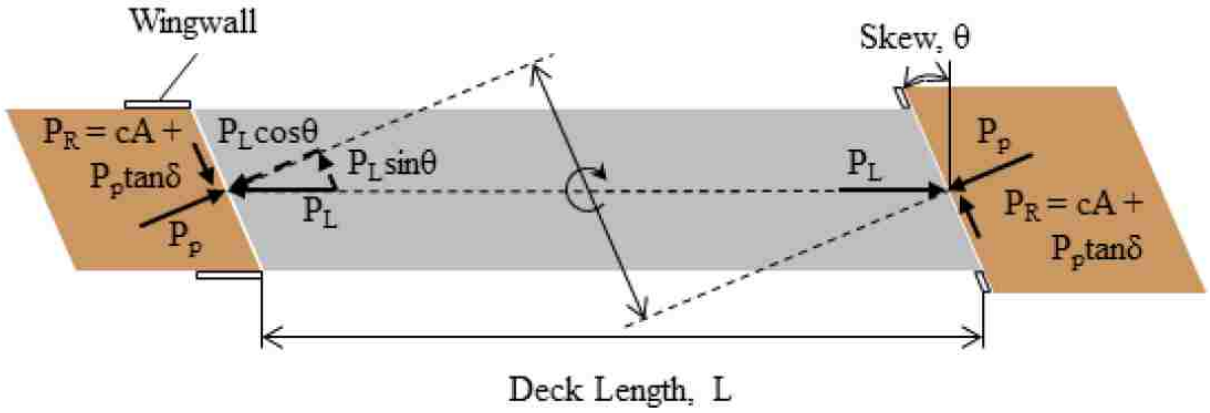

Figure 2-10: Typical forces on a skewed bridge from lateral loading (Franke 2013)

For a skewed bridge to be able to resist rotation and remain in force equilibrium, one of two conditions must be met: (1) horizontal wall friction must be sufficient to resist the couple moment or (2) additional resistance from an external source must be provided. To satisfy the first condition, the factor of safety, FS, given in Equation (2-9), must be greater than 1.0. To satisfy the second condition, sufficient lateral restraint must be provided to resist rotation. This lateral resistance is usually provided by shear keys or seismic restraints. Another solution would be to increase the bent size to allow more bridge rotational movement before unseating occurs.

$$FS = \frac{cA + P_p tan\delta}{P_L sin\theta} \geq 1 \qquad (2\text{-}9)$$

where,

$FS = Factor\ of\ safety$

$c = Soil\ cohesion$

$A = Wall\ surface\ area$

$P_p = Passive\ soil\ resistance$

$\delta = Wall\ friction\ angle$

$P_L = Longitudinal\ Force$

$\theta = Skew\ angle$

Passive soil resistance (P_p) is an important aspect of skewed bridge geometry that must be considered in design. The development of sufficient passive soil resistance is essential to resist longitudinal displacement. Consequently, properly predicting the development and achievement of ultimate passive soil resistance is essential during bridge design to ensure that the abutment will be able to withstand substantial seismic events and thermal expansions.

2.4 Passive Force Skew Reduction Factors

The relationship between abutment skew angle and reduction in passive resistance of the backfill has recently been explored by several researchers. Numerical analyses, lab tests, and large-scale field tests have been employed to determine an appropriate relationship between passive force reduction factor (R_{skew}) and skew angle. Shamsabadi et al. (2006) performed numerical analysis using 3D PLAXIS modeling. The model results indicate a significant reduction in passive resistance with increasing skew angle.

Rollins and Jesse (2012) performed nine small-scale laboratory tests. A 4.1-ft (1.26-m) wide and 2-ft (0.61-m) high concrete wall was pushed longitudinally into a densely compacted sand backfill. Tests were conducted at skew angles of 0°, 15°, 30°, and 45°. The backfill extended 10 to 13 ft (3 to 4 m) behind the backwall and 1-ft (0.3-m) below the base of the wall to allow for the formation of a log spiral failure surface. The backfill was confined by low interface friction sidewalls to approximate plain-strain (2D) conditions.

Between 2012 and 2015, Rollins performed several large-scale field tests with the results being published by several of his graduate students (Franke 2013, Marsh 2013, Palmer 2013, Smith 2014, and Frederickson 2015). All of the tests were performed using an 11-ft (3.35-m) wide and 5.5-ft (1.68-m) high pile cap that was pushed longitudinally into various types of backfill. The backfill extended approximately 20 to 25-ft (6.1 to 7.6-m) behind the backwall and 0.5 to 1-ft (0.15 to 0.3-m) below the base of the wall. Tests were conducted at skew angles of 0°, 15°, 30°, and 45°. The pile cap was loaded using two hydraulic actuators which pushed the pile cap into the backfill at discrete increments until backfill failure was reached. The loading was applied to produce uniform deformation (or no rotation) to both sides of the pile cap in all tests.

Franke's (2013) test included longitudinal MSE wingwalls extending 24-ft (7.32-m) from the face of the pile cap and a poorly-graded sand backfill. Tests were conducted at skew angles of 0°, 15°, and 30°. Marsh's (2013) test included transverse wingwalls extending 4-ft from each side of the pile cap and a poorly-graded sand backfill. Tests were conducted at skew angles of 0°, 15°, and 30°. Palmer's (2013) test also included 4-ft (1.2-m) transverse wingwalls and poorly-graded sand backfill, but the backfill was only 3.5-ft (1.07-m) high instead of being filled to the top of the pile cap as was done in previous tests. Tests were conducted at skew angles of 0°, 15°, and 30°. Smith's (2014) test included longitudinal reinforced concrete wingwalls and a poorly-graded sand

backfill. The wingwalls were 5.5-ft (1.68-m) high, 1-ft (0.3-m) thick and 10-ft (3-m) long. At 5-ft (1.5-m) out, the bottom of the wingwall tapered upward at a 2H:1V slope, making the tapered end 3-ft (0.91-m) high. Only 6-ft (1.83-m) of the wingwall extended into the backfill zone because 4-ft (1.2-m) of the wall were used to connect it to the pile cap. Tests were conducted at skew angles of 0° and 45°. Frederickson's (2015) test included 4-ft (1.2-m) transverse wingwalls and a well-graded gravel with silt and sand backfill. Tests were conducted at skew angles of 0° and 30°. The passive force reduction factor (R_{skew}) was plotted against skew angle for all of the previously described tests, as shown in Figure 2-11.

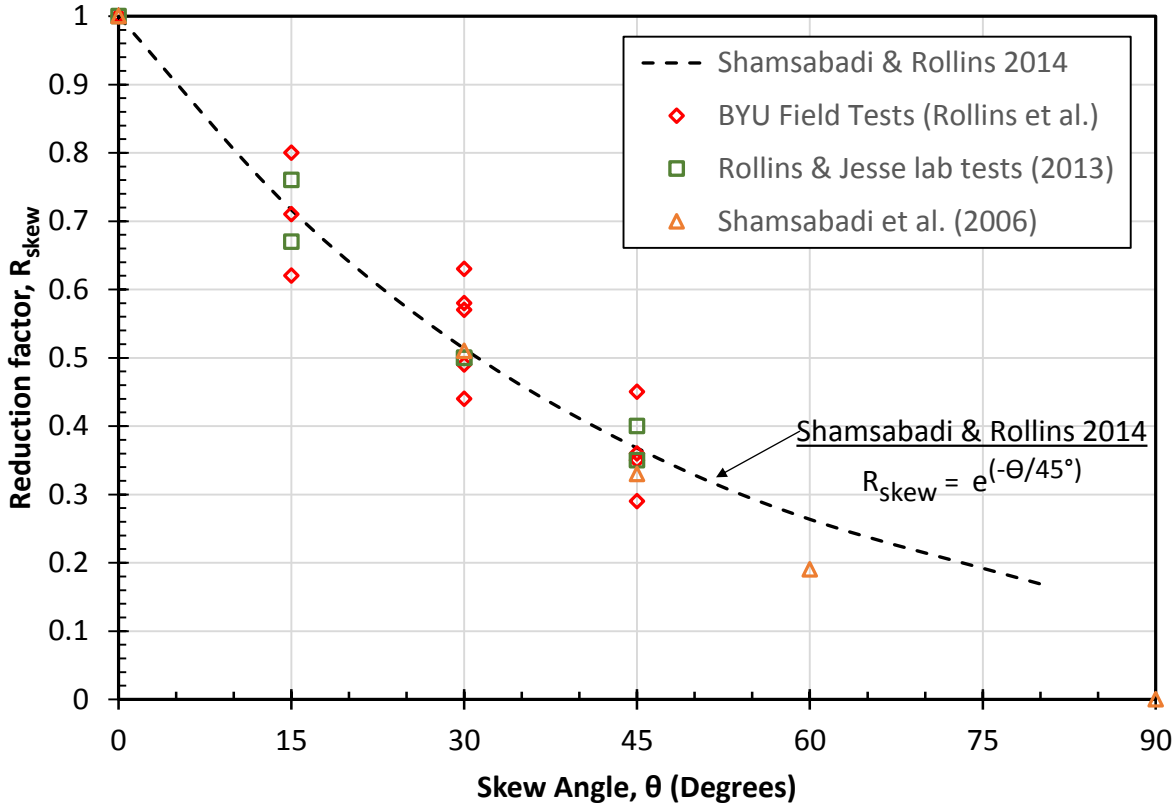

Figure 2-11: Reduction factor, R_{skew} (passive force for a given skew angle normalized to non-skewed passive force) plotted versus skew angle based on previous BYU field tests (Franke 2013; Marsh 2013; Palmer 2013; Smith 2014; Frederickson 2015), lab tests (Rollins and Jessee 2012), and numerical analyses (Shamsabadi et al. 2006)

Based on the data points shown in Figure 2-11, Shamsabadi and Rollins (2014) proposed a reduction curve to estimate passive force reduction factor given the abutment skew angle. The equation for the Shamsabadi and Rollins (2014) reduction factor (R_{skew}) is given by Equation (2-10).

$$R_{skew} = e^{\left(-\theta/45\right)} \quad (2\text{-}10)$$

where

θ = skew angle (in degrees)

2.4.1 Narrow Abutment Effect

It has been observed that the skew angle is effectively reduced when the abutment is particularly narrow and longitudinal wingwalls are in place. Snow (2018) performed PLAXIS modeling of 2-lane, 4-lane, and 6-lane abutments to determine the effect of abutment width on passive force skew reduction factors. It was determined that narrower bridge abutments have higher reduction factors. This results because the skew angle is effectively reduced during the loading process. A wedge of backfill material between the obtuse corner of the abutment and the side wall gets caught in a pocket resulting from the normal force against the skewed abutment wall and the side wall friction. This wedge of sand moves with the abutment and effectively reduces the skew angle, which in turn increases the passive force skew reduction factor. This soil wedge that moves with the abutment can be observed in both the longitudinal displacement and heave plots produced in PLAXIS. The longitudinal displacement plot in Figure 2-12 shows that the soil wedge displaces more than the rest of the soil along the abutment-backfill interface. The heave

plot in Figure 2-13 shows that there is very little heave in the soil wedge. This is because the soil wedge is moving with the abutment instead of compressing and heaving.

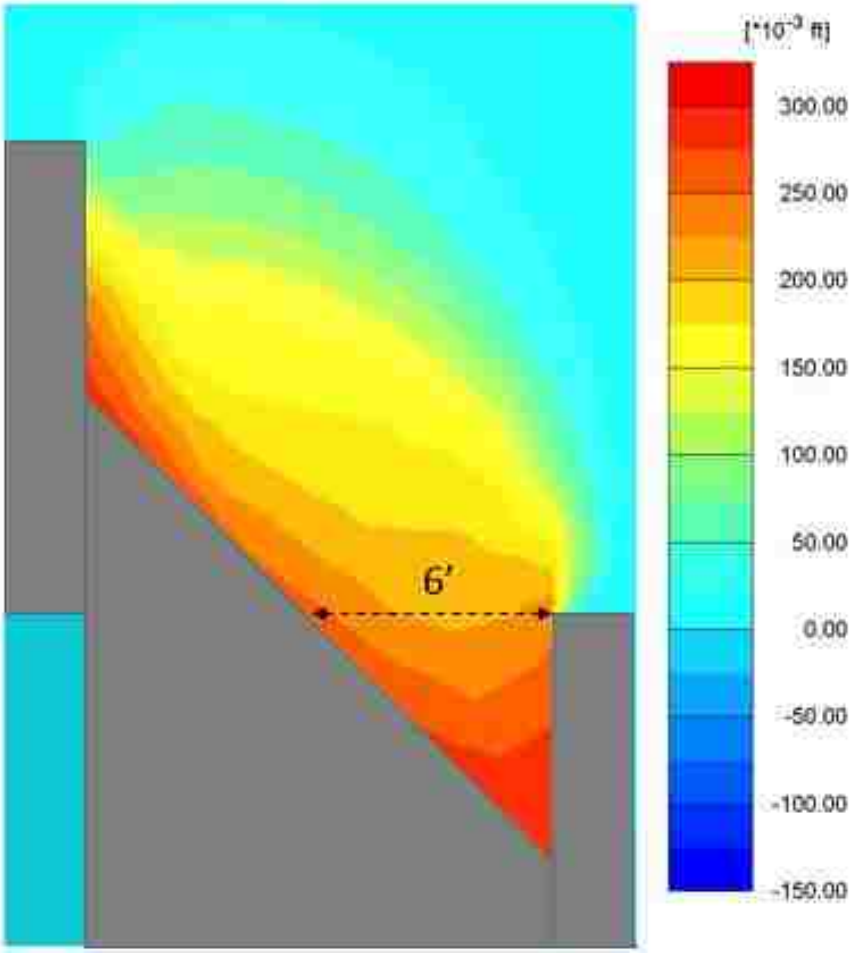

Figure 2-12: Longitudinal displacement for calibrated 45° skew, illustrating the wedge of backfill that gets caught between the obtuse end of the skewed abutment and the sidewall (Snow 2018)

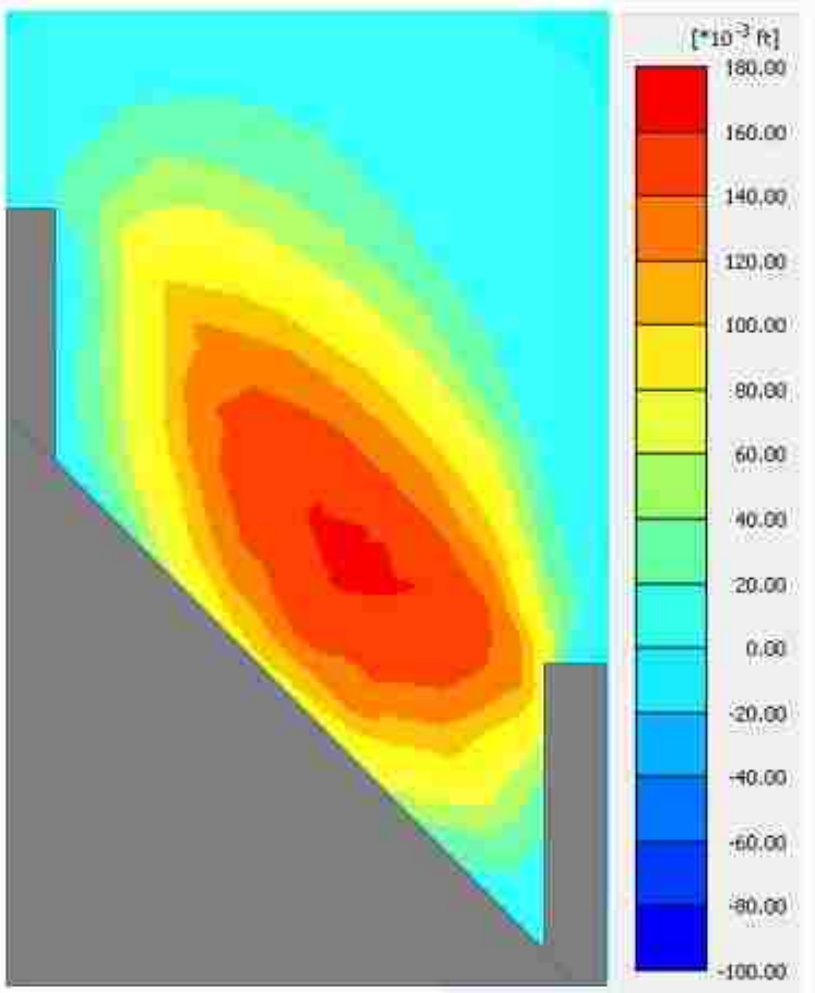

Figure 2-13: Heave for calibrated 45° skew, illustrating the wedge of backfill that gets caught between the obtuse end of the skewed abutment and the sidewall (Snow 2018)

Tests reported by Smith (2013) also show an effective reduction in skew angle as a soil wedge gets caught and moves with the abutment, as illustrated by the heave plot shown in Figure 2-14. The backfill heave in the soil wedge between the obtuse corner of the skew wedge and the side wall is between 0 and 0.25 inches. In contrast, the soil adjacent to the rest of the skew wedge experienced heave between 0.25 and 1.0 inches. As the soil wedge moves with the skewed abutment, it effectively reduces the 45° skew angle down to about 36°, as shown in Figure 2-14.

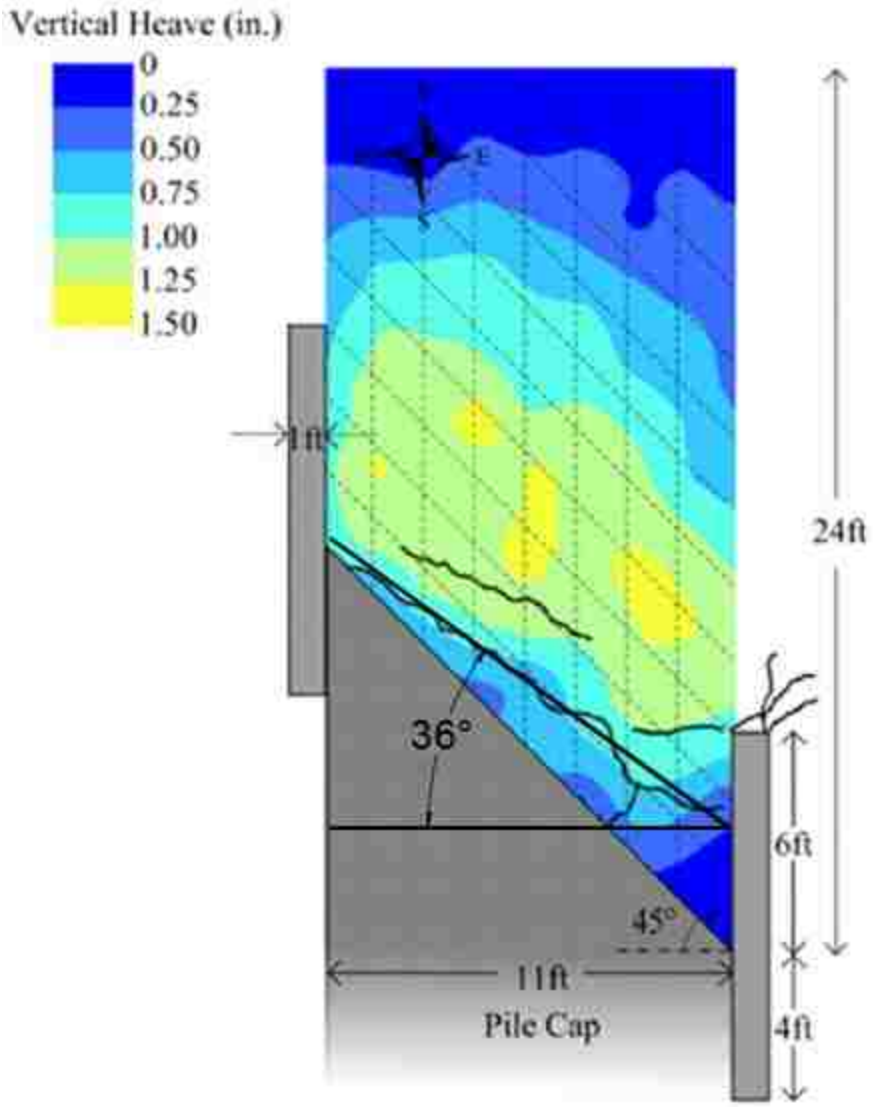

Figure 2-14: Heave contours and surface cracks from Smith's (2013) 45° skew test

With wider abutments, the effective reduction in skew angle decreases. In Snow's (2018) PLAXIS analysis of four-lane and six-lane abutments, a similar sand wedge formed between the obtuse corner of the skew wedge and the side wall. However, because the abutment width was much wider, the soil wedge did not decrease the effective skew angle as much as it did for the narrow abutment case.

Effective skew angle should be considered when selecting a passive force skew reduction factor during the design of narrow skewed bridges, such as a two-lane highway. However, when the bridge abutment is wider, such as with a four- or six-lane highway, the effective reduction in skew angle is much smaller and does not have as much of an effect on the skew reduction factor and may not need to be considered. An example of a narrow skewed bridge where the narrow abutment effect would need to be considered is shown in Figure 2-15. An example of a wide skewed bridge where the narrow abutment effect need not be considered is shown in Figure 2-16.

Figure 2-15: A narrow skewed bridge located near utility exit 133 off of Interstate-80, about 5 miles east of Salt Lake City, Utah (adapted from Google Earth)

Figure 2-16: A wide skewed bridge located on Interstate-15 in Lehi, Utah (adapted from Google Earth)

2.5 Backfill Soil Pressure Distribution

The horizontal backfill soil pressure distribution has been measured during previous large-scale tests performed by Franke 2013 and Smith 2013. The pressure was recorded using six pressure cells which were installed horizontally across the face of a skewed backwall to measure the pressure as the abutment was pushed into the backfill. In both of these tests, uniform longitudinal loading was applied to the abutment, thus limiting the rotation of the abutment

backwall. Franke 2013 recorded significantly higher pressures on the acute side of a 30° skewed abutment, especially at displacement greater than 1 inch, as shown in Figure 2-17. Smith 2013 also recorded higher pressures on the acute side of a 45° skewed abutment, as shown in Figure 2-18.

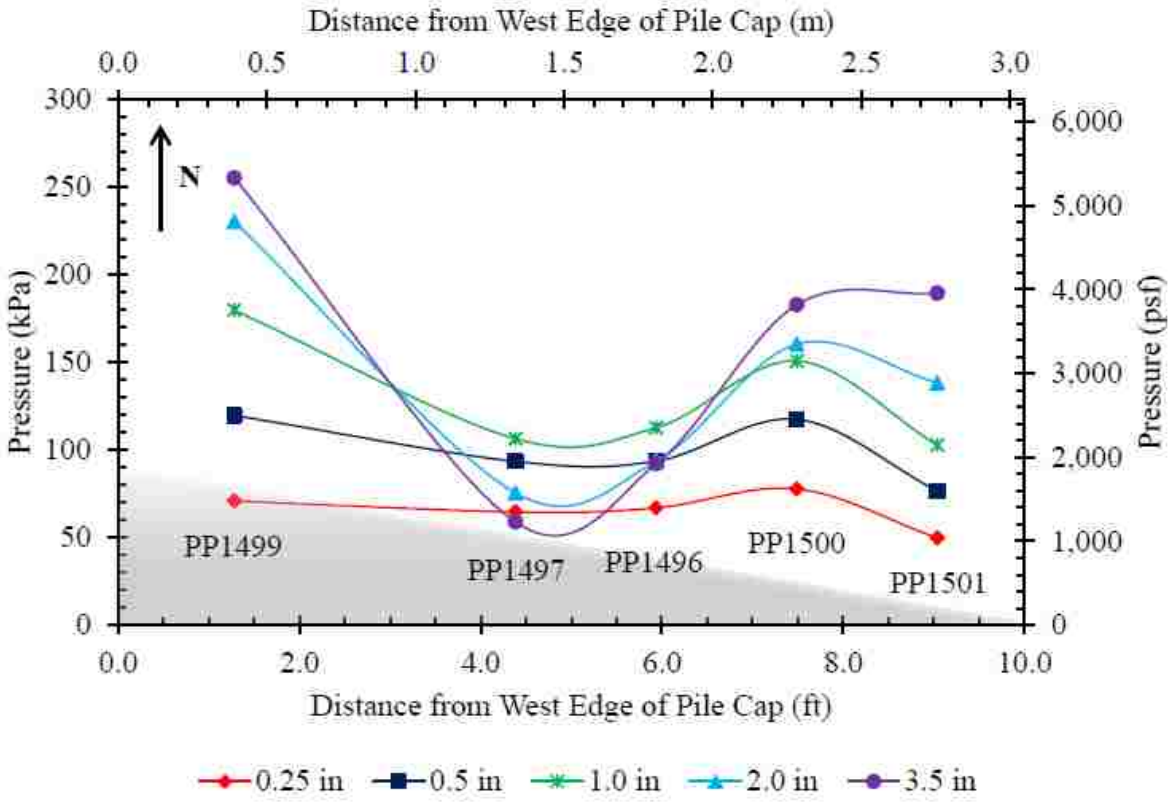

Figure 2-17: Pressure distribution across 30° skewed abutment (west edge is the acute side) (Franke 2013)

Previous field observations have shown that the backfill soil pressure is typically higher on the obtuse corner of a skewed abutment than on the acute corner. This is a result of rotation of the abutment during seismic events or thermal expansion. Findings by Apiakyorapinit et al. (2012)

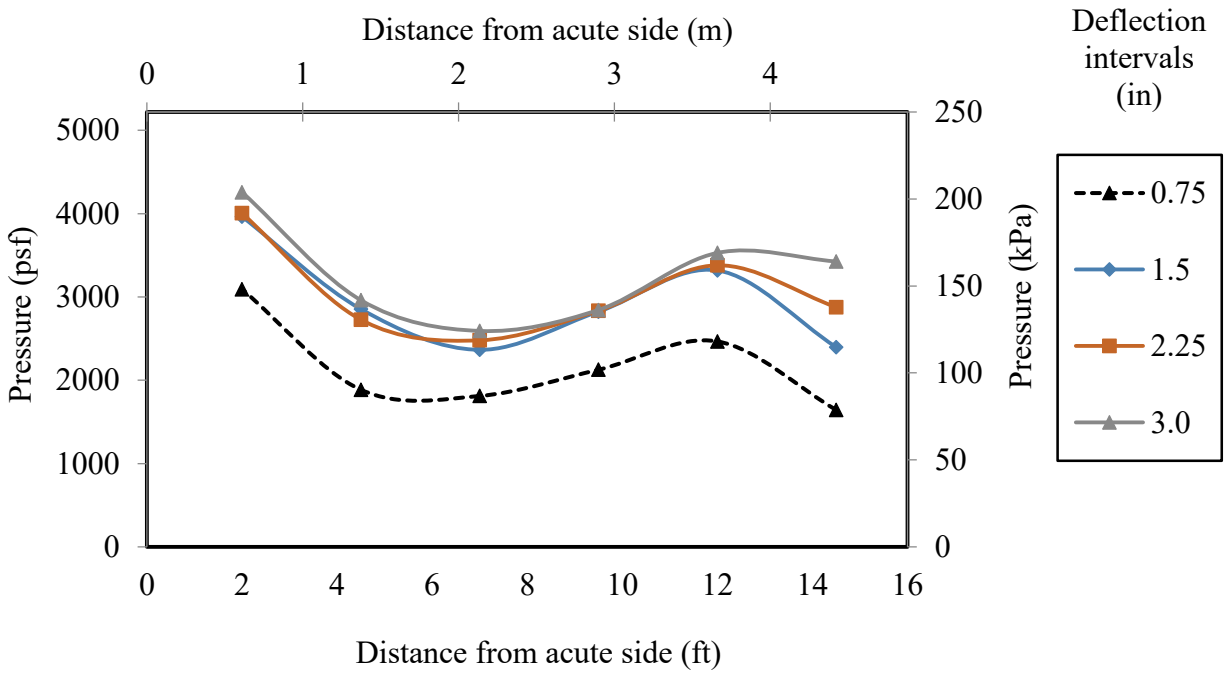

Figure 2-18: Pressure distribution across 45° skewed abutment (Smith 2013)

explain that stresses on skewed bridge girders are highest on the obtuse side where the girders are pushed into the backfill. Sandford and Elgaaly (1993) also found that pressures on the obtuse side of a skewed bridge abutment tend to be greater than on the acute side. Because rotation was extremely limited during Franke's (2013) and Smith's (2013) test, their findings did not match what was observed in these field studies.

If rotation of the abutment is introduced in a large-scale test, it would be expected that pressure on the obtuse side would be higher than on the acute side. The test performed in this study is the first time where an inclined, or non-uniform, loading scenario has been tested.

3 SITE LAYOUT

3.1 Overview

All tests were performed at a site immediately north of the control tower at the Salt Lake International Airport (40°47’55.80”N, 111°59’8.89”W), as shown in Figure 3-1.

Figure 3-1: Aerial Photograph of test site and Salt Lake International Airport control tower (adapted from Google Earth)

The site consisted of low-plasticity silts and clays, had almost no plant growth, and was subject to full sun exposure. The area immediately around the excavation consisted of a poorly graded sandy gravel due to previous material used at the site. Temperatures ranged from 63° to 102°F (17° to 39°C) during testing.

3.2 Geotechnical Characterization

It was not necessary to perform a geotechnical test at this time because several investigations have previously been performed at or near the site. Some of these investigations include cone penetrometer, dilatometer, standard penetration, vane shear, and shear wave velocity tests. The soil profile at the test site consists of 5 ft (1.52 m) of sandy gravel fill underlain by layers of silty clay and sand down to a depth of 100 ft (30.5 m). A portion of the upper 8 ft (2.44 m) was excavated and replaced with clean sand in 2004 in the test site vicinity (Rollins et al 2010). Rollins et al. (2010) concluded that the site was represented best by the CPT profile shown in Figure 3-2. During excavation, it was found that the water table was located approximately 5 ft below the ground surface. This was in agreement with the CPT shown in Figure 3-2. Further details concerning the geotechnical characterization of the site may be found in previous publications (Christensen 2006; Rollins et al. 2010; Strassburg 2010).

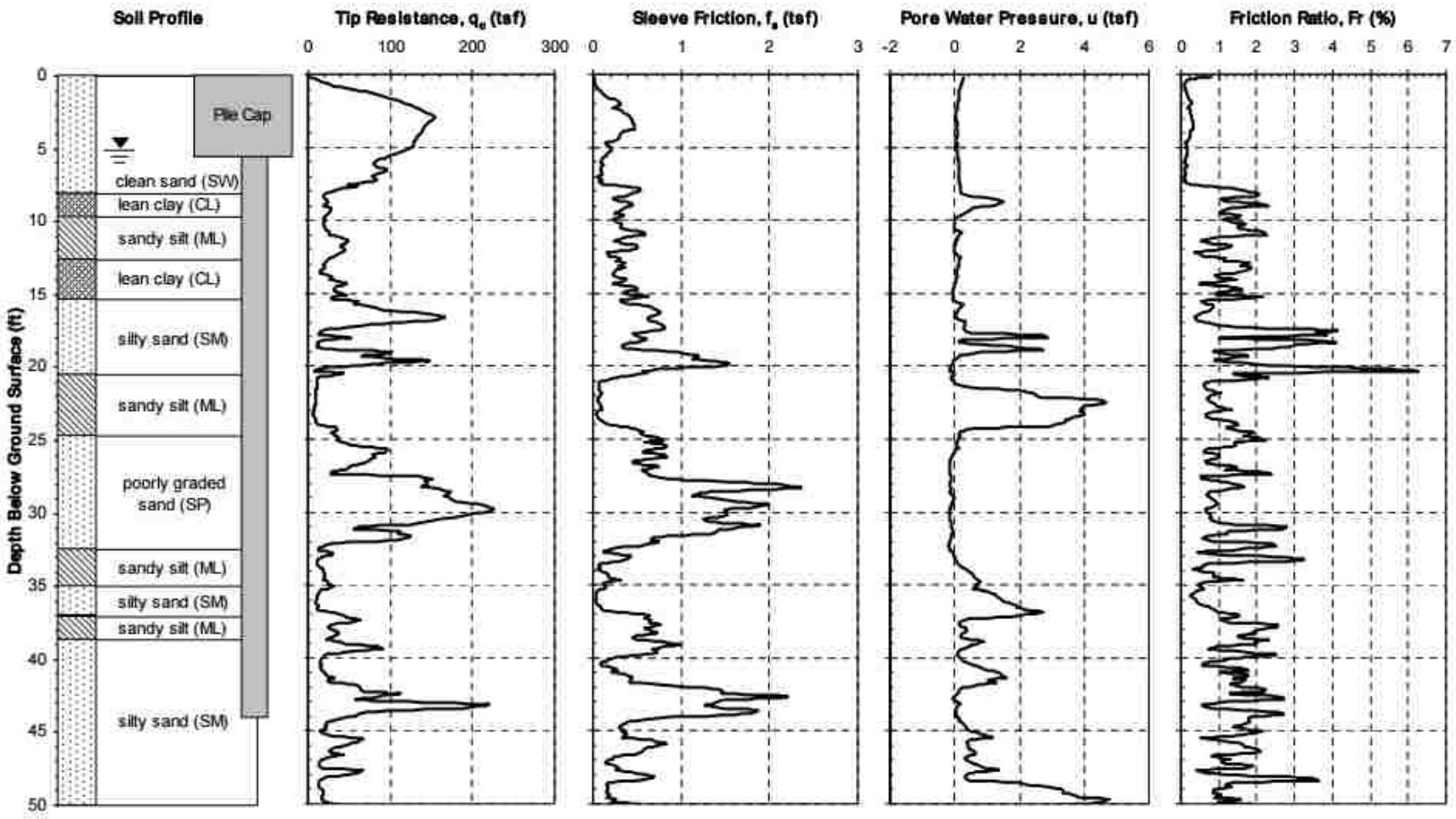

Figure 3-2: CPT soil profile of Salt Lake International Airport test site (Rollins et al. 2010)

3.3 Test Layout

All testing was performed using an existing pile cap and reaction frame that has been used for previous tests (Franke 2013, Fredrickson 2015, Marsh 2013). The pile cap was 5.5-ft tall, 11-ft wide, and 15-ft long (1.68-m by 3.35-m by 4.57-m). The cap was anchored in place by six piles driven to a depth of approximately 43 ft (13.1 m) (Marsh 2013). The reaction system consisted of two 4-ft (1.22-m) diameter concrete shafts along with an AZ 18 sheet pile wall placed against the shafts on the north side. Deep I-beams were placed along the north side of the sheet pile wall and along the south side of the concrete shafts to tie the system together. Plan and profile views of the complete test setup are illustrated in Figure 3-3.

Loading was accomplished using two hydraulic actuators placed between the reaction frame and pile cap. Extension pieces were placed on the north side of each actuator to allow the actuator to span the full distance between the reaction frame and pile cap. Each actuator was held in place by four Dycherhoff and Wildmann AG (DYWIDAG) bars on the north and south ends. Together, the two actuators could apply up to 1,200 kips (5,338 kN) of lateral load to the pile cap. Figure 3-4 shows the hydraulic actuator setup.

Two large-scale lateral load tests were performed on 0° and 30° skewed abutments. The 30° skew angle was created by attaching two previously constructed 15° concrete wedges to the backside of the pile cap. The skew wedges were held in place by dowel rods placed through holes on the center of the skew face and metal plates placed on the top and sides of the pile cap and skew wedges. The wedges were supported by a railroad tie base overlain by 0.75-in. (1.9-cm) plywood. One-inch (2.5-cm) diameter rollers were placed on the plywood to minimize friction. Figure 3-5 shows the skew wedge base.

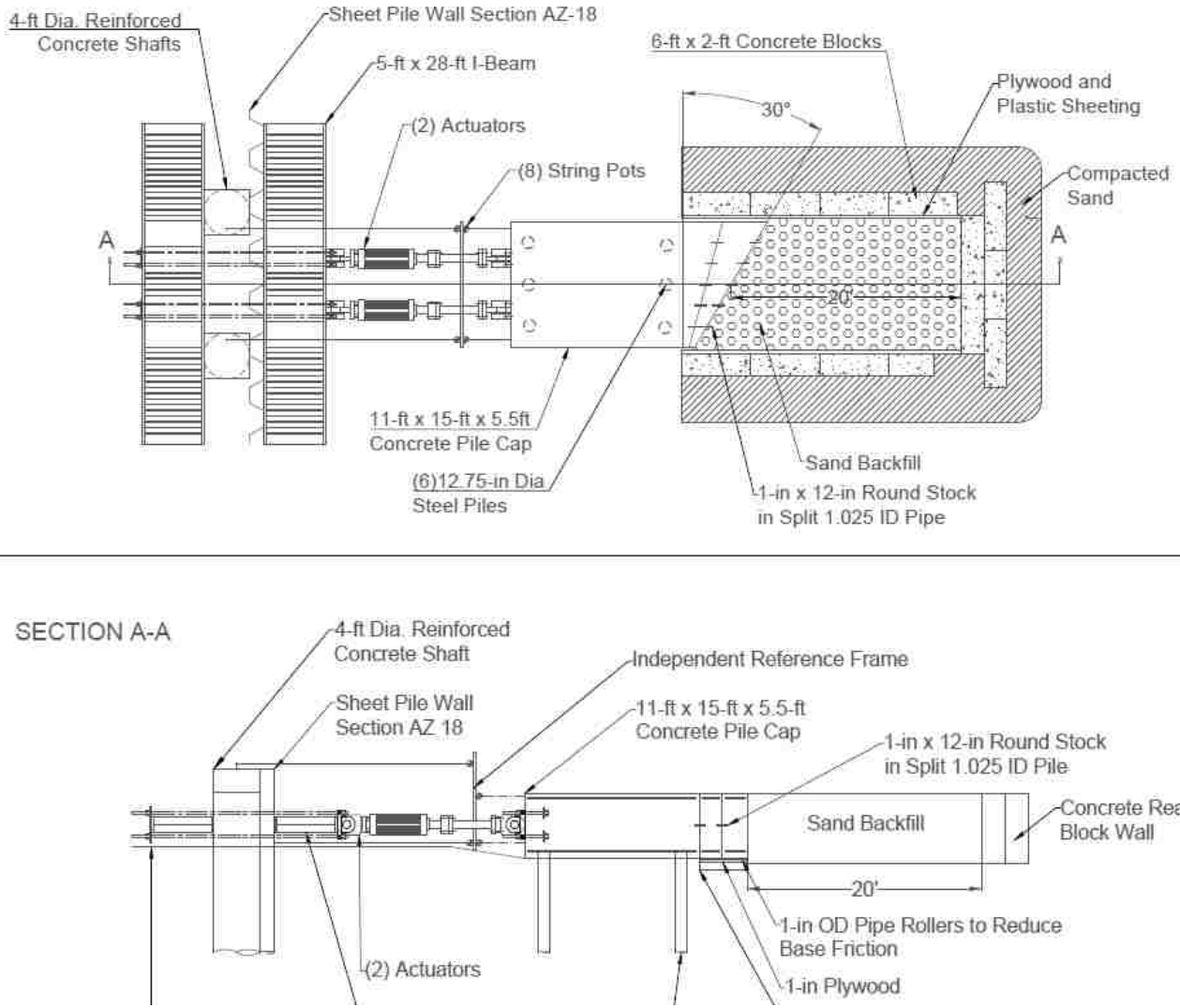

Figure 3-3: Plan and profile view of the site layout at Salt Lake International Airport

Figure 3-4: Hydraulic actuator setup as viewed from the west side

Figure 3-5: Skew wedge base composed of railroad ties, 0.75-inch plywood, and rollers

The backfill area was excavated to a depth 6-in. (15.2-cm) below the simulated abutment base out to a distance of 22-ft (6.71-m) from the abutment and then sloped steeply upward to the ground surface. As shown in Figure 3-6, interlocking pre-cast blocks [6-ft x 2-ft x 2-ft (1.83-m x 0.61-m x 0.61-m)] faced with plywood sheeting were placed along both sides of the sand backfill to hold it in place and allow the backfill to fail in a 2D plane strain fashion. Before the backfill placement, two layers of plastic sheeting with grease between them were placed against the plywood sheet facing on each side to reduce friction and better simulate a 2-D geometry typical of a wider abutment wall.

Figure 3-6: Interlocking pre-cast block walls with plywood sheeting

Because the water table was located approximately 5-ft (1.52-m) below the ground surface, it had to be lowered below the base of the 6-ft excavation to ensure it did not interfere with the

backfill placement process. Dewatering was accomplished with the use of pumps placed in sump boxes on the east and west sides of the pile cap. A perforated conduit was placed from the end of each concrete block wall to a sump box to extend the effective area of each pump. The conduit was sloped at 1.5% to allow the water to flow into the sump boxes. Once the backfill was placed, a small generator ran continuously to supply power to the two pumps. The pumps were operated frequently to keep the site dewatered throughout the testing period.

3.4 Instrumentation

3.4.1 Longitudinal Load Instrumentation

There were two hydraulic actuators that applied longitudinal load to the south side of the pile cap. These actuators contained pressure transducers that measured the applied load. The combined load applied by the two actuators was continuously recorded during the loading process. The difference between the applied load with backfill and the load with no backfill was used to calculate the passive resistance of the sand backfill.

3.4.2 Longitudinal Displacement Instrumentation

Eight string potentiometers (linear position sensors) were attached to an independent reference beam located on the south side of the pile cap. Four potentiometers were attached to the four corners of the pile cap with strings attached to measure displacement and rotation of the pile cap. The other four potentiometers were attached to two points on the 28 x 5-ft (8.53 x 1.52-m) I-beam and to the top of the two 4-ft (1.22-m) diameter concrete shafts. As load was applied to the pile cap, the potentiometers measured the movement of the I-beam and concrete shafts holding the

actuators in place as well as the longitudinal movement of the pile cap. This data was used to make adjustments in order to prevent excessive rotation of the pile cap.

3.4.3 Backfill Compressive Strain Instrumentation

Ten string potentiometers were installed near the centerline of the cap on top of the north side of the pile cap, as shown in Figure 3-7. For the 30° skew test, nine of the strings were attached to stakes placed in the backfill between 2 and 18 feet from the pile cap at 2 foot intervals as shown in Figure 3-8. A single string potentiometer was placed on the furthest skew wedge to record any compression that could occur between the wedges and pile cap. Because there was no skew wedge in the 0° skew test, the extra potentiometer was attached to an additional stake placed 20 feet from the pile cap. As load was applied to the pile cap, the potentiometers measured the change in distance between the pile cap and each stake. This data was used to calculate the amount of compressive strain that occurred throughout the backfill. The layout for the 0° skew test was identical minus the skew wedges and with the additional stake 20 feet from the pile cap.

Figure 3-7: String potentiometers mounted on the pile cap

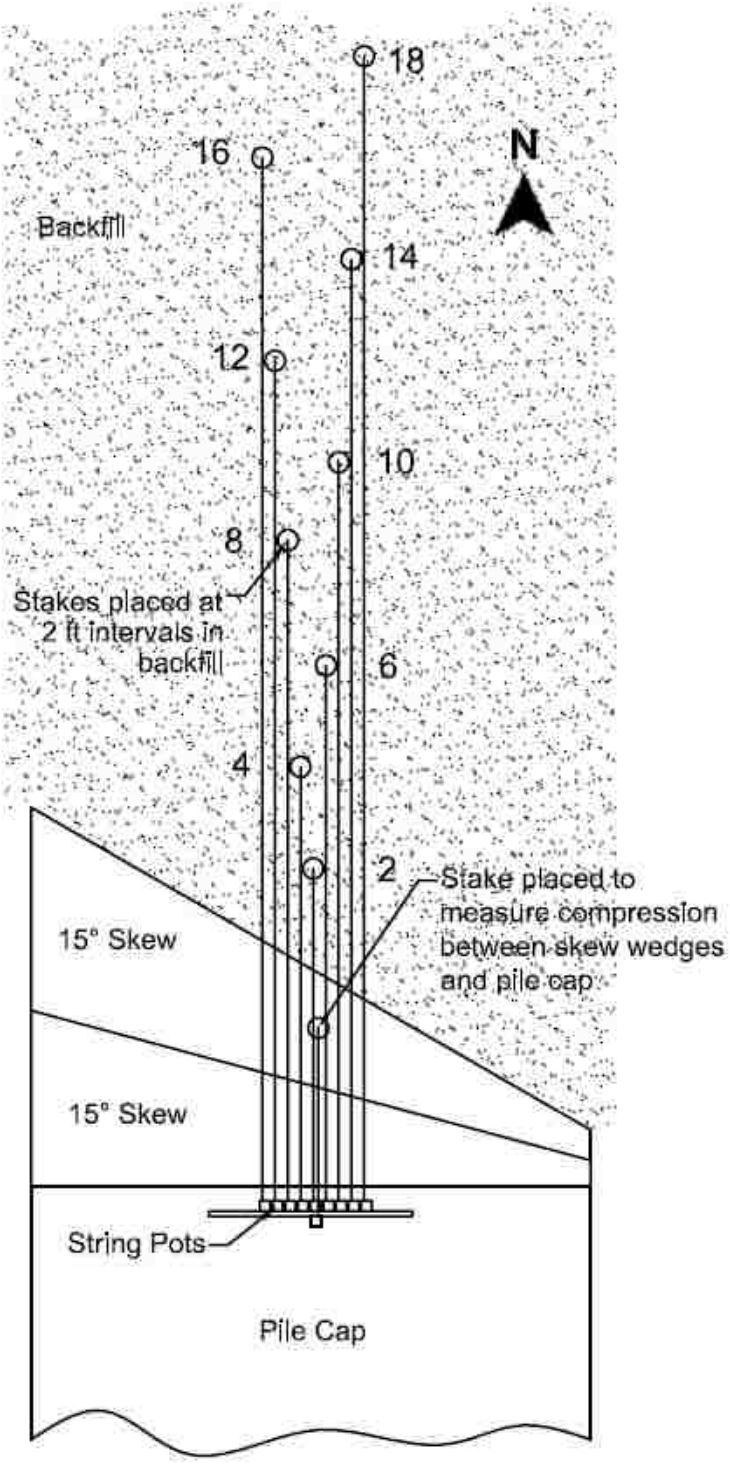

Figure 3-8: String pot layout for compressive strain in backfill (Remund 2017)

3.4.4 Backfill Surface Movement

To measure the heave and lateral displacement of the entire backfill, a grid was painted on the surface of the backfill and monitored before and after loading. A 1-ft by 2-ft grid was painted on the surface of the sand backfill in the first 4 feet from the pile cap, while a 2-ft by 2-ft grid was used from that point to the back of the backfill. The lateral gridlines ran parallel to the abutment skew for both the 0° and 30° skew tests. An elevation rod was held at each intersection point of the painted gridlines and the elevations were measured before and after loading using an auto level with a resolution of 0.001feet (0.012 inch). The difference in these elevations at each grid point were used as the backfill surface heave measurement. A total station was also used to survey the grid points before and after loading to track the 3D movement of each point.

A Digital Image Correlation (DIC) camera system was set up just past the north end of the backfill to monitor the movement of the backfill within 12 feet of the pile cap. A uniform pattern of black diamond-shaped dots was painted onto this portion of the backfill to help the camera locate and track the movement of points on the backfill. Photos of the two DIC cameras mounted on a tripod and the pattern of black dots are shown in Figure 3-9 and Figure 3-10. The cameras were positioned a specified distance from each other and produced overlapping fields of view. This allowed a computer algorithm to track the movement of thousands of points and define the displacement of the ground surface at each stage of loading. Because the cameras were set up to take the images at an angle, some distortion was expected. However, the DIC system uses a complex algorithm to correct back for shift of image due to distortions. ISTRA 4D software was used to analyze the digital images from the camera to determine the movement of the backfill.

Figure 3-9: DIC cameras on tripod just past the north edge of the backfill

Figure 3-10: Uniform pattern of black dots painted on first 12 feet of backfill to aid the DIC camera system in tracking ground surface displacement

3.4.5 Backfill Horizontal Pressure Distribution

Six pressure plates were installed on the face of the 30° skew wedge to measure the backfill pressure against the wedge face relative to the horizontal position of the wedge face. The pressure plates were located approximately 22 inches (0.559 m) up from the base of the wedge, which is one-third of the wall height. They were spaced 21.5 inches (0.546 m) center to center along a horizontal line, with the center of the first plate located 17.75 inches (0.451 m) in from the west edge as shown in the photo in Figure 3-11.

Figure 3-11: Photograph of embedded pressure plates showing horizontal spacing dimensions

The pressure plates were originally mounted to the inside of the concrete form prior to placing the concrete to ensure that the plates were flush with the concrete surface, but were subsequently removed. For this set of tests, the pressure plates were re-attached to the face of the wedge with bolts attached to the conrete; however the fit was not quite as good as in the original

installation. Plumbers putty was applied around the periphery of each cell to fill the small gap between the concrete and the pressure plate and prevent sand and moisture from infiltrating behind the plate. Steel channels [2 x 1 x 1/8 inch (50.8 x 25.4 x 3.2 mm)] channels were used to protect the pressure plate cables from the backfill materials. A photo of the pressure plates just prior to backfill placement is provided in Figure 3-12.

Figure 3-12: Photograph of pressure plates and steel channels on skew wedge

3.5 Geotechnical Backfill Characterization

3.5.1 Backfill Soil and Compaction

Sand backfill was used in both tests. The backfill area was 6 feet deep and the sand was compacted in a series of twelve 6-inch lifts. After each lift was compacted, a nuclear density gage

test was performed in three places to measure the relative compaction and moisture content. The dry unit weight was determined by multiplying the relative compaction by the Proctor maximum density, which was determined to be 112. The moist unit weight was calculated using the dry unit weight and moisture content. There was an error in measuring the moisture content with the nuclear density gage on the first two lifts for the 30° skew test. Consequently, there is no moisture content and moist unit weight data for the 30° skew for the first two lifts. Plots showing moisture content, dry unit weight, moist unit weight, and relative compaction with respect to elevation above the base of the pile cap for both tests are shown in Figure 3-13, Figure 3-14, Figure 3-15, and Figure 3-16, respectively.

As would be expected for backfill placed near the water table, the moisture content, and thus the moist unit weight, increased slightly with depth. The first lift of backfill for the 0° skew test was placed below the natural water table and therefore had a very high moisture content (approximately ranging from 12% to 16%). The average moisture content for all lifts in the 0° and 30° skew tests was 8.1% and 7.5%, respectively. These values are close to the optimal moisture content of 8%. The average relative compaction for all lifts in each test was also very close to the optimal compaction of 95%, with an average of 95.3% for the 0° skew backfill and 94.7% for the 30° skew backfill. The average compaction, moisture content, dry unit weight, and moist unit weight for backfill in the 0° and 30° skew tests is summarized in Table 3-1.

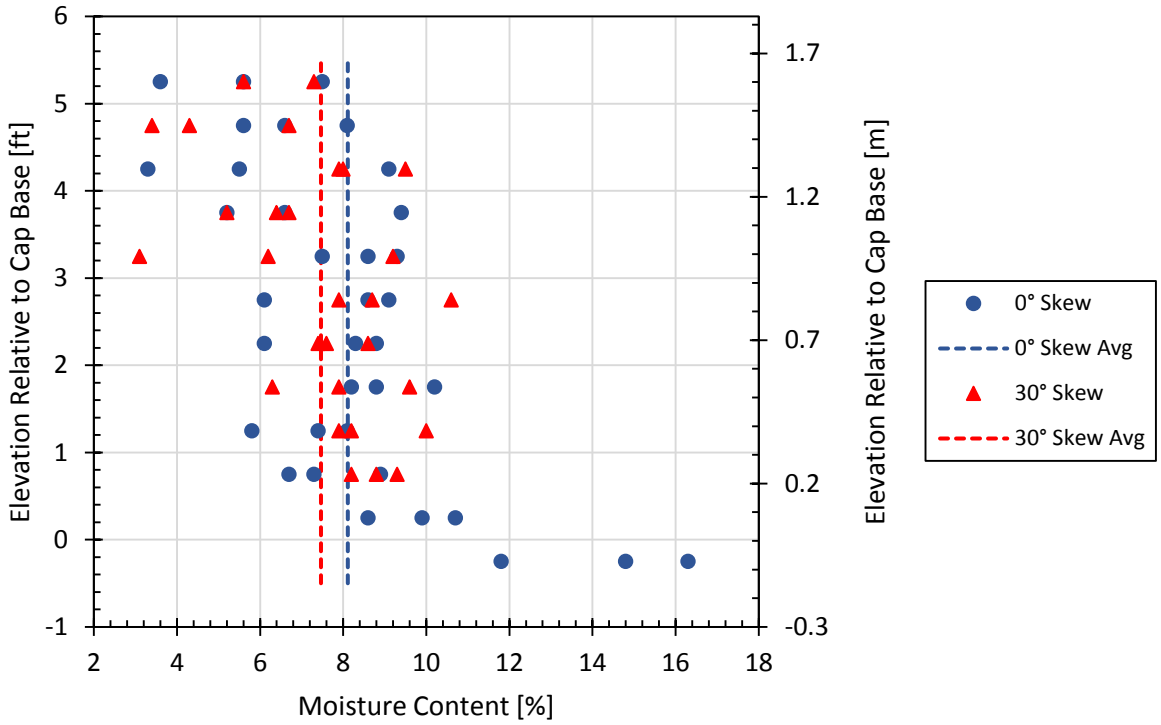

Figure 3-13: Moisture content with respect to depth for all tests

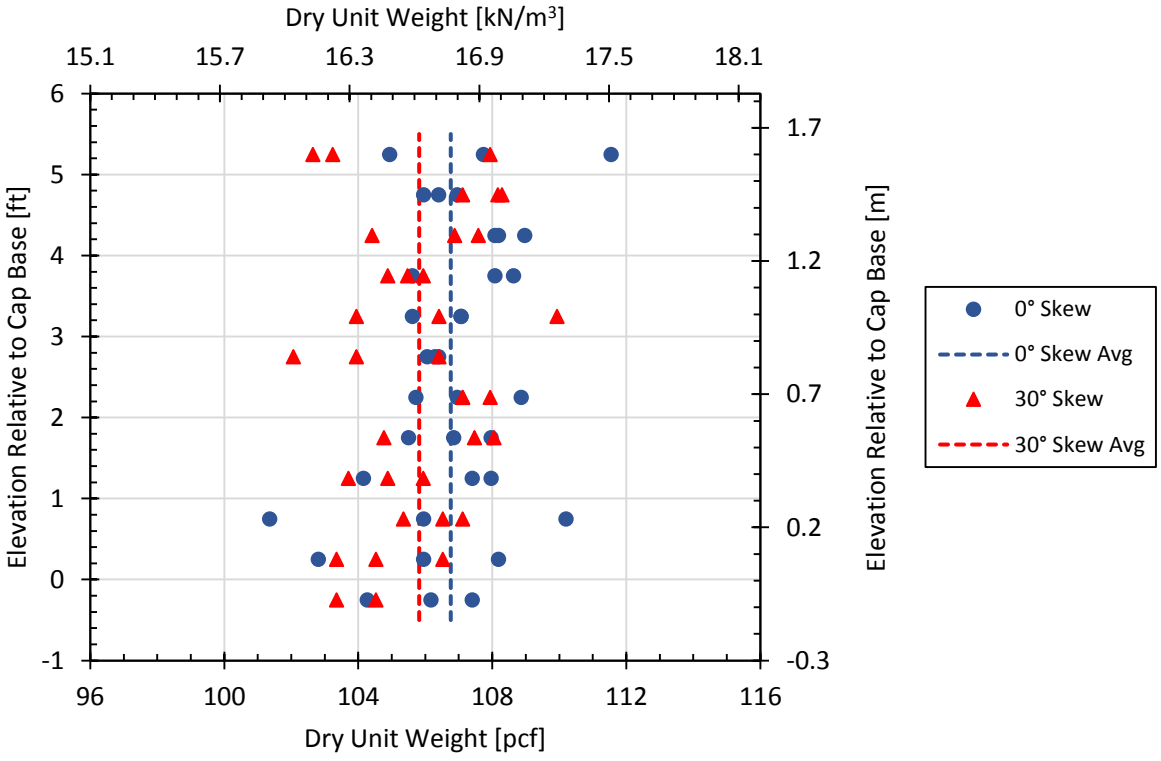

Figure 3-14: Dry unit weight with respect to depth for all tests

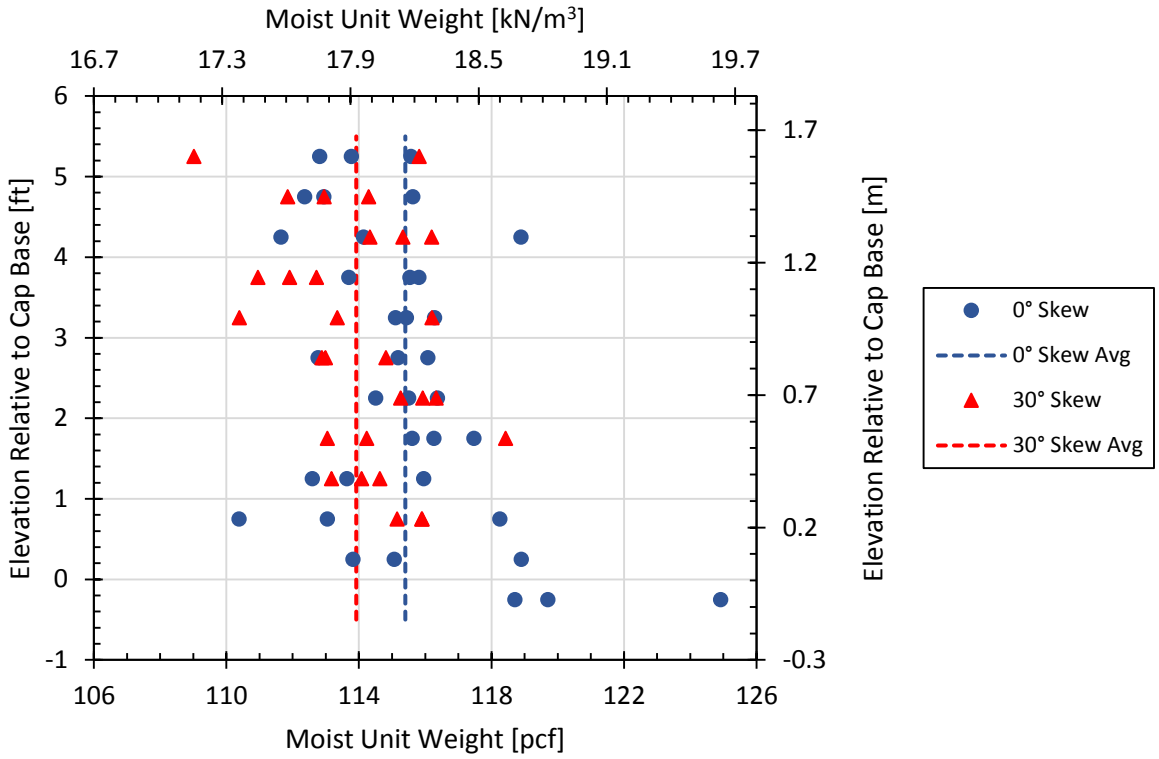

Figure 3-15: Moist unit weight with respect to depth for all tests

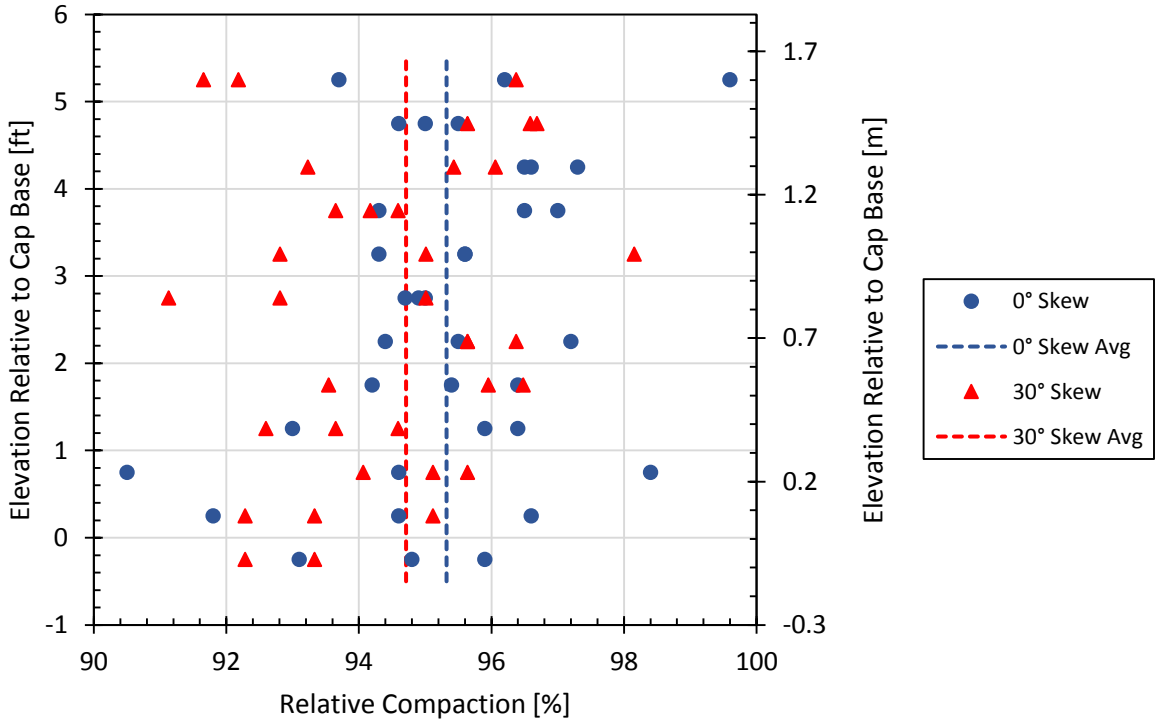

Figure 3-16: Relative compaction with respect to depth for all tests

Table 3-1: Average Compaction, Moisture Content, and Unit Weights for all Lifts

	Relative Compaction (%)	Moisture Content (%)	Dry Unit Weight (pcf)	Moist Unit Weight (pcf)
0° Skew Sand Backfill	95.3	8.1	106.8	115.4
30° Skew Sand Backfill	94.7	7.5	105.8	114.1

3.5.2 Backfill Soil Strength Parameters

The backfill friction angle (φ) and cohesion (c) were determined from in-situ direct shear tests performed on the sand backfill at the test site. The shear box used for the in-situ tests was 1.5-ft by 1.5-ft wide and 8-in. high. A block of sand was formed by scraping sand from the edges of the shear box. The shear was gradually tapped further down the sand block until the sand was flush with the top of the box. The normal force was applied by stacking 16-kg weights on top of the center of the box. Two tests were performed with 24 and 48 weights (384-kg and 768-kg (846.6-lbs and 1693.1-lbs)) stacked to apply normal force. The peak horizontal force at failure in the test with 24 weights was 1053 psf and the peak in the test with 48 weights was 1833 psf, as shown in Figure 3-17.

The shear stress applied by the peak horizontal force at failure was calculated by dividing the force by the surface area of the shear box. The normal stress was calculated by adding the stress applied by the weight of the sand and the 16-kg weights together. Figure 3-18 shows the normal stress plotted against the shear stress for each test. A failure envelope was determined by drawing a line through the two points. The friction angle of the backfill based on the slope of this line was 42.7°. The cohesion of the backfill was about 52 psf, as determined from the intercept of the failure envelope with the shear stress axis.

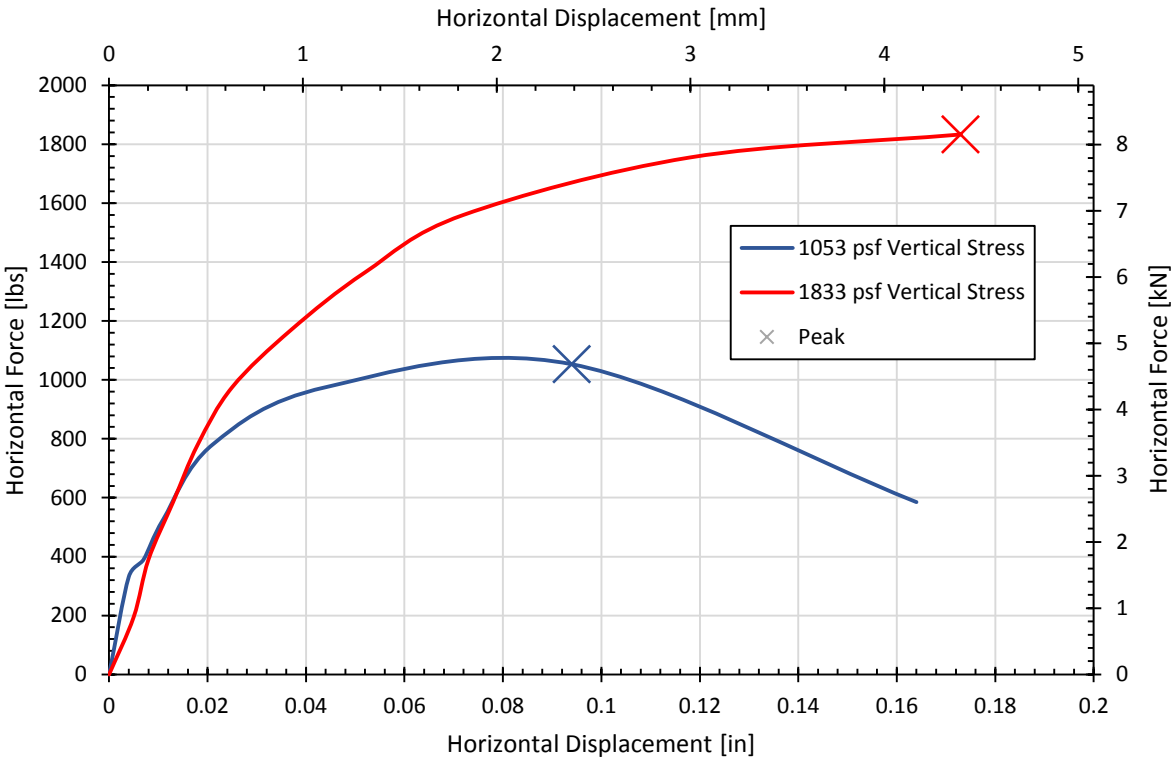

Figure 3-17: Horizontal load-deflection plot for direct shear test

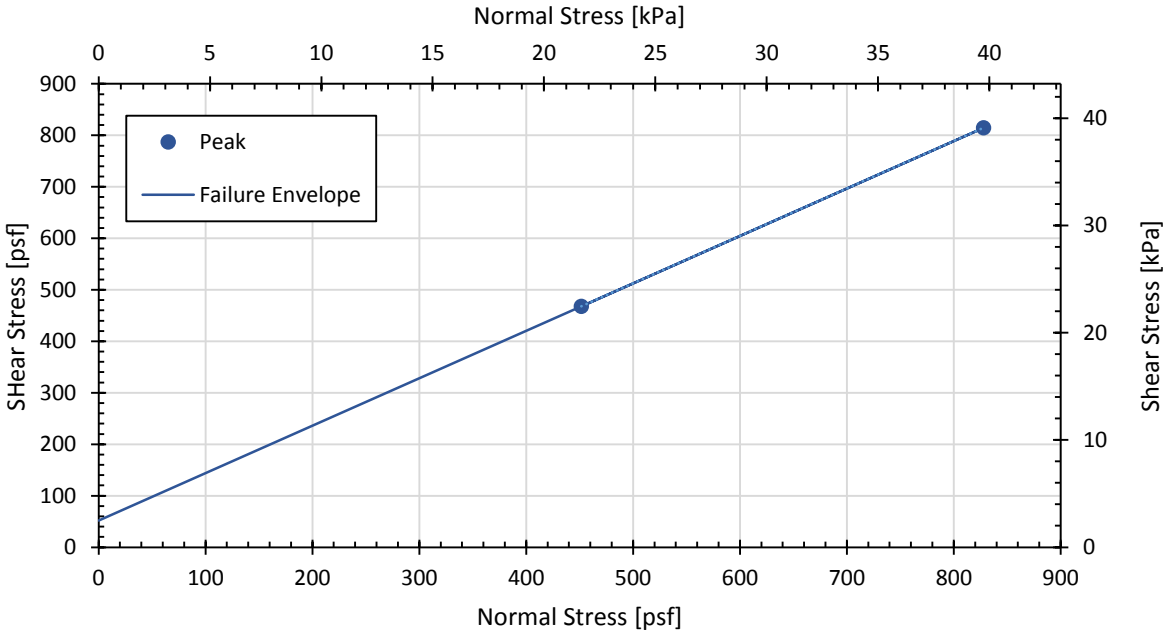

Figure 3-18: Normal stress versus shear stress for direct shear test

3.6 Testing Procedure

Two 600-kip (2669-kN) hydraulic actuators applied the load to displace the concrete pile cap until the sand backfill reached failure. The actuators were calibrated to displace 0.25 in. (6 mm) within 1 minute, hold the position for at least 2 minutes, and then displace another 0.25 in. (6 mm). The position was held between displacements to allow incremental measurements to be taken as well as the reduction in load over time to be observed. This procedure continued until a pile cap displacement of 3.5 to 4.0 inches (8.9 to 10.2 cm) was reached.

To accomplish inclined loading, the actuator on the east (obtuse) side was displaced about 0.25 to 0.33 inches further than the actuator on the west (acute) side, inducing an average rotation angle of about 0.15 degrees. Professor Ian Buckle from the University of Nevada-Reno has determined that bridge superstructure rotation for skewed bridges typically falls within the range of 0.11 to 0.46 degrees (2 to 8 x 10^{-3} radians) (I. Buckle, Univ. of Nevada Reno, personal communication, 2016). Although this is a small rotation, it is sufficient to produce 2.5 to 10 inches of displacement at the end of a bridge with a 100 ft span. In the case of the simulated abutment at the Salt Lake International Airport, the 0.25 to 0.33 inches of extra displacement on the obtuse side provided enough rotation to fit within this range.

4 PASSIVE FORCE TEST RESULTS

4.1 Force-Deflection Relationship

Before the sand backfill was put in place, a baseline test was performed with no backfill present to measure the lateral resistance of the pile cap, piles, skew wedge, etc. The baseline curves in Figure 4-1 and Figure 4-2 represent the lateral resistance before placement of the backfill for the 0° and 30° skew tests. The tests were again performed after the backfill was in place. Total force was measured by adding the loads from the two actuators together. Pile cap deflection was calculated by averaging the displacements measured by four string pots placed on each corner of the back side of the pile cap. The passive force (net force) provided by the backfill was calculated by taking the difference between the total force with and without the sand backfill in place.

During the 30° skew test, the pump supplying hydraulic fluid to the actuators overheated after the pile cap reached a deflection of 2.5 inches causing the system to shut-down. As a result, the total force dropped down to 0 and the pile cap displacement dropped back to about 1.0 inch. After the actuator system was repaired, the pile cap was again incrementally loaded until the pile cap displacement reached 3.75 inches. This can be seen in Figure 4-2 on the plot showing the total force. Figure 4-3 shows the 0° and 30° skew passive force versus deflections curves for pile cap deflections ranging from 0 to 3.75 inches. The part of the net force affected by the unloading and reloading of the pile cap was cut out to show a better representation of the passive force assuming the loading was applied without interruption. As expected, the passive resistance was lower in the

30° skew test than it was for the non-skewed test. A discussion of the skew passive force reduction factor is included in section 4.5.

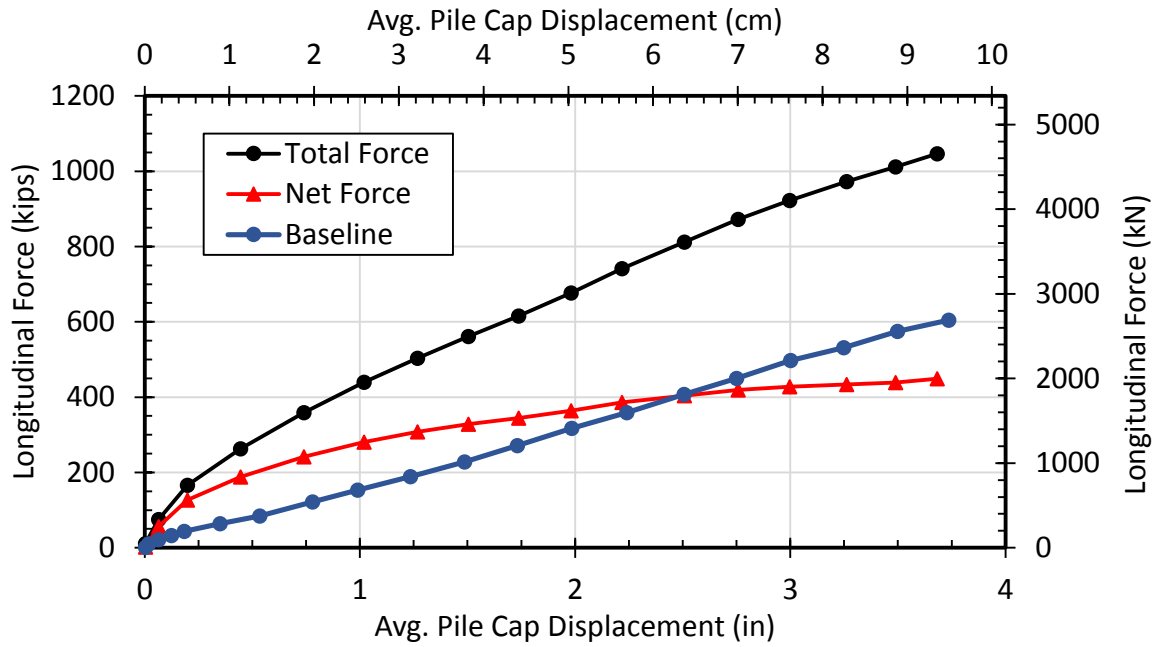

Figure 4-1: Total, baseline, and net force-deflection curves for 0° skewed abutment

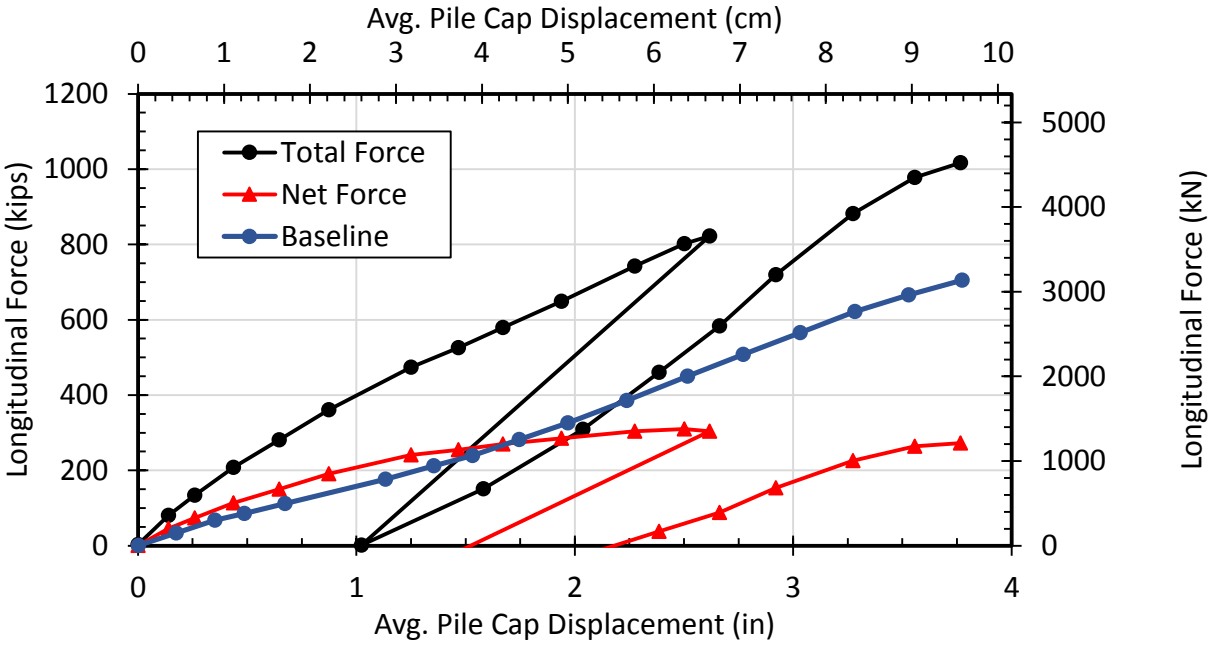

Figure 4-2: Total, baseline, and net force-deflection curves for 30° skewed abutment

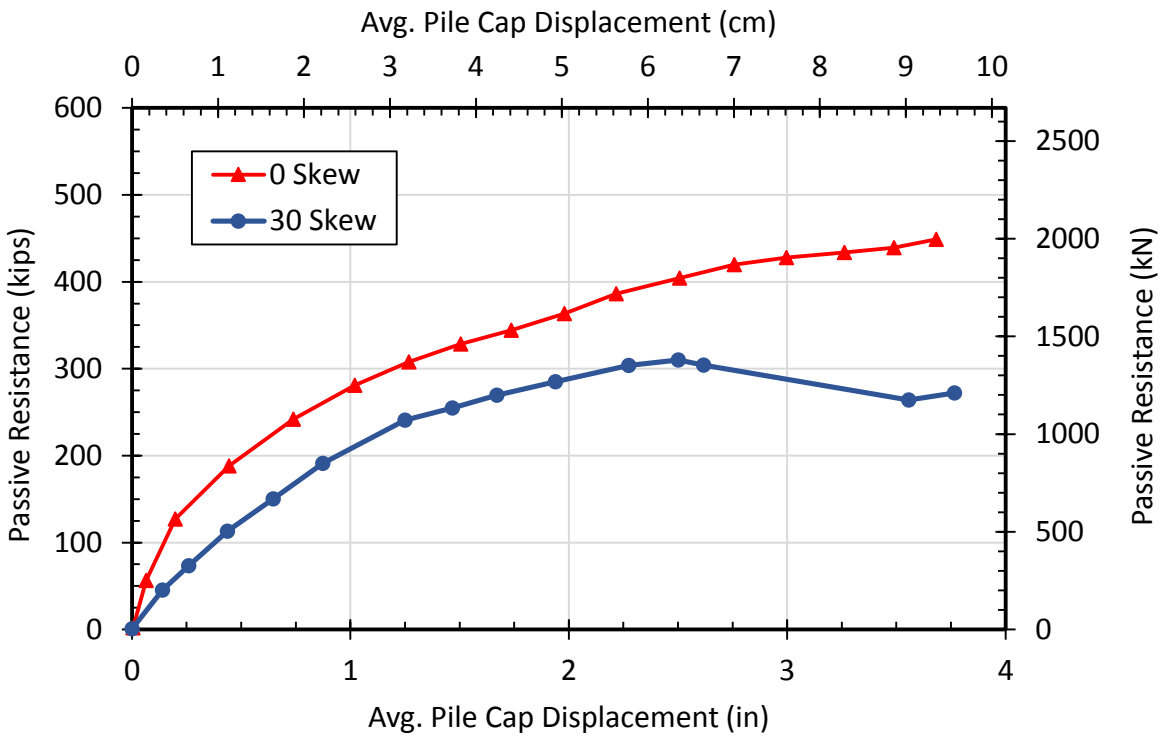

Figure 4-3: Passive resistance-deflection curves for 0° and 30° skewed abutments

4.2 Surface Heave

Before the 0° and 30° skew tests were performed, a 2 ft by 2 ft grid was painted onto the surface of the backfill. Additional gridlines were painted at 1 ft intervals in the first 4 ft behind the pile cap because more movement was expected in that area. Figure 4-4 and Figure 4-5 show the grid line layout for the 0° and 30° skew tests. The grid points were surveyed using an auto level before and after the test was conducted. The surface heave at each grid point was calculated by taking the difference in the elevations before and after the test. These heave values were then entered into ArcMap to create heave contours using the kriging interpolation method. The heave contours and surface cracks for the 0° and 30° tests are presented in Figure 4-6 and Figure 4-7. The same heave interval was used for both figures so they can be compared against each other.

Figure 4-4: Photo of the grid line layout for the 0° skew test

Figure 4-5: Photo of the grid line layout for the 30° skew test

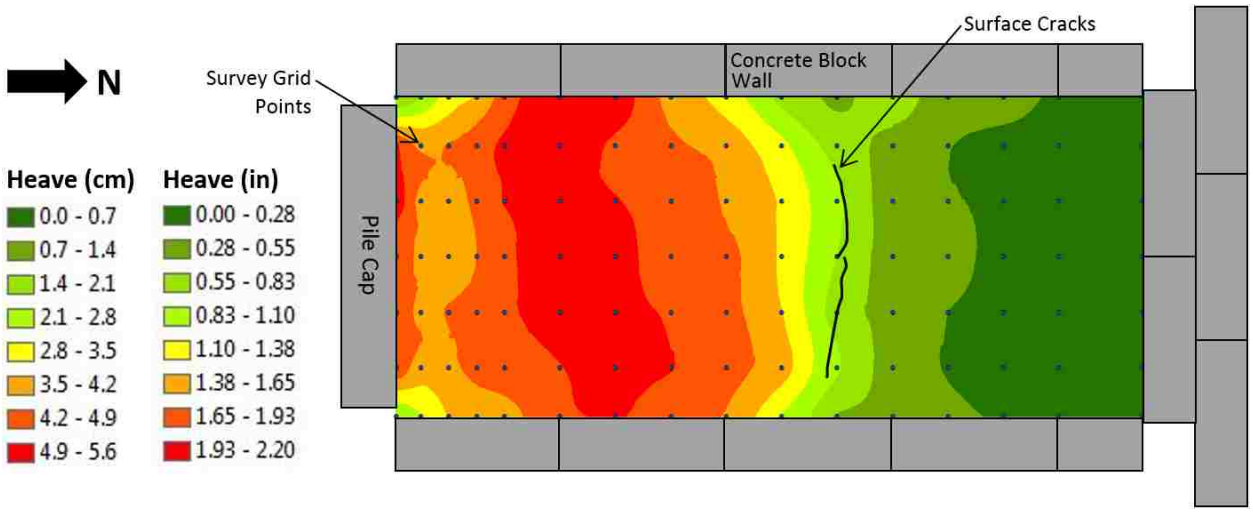

Figure 4-6: Heave contours and surface cracks for non-skewed abutment

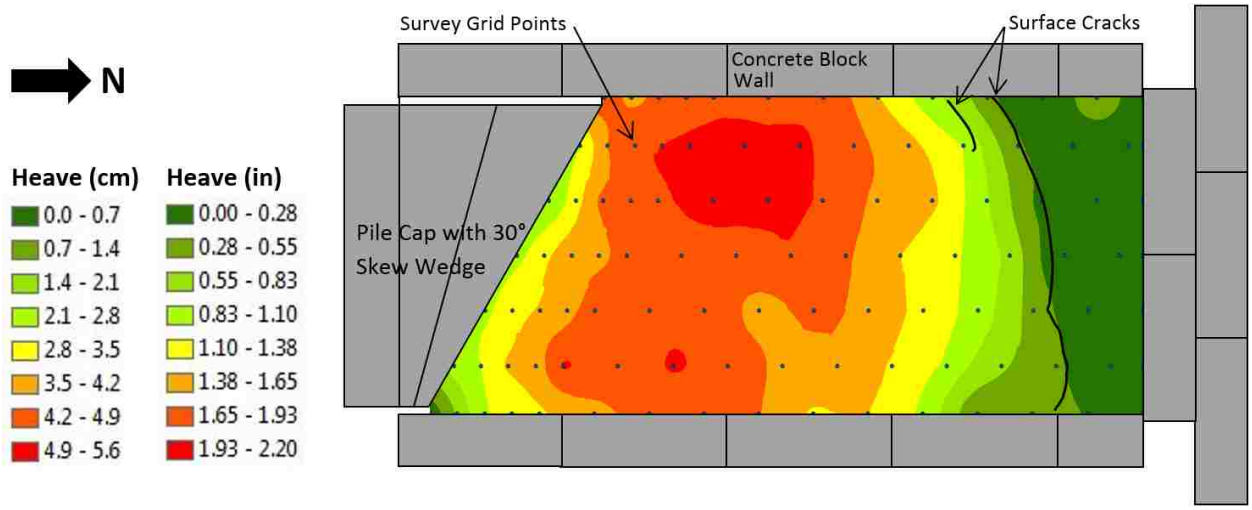

Figure 4-7: Heave contours and surface cracks for 30° skewed abutment

For the non-skewed test, the plot in Figure 4-6 shows that the greatest heave (1.93-2.20 inches) occurred in the area between 4 and 8 feet away from the pile cap. This represents a heave of about 3% relative to the wall height of 66 inches. The surface cracks, where the failure surface daylighted, formed almost uniformly across the backfill about 16 feet away from the pile cap.

Heave in this vicinity was about 0.75 inches. There was not very much heave near the corners of the pile cap relative to the rest of the backfill across the face of the cap.

For the 30° skew test, the plot in Figure 4-7 shows that the greatest heave occurred mainly on the acute side of the skew wedge in the area between 4 and 8 feet away from the wedge. This is interesting because there was more force being applied to the pile cap on the obtuse side due to the inclined loading applied in this test. Nevertheless, the maximum heave was still about 3% of the wall height, similar to that for the 0° skew. The surface cracks did, however, appear to be affected by the inclined loading. The crack surfaced at approximately 22 feet away from the obtuse side of the skew wedge and only 14 feet away from the acute side.

4.3 Failure Surface

To determine the location of the internal failure surface, a 2-inch (51 mm) diameter hand auger was used to core holes in the backfill which were then filled and compacted with red-dyed sand. The sand columns were located at a transverse offset of 2 feet on either side of the longitudinal centerline at distances of 2, 4, 6, 10, and 14 feet from the pile cap. After the final pile cap displacement was completed, a trench was excavated adjacent to the red soil columns. The offset in the column indicates the location of the failure surface, as shown in Figure 4-8. The depths of the offsets in each soil column were used to plot the failure surfaces for the 0° and 30° skew tests, as shown in Figure 4-9 and Figure 4-10.

Figure 4-8: Offset in red sand columns showing the failure surface of the 30° skew test

In the non-skewed test, there was an upper and lower failure surface on both the east and west sides of the backfill as shown in Figure 4-9. The upper west failure surface began at the top of the wall and intersected with the lower surface between 7 and 8 feet from the pile cap while the upper east failure surface only extended four feet from the pile cap. The lower east failure surface was slightly deeper than the lower west failure surface until they both reached the surface about 16 feet from the pile cap. Heave was largely constrained within the boundaries of the failure zone. The failure surfaces day-lighted where the heave was approximately 0.83 inches (2.10 cm) and decreasing.

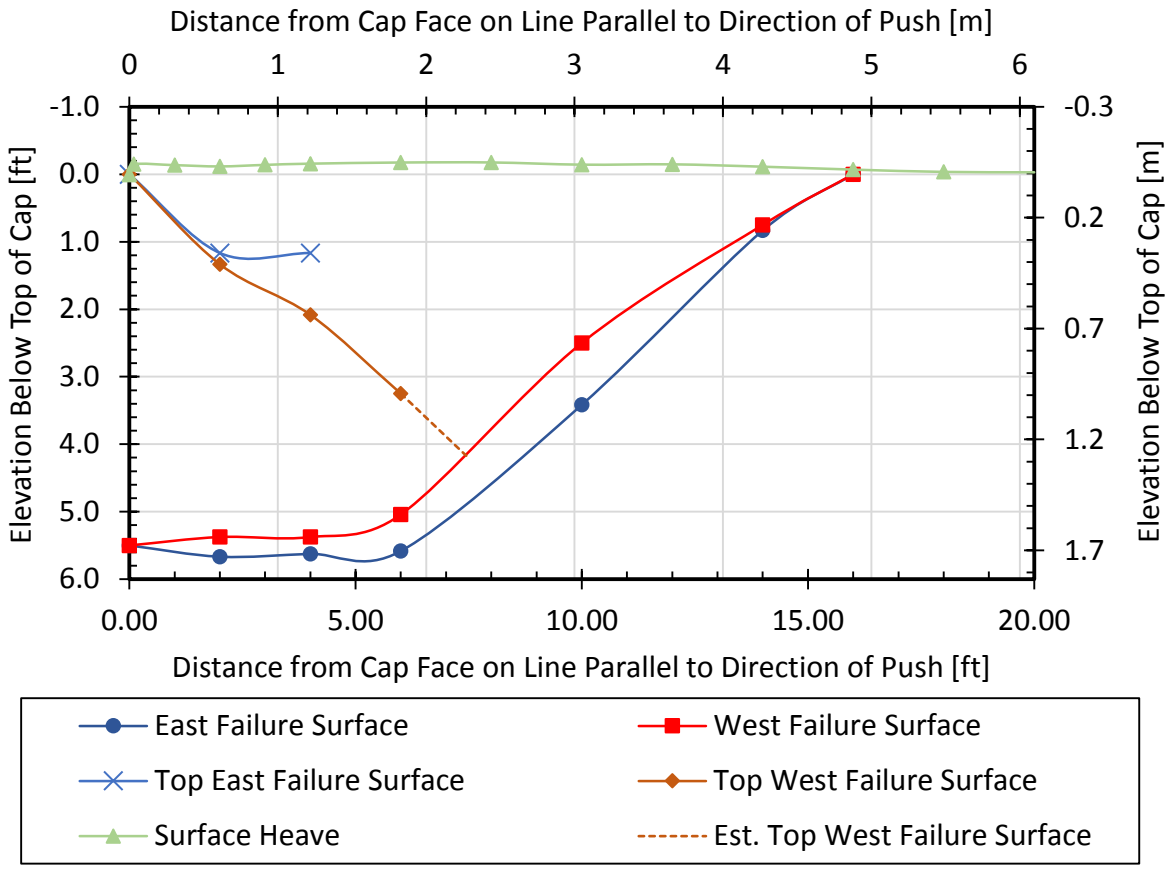

Figure 4-9: Backfill shear failure surface for non-skewed abutment

In the 30° skew test, there were no upper failure surfaces observed. The east failure surface extended much further past the pile cap than the west failure surface did. This is presumed to be a result of the inclined loading where the actuator on the east side of the pile cap was pushed further than the west side. The east failure plane surfaced at 21 feet from the pile cap where there was no heave while the west failure plane surfaced at 17 feet in 0.07 inches (0.18 cm) of heave.

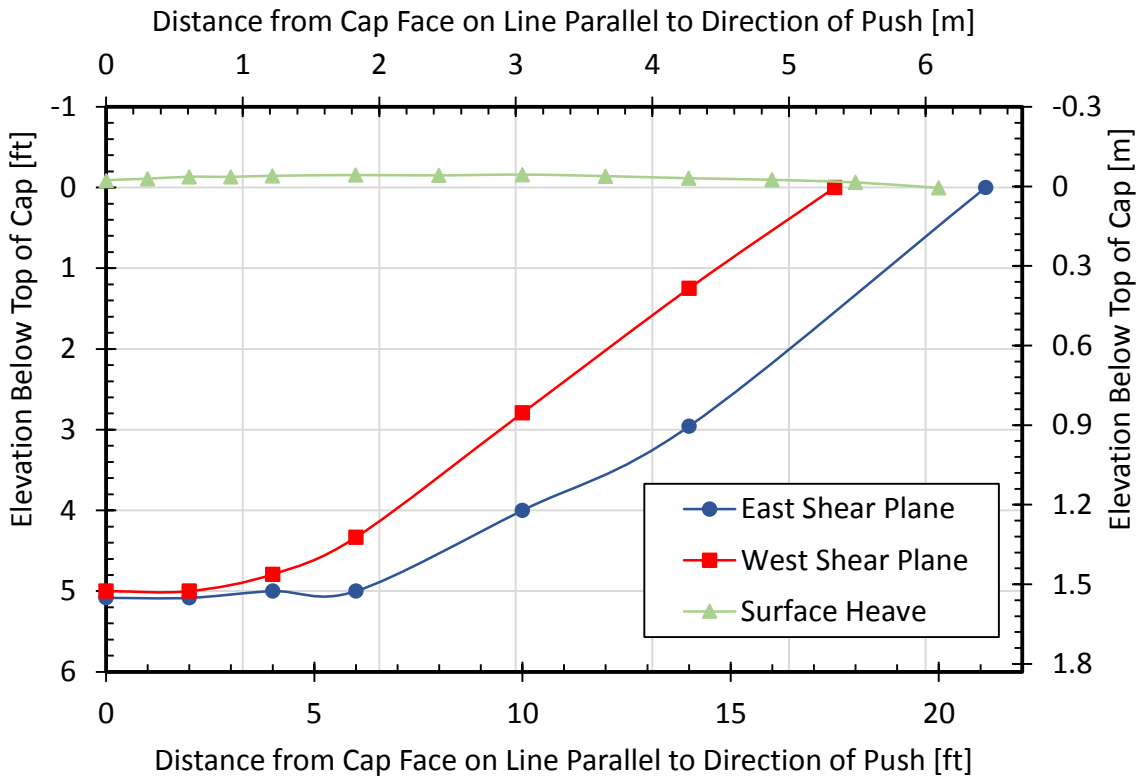

Figure 4-10: Backfill shear failure surface for 30° skewed abutment

4.4 Lateral Surface Movement

Lateral ground surface movement was tracked by surveying the difference in grid points before loading and after the last load increment was applied (see detailed explanation in Section 3.4.4). The vector plots shown in Figure 4-11 and Figure 4-12 were produced by scaling the surveyed movements by a factor of four to make the displacements easier to see. These surface movements were divided into interval classes represented by the different colors shown in the figures. Ground displacement decreases rapidly from the cap face and is typically less than one inch behind the failure zone at 16 ft. For the 0º skew test, the displacement vectors are typically aligned with the direction of loading; however, displacements are somewhat higher on the east side as a result of the inclined loading. In contrast, for the 30º skew test, the displacement vectors

tend to have an eastward alignment, somewhat normal to the face of the skewed abutment wall. However, the walls adjacent to the backfill prevent excessive eastward movement.

Contour plots of displacement are also shown in Figure 4-13 and Figure 4-14 using the surveyed movements of the grid points. The surface cracks are also shown on these contour plots to provide a frame of reference. Although these plots are based on the same data as those in Figure 4-11 and Figure 4-12 they provide a somewhat different perspective from the vector plots. For example, in Figure 4-13 the plot clearly shows that the maximum ground displacement is higher on the east (obtuse) corner of the wall. In contrast, the contour plot in Figure 4-14 shows a much more complicated pattern. The ground displacements appear to be greater in the soil on the east side near the wall face; however, further back from the wall the displacements become greater on the west (acute) side of the wall. This could help explain why the failure surface occurs closer to the wall on the west side than on the east side in this test.

The DIC camera system data was also used to track lateral surface movement of the backfill within 12 feet of the pile cap and the results are shown in Figure 4-15 and Figure 4-16 for the 0° and 30° skew tests, respectively. The displacement data determined using the DIC camera very closely matched that which was determined by surveying the grid points. This was the first time that reliable results were produced from DIC camera data in a large-scale bridge abutment test. Additional processing will be undertaken with this data set to understand better the strain distribution in the backfill soil.

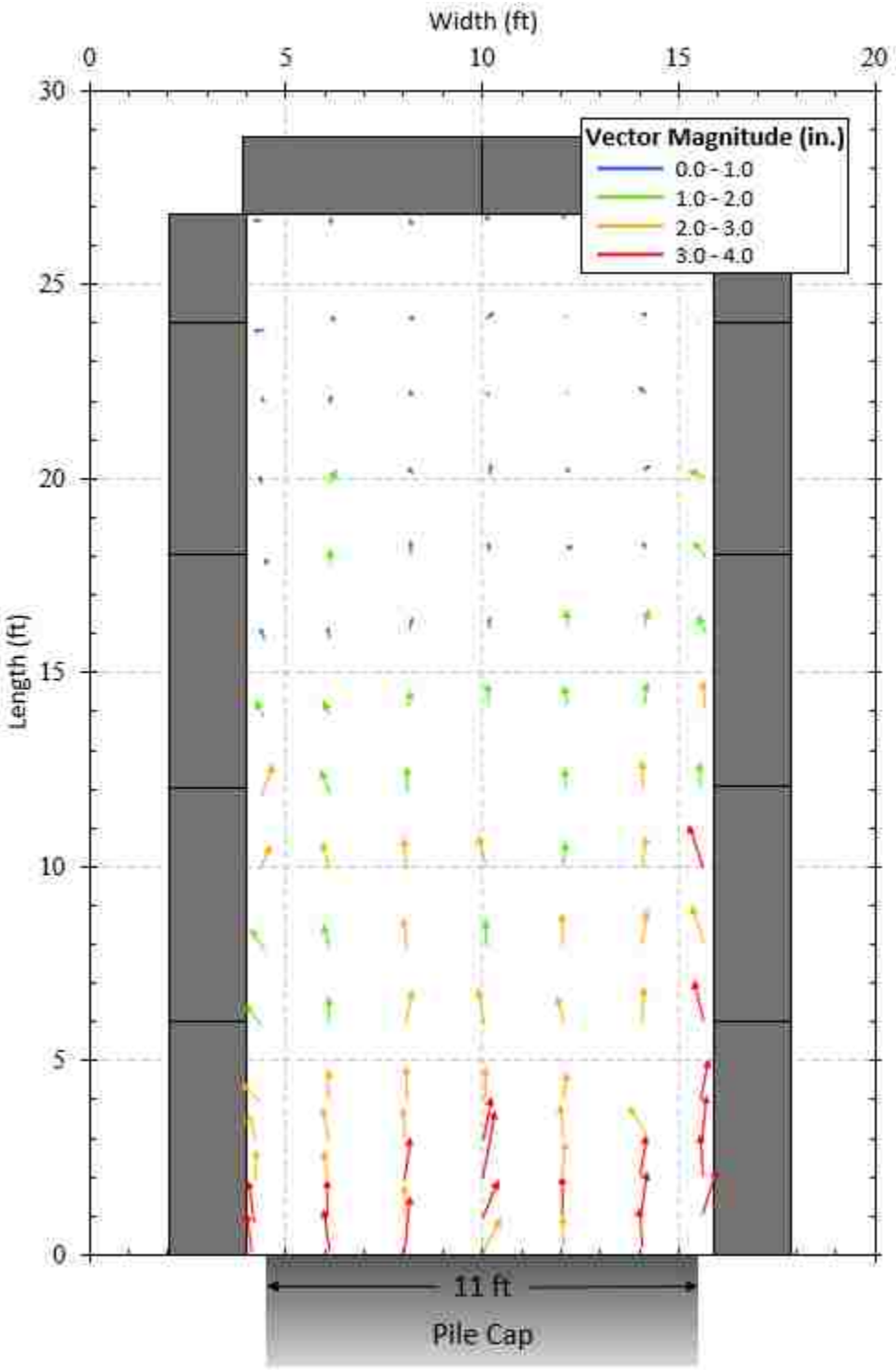

Figure 4-11: Vector plot of 0° skew test lateral surface movement (4:1 scaling)

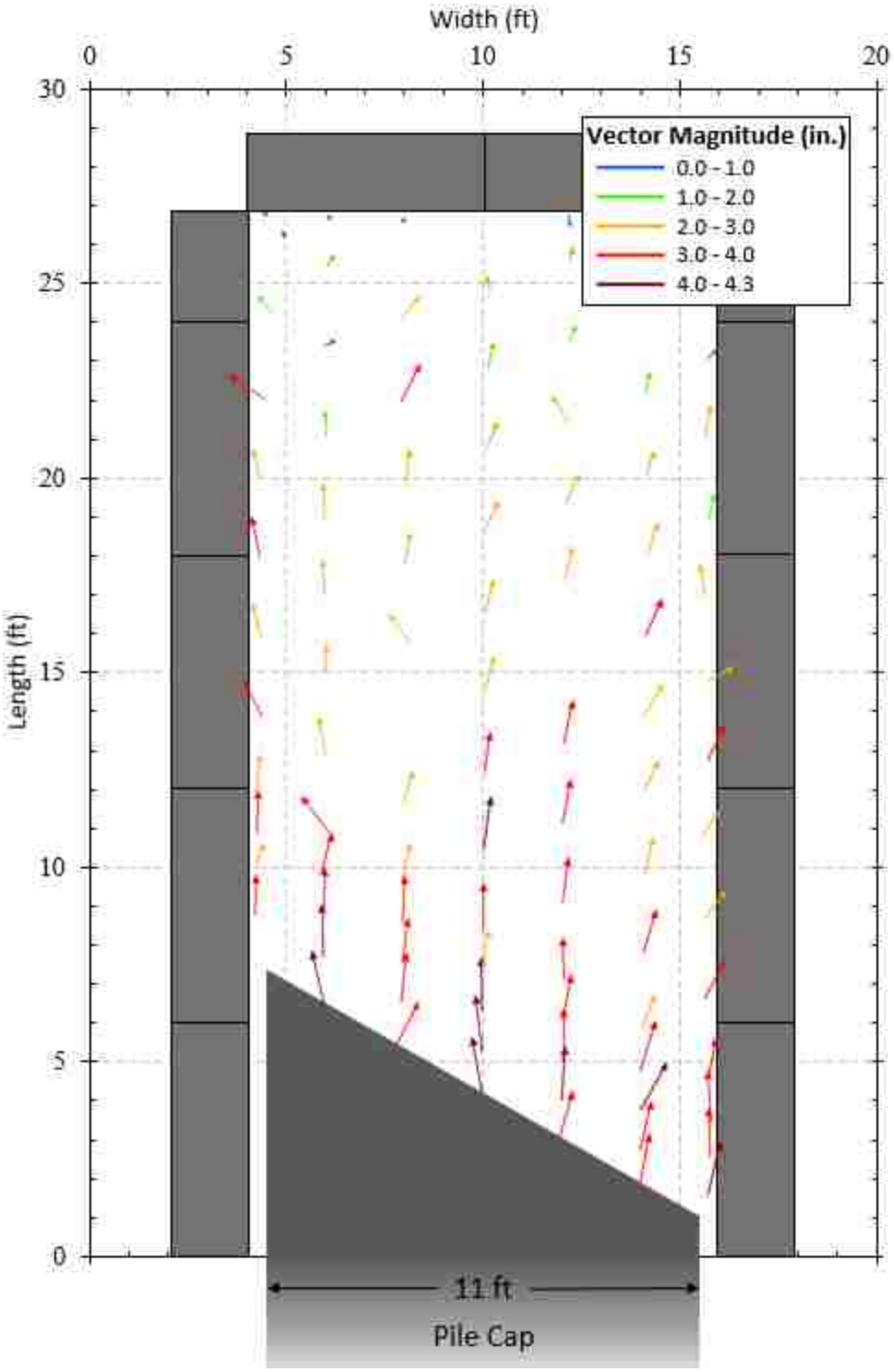

Figure 4-12: Vector plot of 30° skew test lateral surface movement (4:1 scaling)

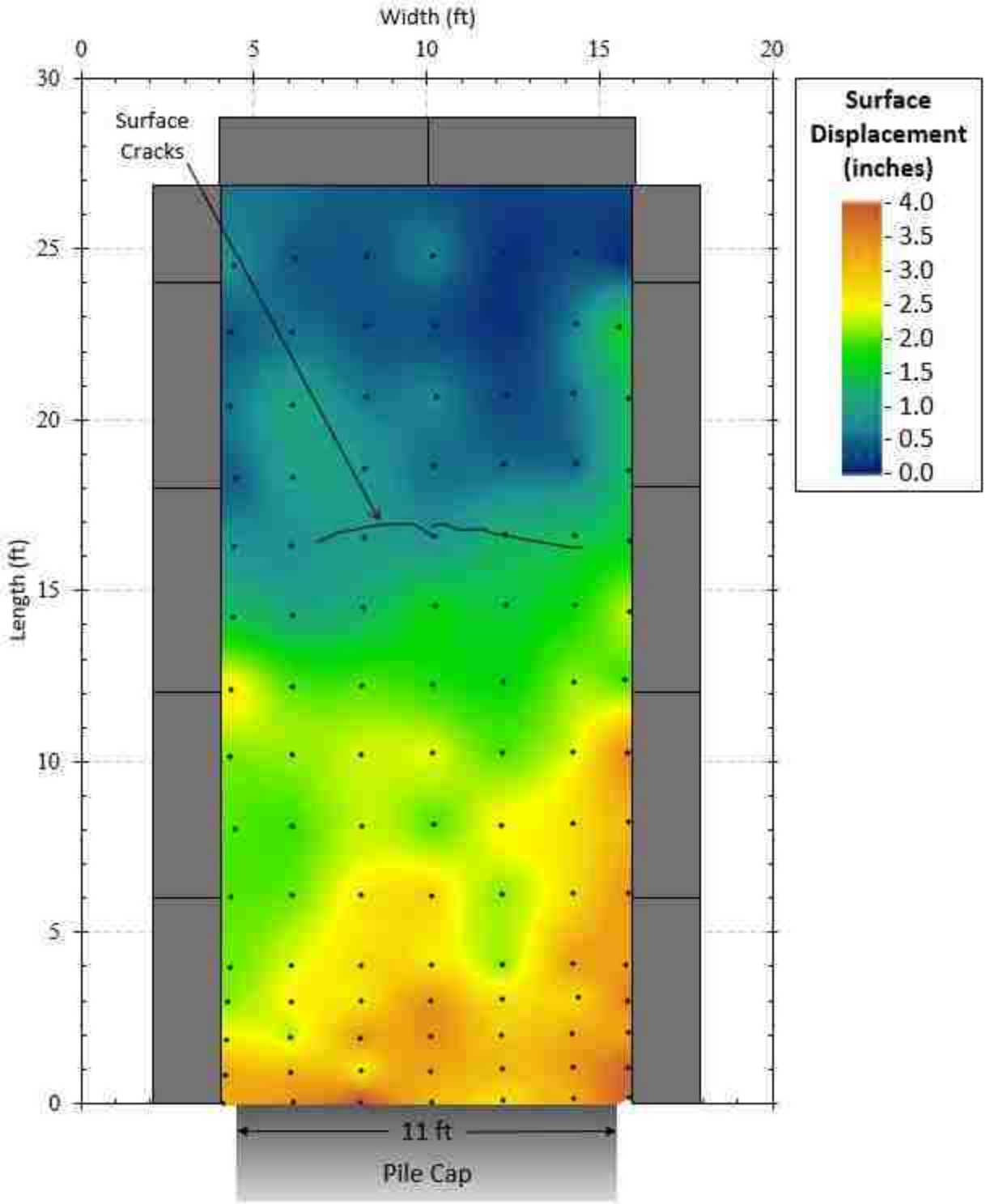

Figure 4-13: Contour plot of 0° skew test lateral surface movement

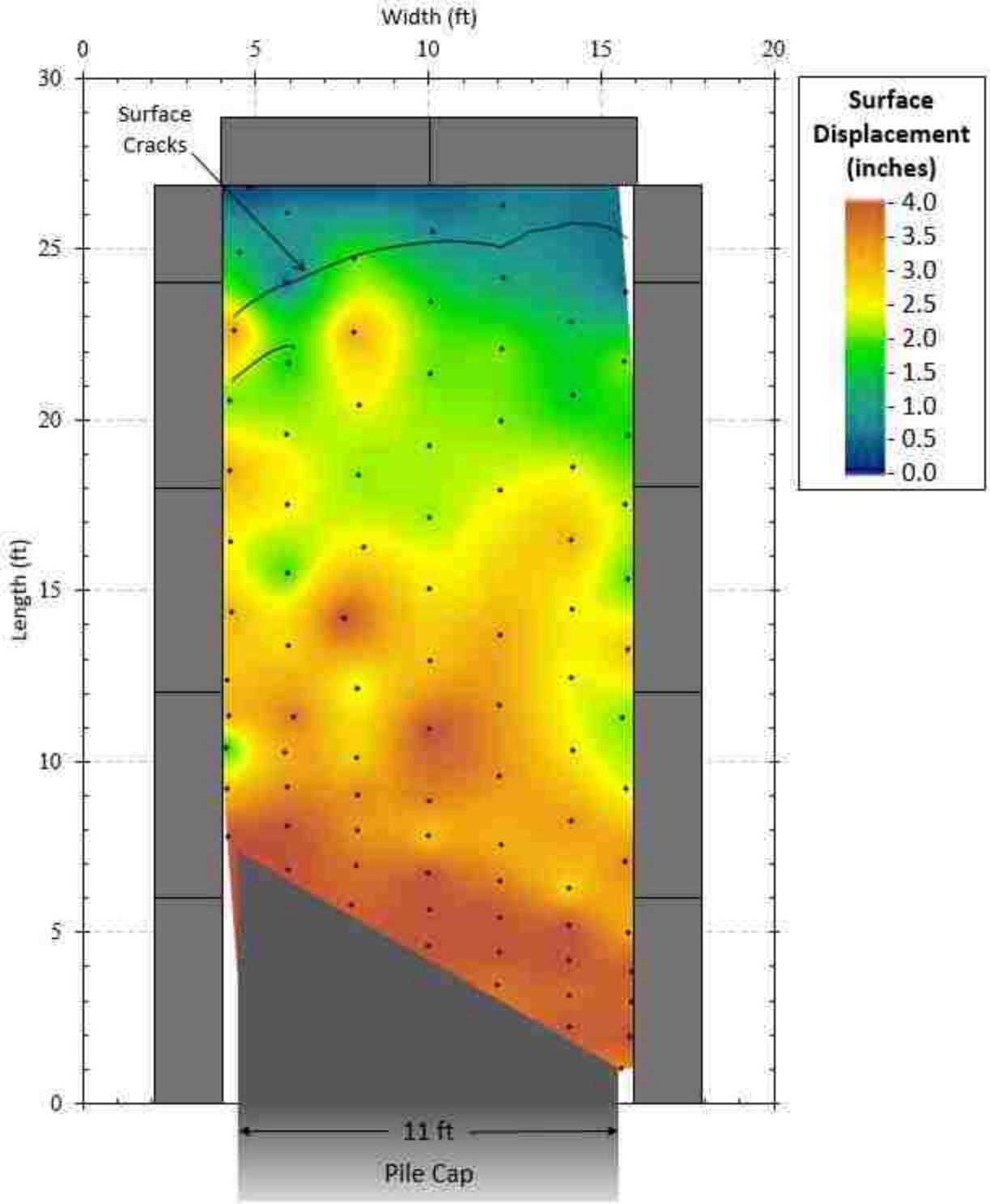

Figure 4-14: Contour plot of 30° skew test lateral surface movement

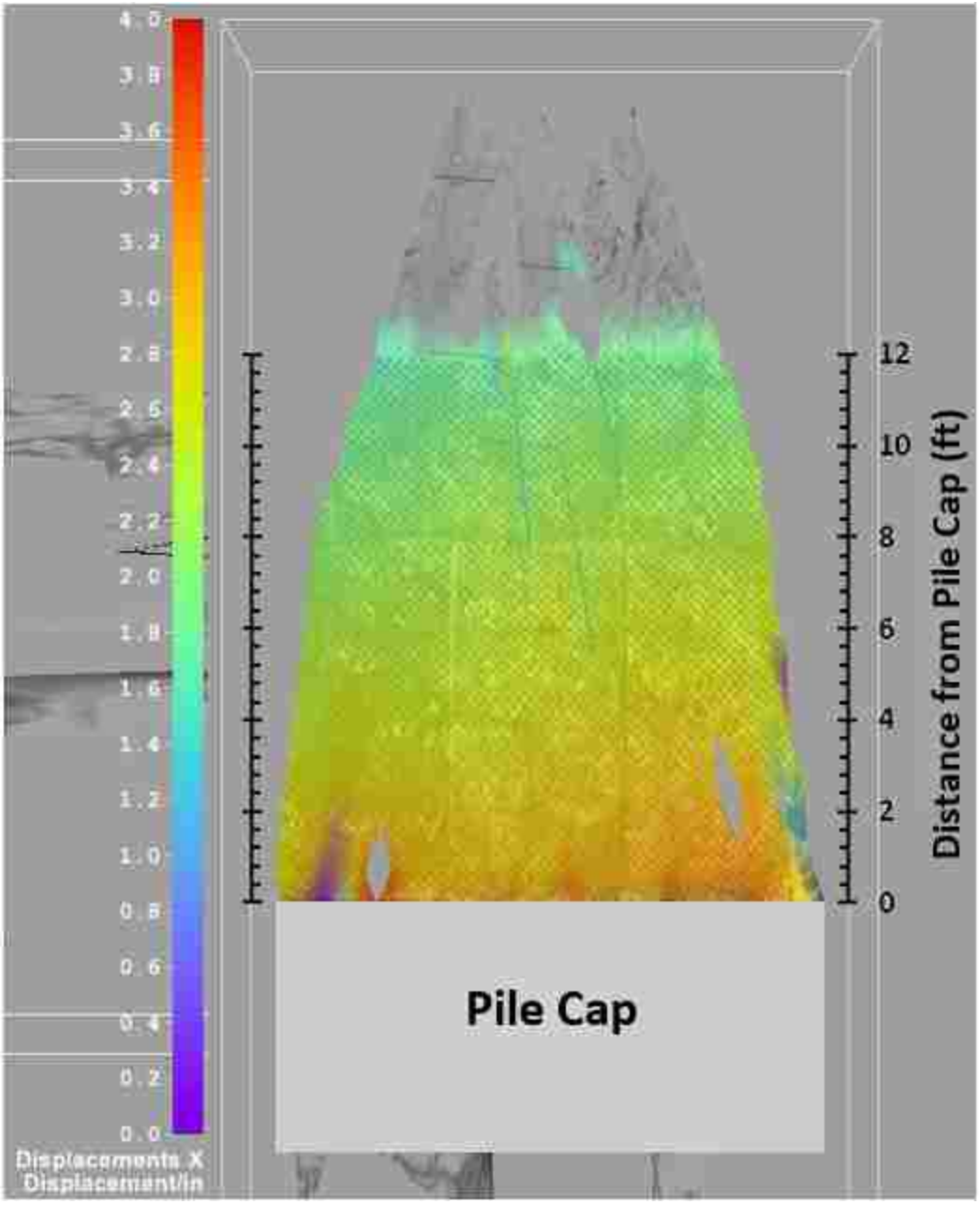

Figure 4-15: Contour plot of longituinal displacement for the 0° skew test produced using DIC camera data

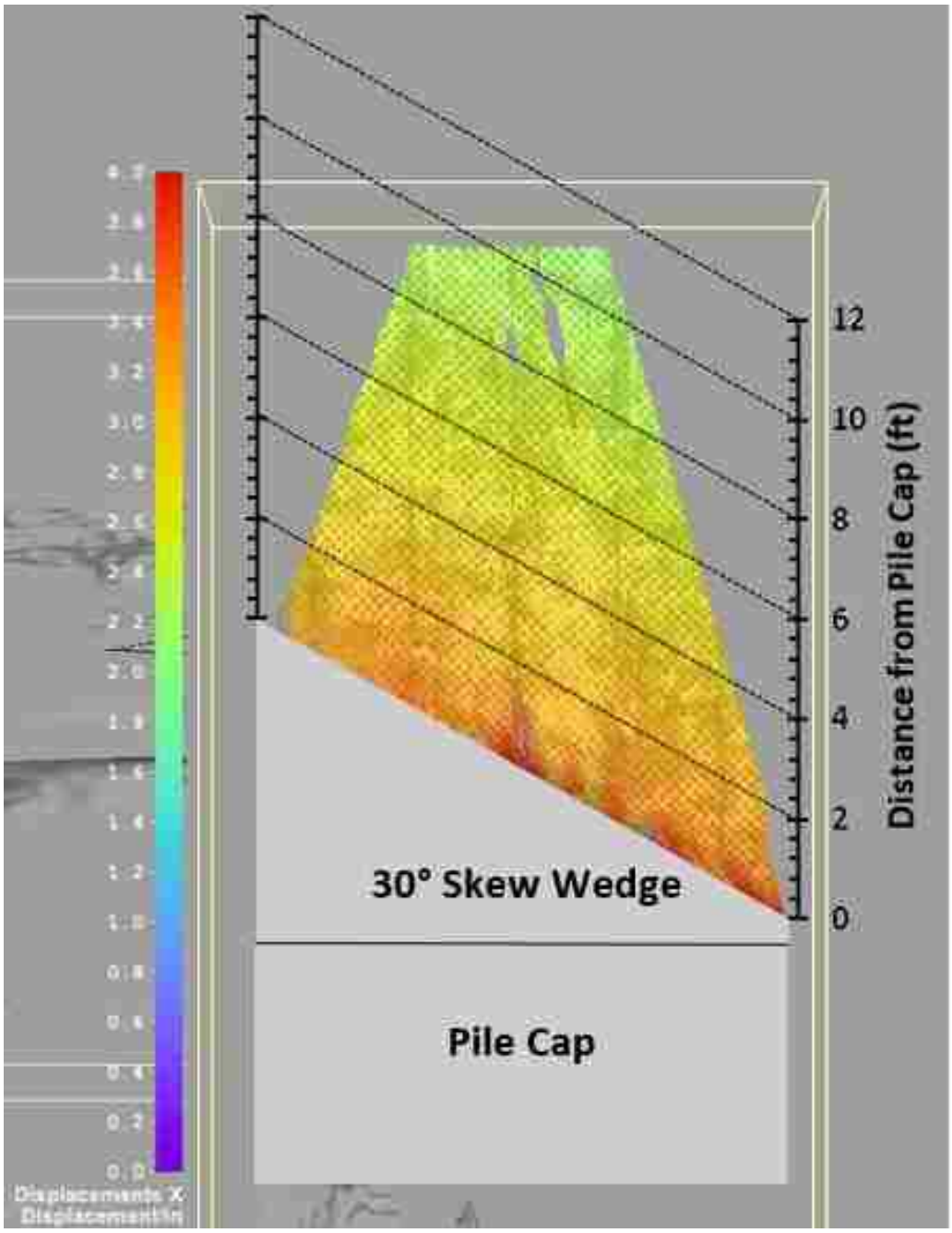

Figure 4-16: Contour plot of longitudinal displacement for the 30° skew test produced using DIC camera data

4.5 Skew Reduction Factor and Effective Skew

The skew reduction factor for the 30° skew was computed by dividing the peak passive force for the skewed abutment (310 kips) by the peak passive force for the non-skewed abutment (448 kips). This resulted in a reduction factor of 0.69. This reduction factor is plotted in Figure 4-17 along with the reduction curve proposed by Shamsabadi and Rollins (2014) and the laboratory tests and numerical model results by Shamsabadi et al. (2006).

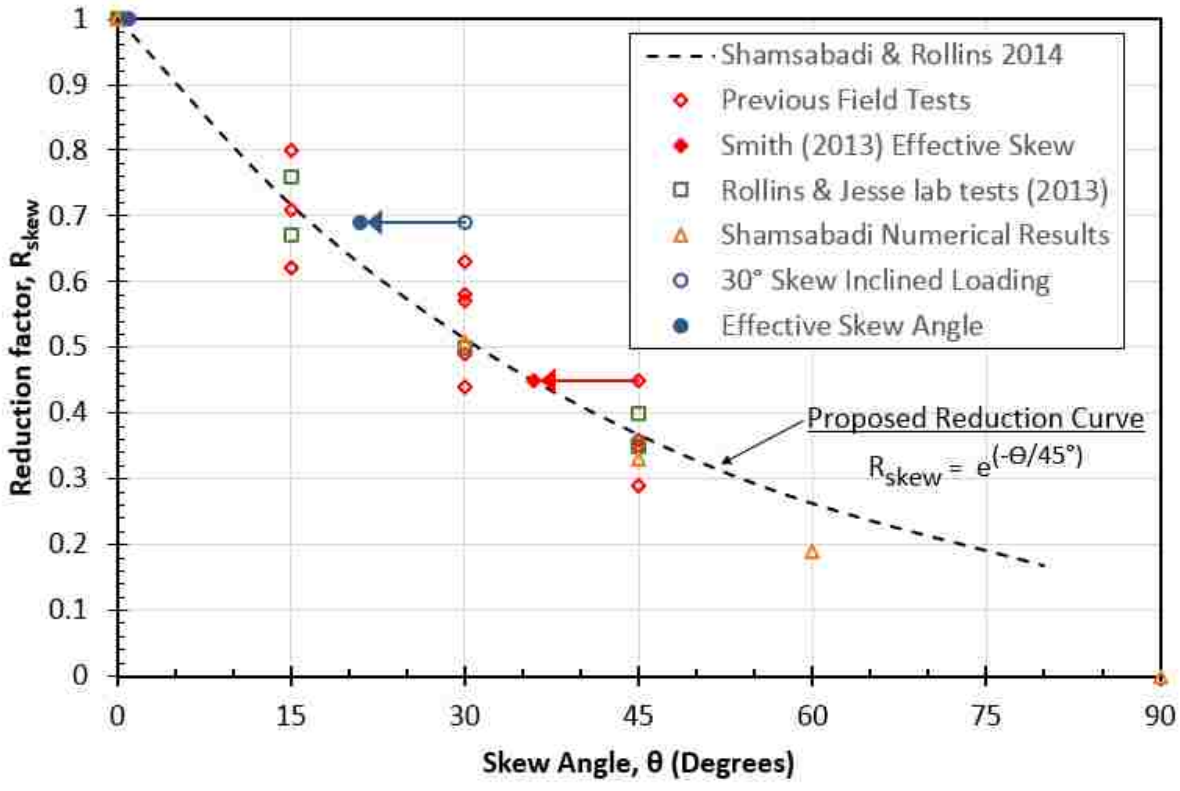

Figure 4-17: Reduction factor, R_{skew} (passive force for a given skew angle normalized to non-skewed passive force) plotted versus skew angle based on previous BYU field tests (Franke 2013; Marsh 2013; Palmer 2013; Smith 2014; Frederickson 2015), lab tests (Rollins and Jessee 2012), numerical analyses (Shamsabadi et al. 2006), and results from field tests in this test

The reduction factor of 0.69 for a skew angle of 30° falls significantly above the proposed reduction curve. This may be because the 30° skew angle provided by the skew wedge is being

effectively reduced during the loading process. A review of the surface heave plots suggests that a wedge of sand between the obtuse corner of the skew wedge and the side wall does not heave nearly as much as the adjacent sand. It appears that this sand wedge gets caught in a pocket resulting from the normal force against the skewed abutment wall and friction on the side wall. Thus, the sand wedge effectively moves with the skewed wall and reduces the 30° skew to an effective skew angle of about 21°. This effective skew is illustrated on the heave plot in Figure 4-18.

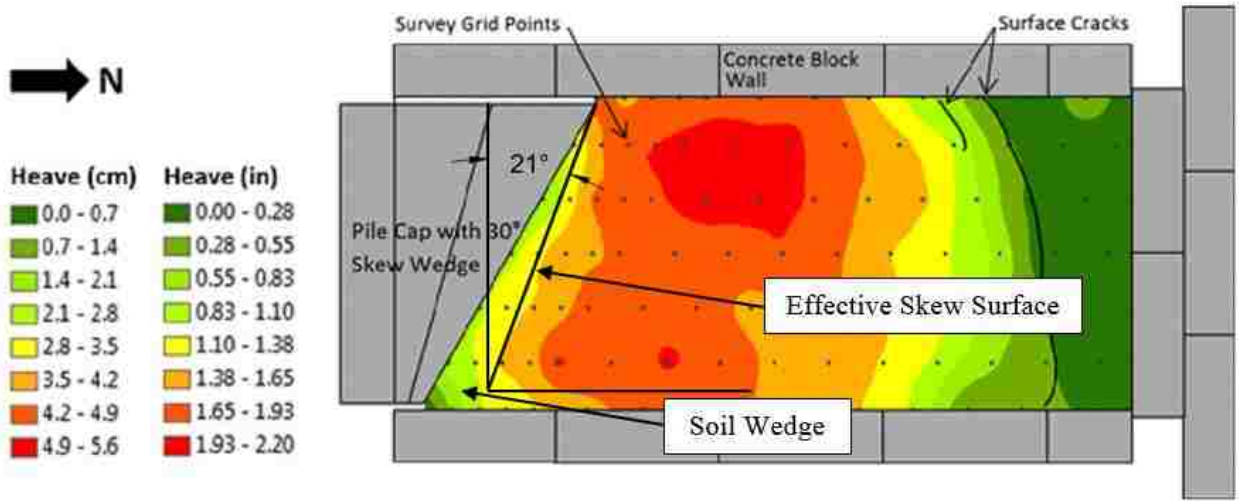

Figure 4-18: Effective skew angle as estimated from surface heave data

The effective skew angle can also be observed on the surface displacement contour plot as shown in Figure 4-19. Just two feet from the skew wedge, the effective skew angle appears to decrease from 30° to about 21°. From these observations, it can be postulated that the effective skew in this test was 21°. The blue arrow and solid blue circle on Figure 4-17 illustrate this effective skew angle and show that the measured reduction factor of 0.69 agrees reasonably well with the proposed reduction curve and previous field tests when shifted over to an effective skew angle of 21°. This validates the claim that the proposed skew reduction curve remains accurate during inclined loading situations.

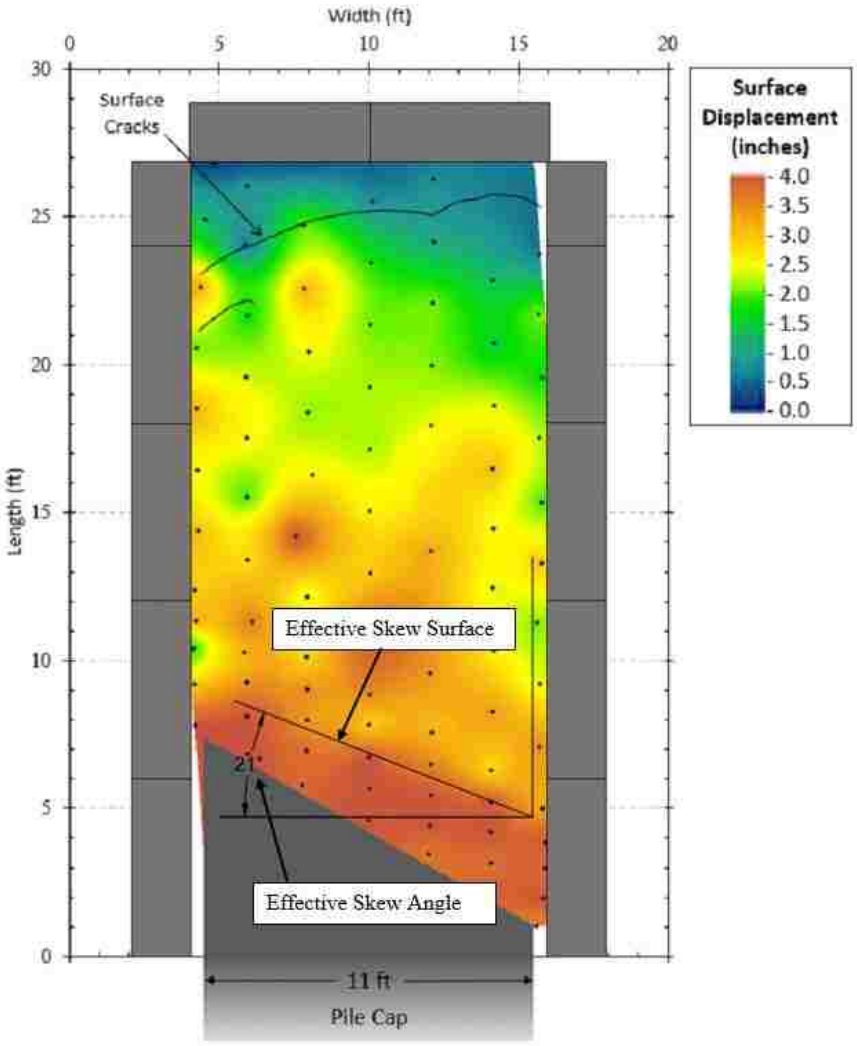

Figure 4-19: Effective skew angle as estimated from surface displacement data

A similar plane strain test including longitudinal wing walls performed by Smith (2013) had a comparable effective reduction in skew angle (refer to Figure 2-14). The red arrow and solid red diamond on Figure 4-17 show that Smith's measured skew reduction factor also moves closer to the proposed reduction curve when effective skew angle is considered. Three-dimensional finite element analyses conducted by Snow (2018) indicate that the overall effect of the "trapped soil wedge" becomes progressively smaller as the width of the abutment wall increases. Therefore, for

more typical two- or four-lane abutments (24 to 48 ft wide) the abnormally high reduction factor observed for the 11 ft wide abutment would not be observed.

4.6 Surface Displacement and Strain

Figure 4-20 and Figure 4-21 show the backfill displacement measured as a function of distance from the backwall based on string pot measurements for a series of wall displacements for the 0° and 30° skew tests, respectively. In both tests, the greatest amount of compression occurred within the two feet of backfill closest to the pile cap. From that point onward, there is a fairly consistent, but gradual decrease in backfill displacement from 2 to 18 feet away from the pile cap as load is transferred from the wall to the backfill soil. In the 0° skew test at a pile cap displacement of 3.68 inches, the rapid decrease in displacement that occurs between 14 and 16 feet from the pile cap is a result of the backfill failure plane surfacing about 16 feet from the pile cap.

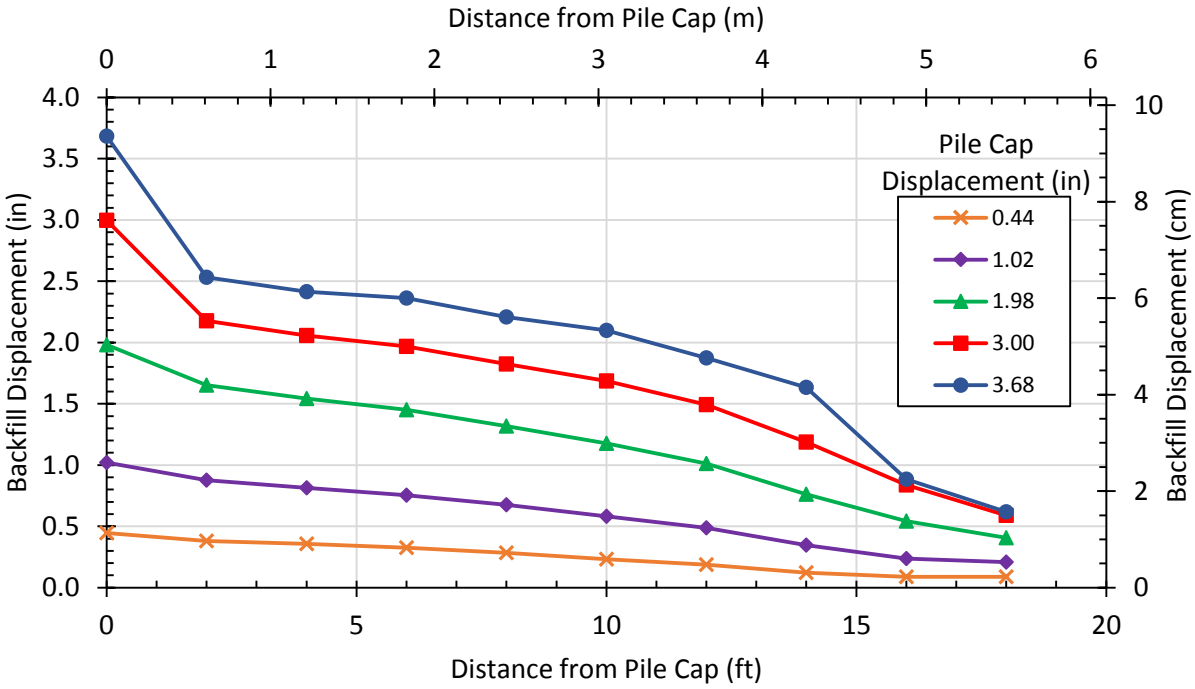

Figure 4-20: 0° Skew backfill displacement at selected pile cap displacement intervals

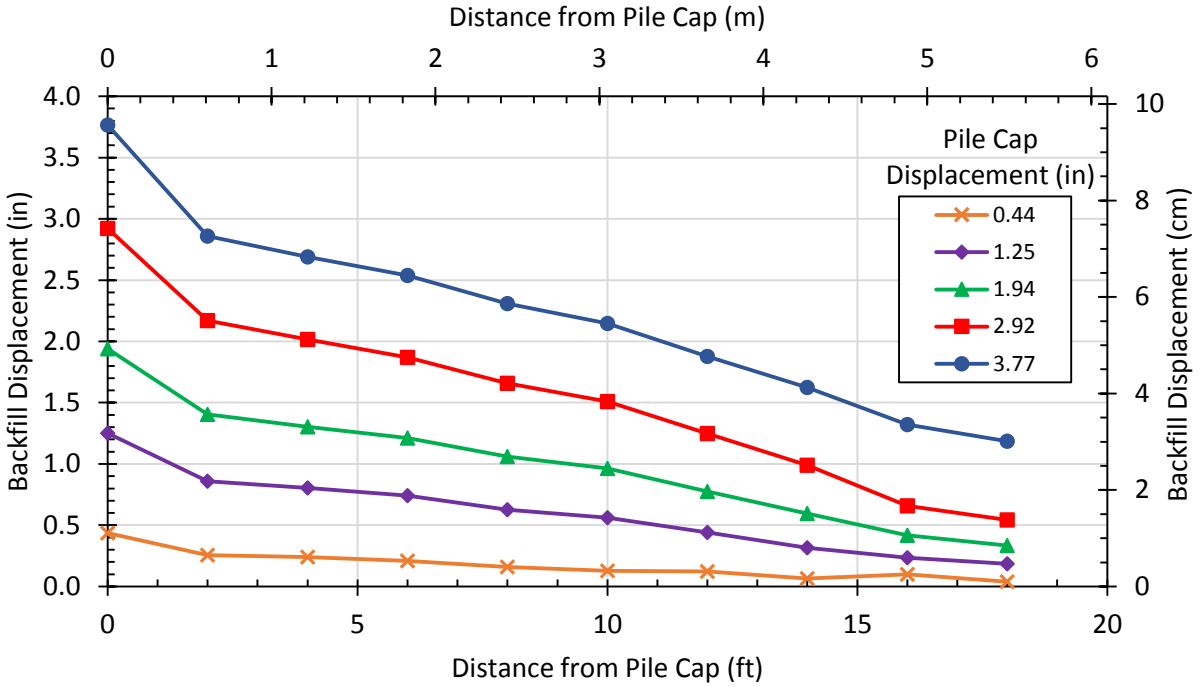

Figure 4-21: 30° Skew backfill displacement at selected pile cap displacement intervals

The compressive soil strain was computed based on the maximum backfill displacements for the 0° and 30° skew tests. Figure 4-22 shows the compressive soil strain versus distance from the center of the pile cap for both tests. The strain was computed by taking the difference in displacements measured by adjacent string pots and dividing by the initial distance between them. This strain was plotted as a constant value between each pair of adjacent string pots. For example, the difference in displacement between the string pots located at 2 feet and 4 feet from the pile cap was divided by the initial 2 foot distance between the string pots to obtain strain. This strain was then plotted as a constant value from 2 feet to 4 feet from the pile cap. The compressive strain was greatest in the first two feet of backfill for both tests, with 4.8% strain in the 0° skew test and 3.8% strain in the 30° skew test. The compressive strain then drops to a relatively low and constant value of around 0.7 to 1.0%. The spike in computed strain between 14 and 16 feet from the pile cap in

the 0° skew test is likely a result of the shear failure plane reaching the surface at about 16 feet which leads to increased compressive strain as the failure wedge collides with the soil behind it.

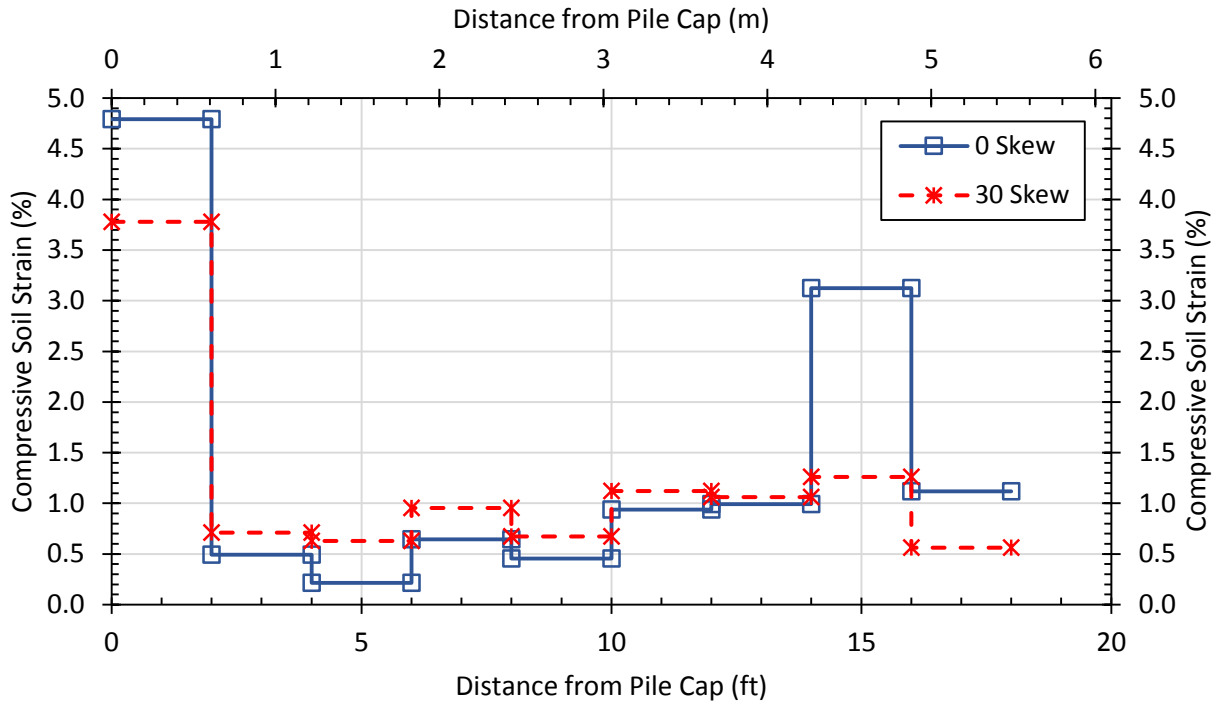

Figure 4-22: Compressive backfill strain for 30° and 0° skew tests

4.7 Pile Cap Rotation

The rotation of the pile cap during the 30° skew inclined loading test was tracked by surveying the northeast and northwest corners of the pile cap at each deflection interval during the loading. The rotation angle was computed by calculating the inverse tangent of the difference in northing coordinates divided by the difference in easting coordinates between the two front corners of the pile cap. Figure 4-23 shows the pile cap rotation angle at each deflection interval between 0 and 3.75 inches. The maximum rotation angle was 0.31° and it occurred when the pile cap was loaded to a deflection of 2.5 inches. At every other deflection interval between 0.25 and 3.75 inches, the rotation angle fluctuated between 0.11° and 0.22°. For the purpose of comparison, the

rotation of the pile cap was also tracked during the 0° skew test without inclined loading, as shown in Figure 4-24. The rotation angle remained very close to zero throughout the loading, fluctuating between -0.07° and 0.05° of rotation with the exception of one outlier where the rotation angle reached -0.12°.

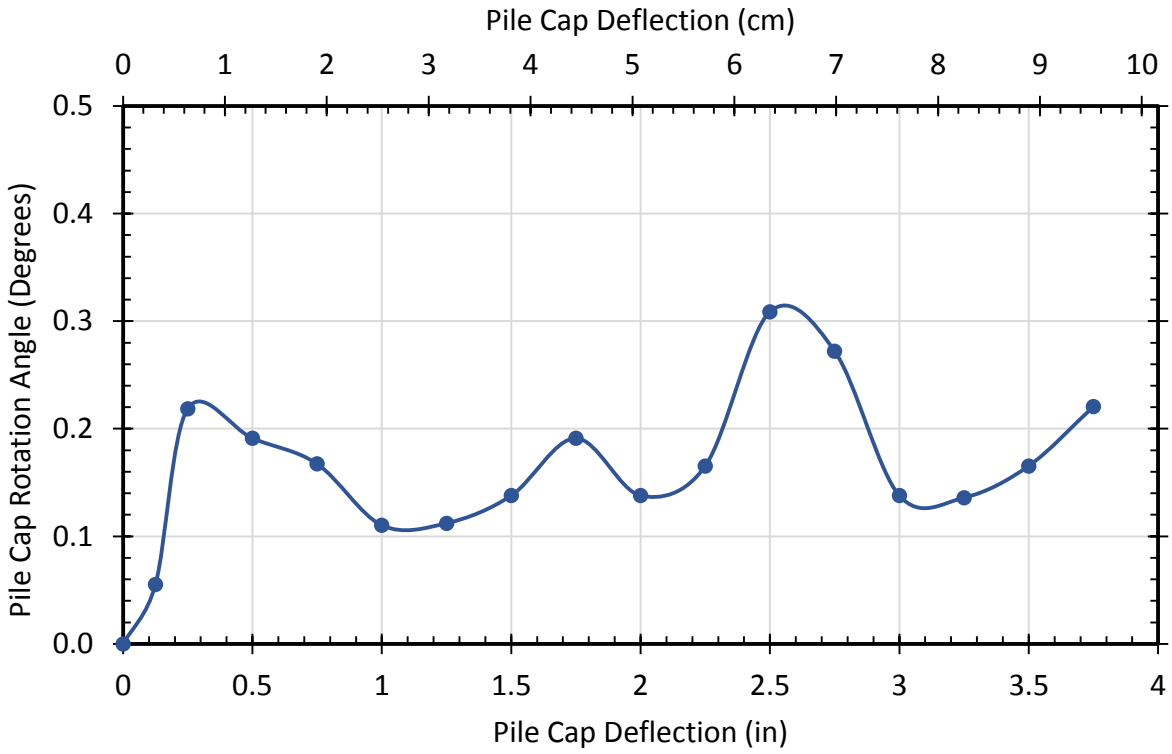

Figure 4-23: Pile cap rotation angle with deflection for the 30° skew inclined loading test

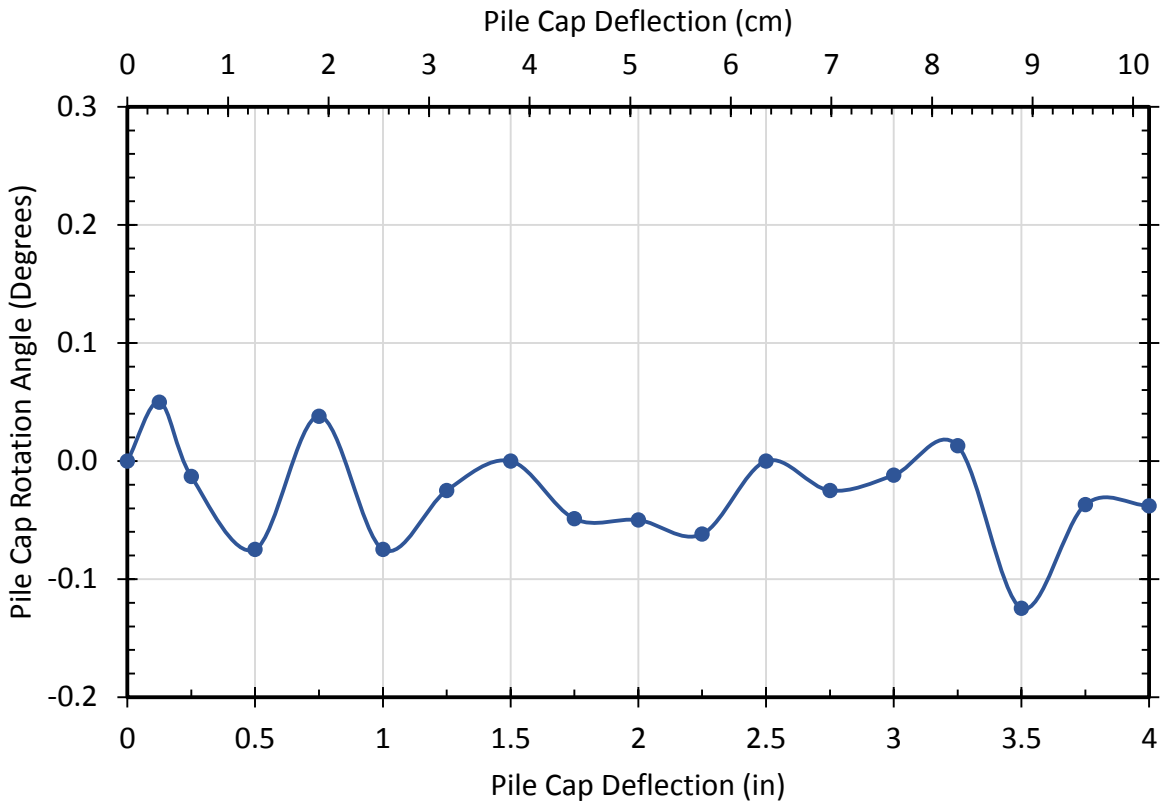

Figure 4-24: Pile cap rotation angle with deflection for the 0° skew uniform loading test

4.8 Backfill Soil Pressure Distribution

The soil pressure distribution across the face of the pile cap was measured using six pressure plates as described in section 3.4.5. Figure 4-25 shows the measured pressure distribution across the face of the 30° skew wedge during the inclined loading test. The pressure distribution is shown for five different pile cap displacement intervals.

As was expected, the soil pressure was the highest on the obtuse side, which is the side that experienced increased loading from the east actuator to produce an inclined loading effect. Four of the other five pressure plates measured very similar pressures to each other. The pressure plate located about 5 feet from the west edge of the pile cap, however, consistently produced lower pressure measurements. It is unclear whether this result represents the actual pressure distribution

or if there is a defect in this particular pressure plate or possibly damage to the wiring or plate during compaction. The plot in Figure 4-26 shows the pressure distribution that would be obtained if the data from the potentially defective pressure plate is neglected. Note that the highest soil pressures were recorded at a pile cap displacement of 1.94 in. rather than the maximum displacement of 3.56 in. This is likely a result of the loading malfunction that occurred during testing which required the pile cap to be unloaded after reaching a deflection of 2.5 inches and then reloaded back up to the maximum displacement of 3.75 inches.

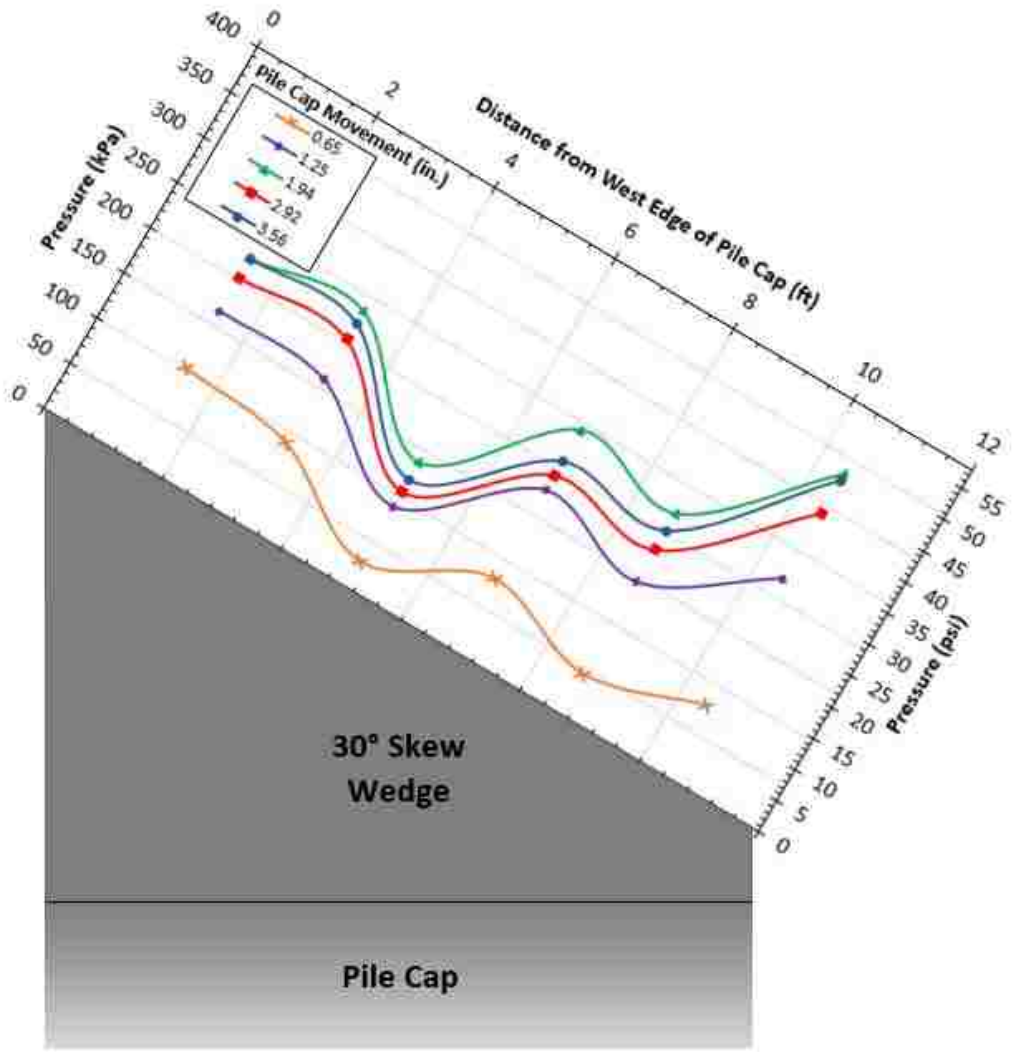

Figure 4-25: Horizontal pressure distribution with pile cap movement

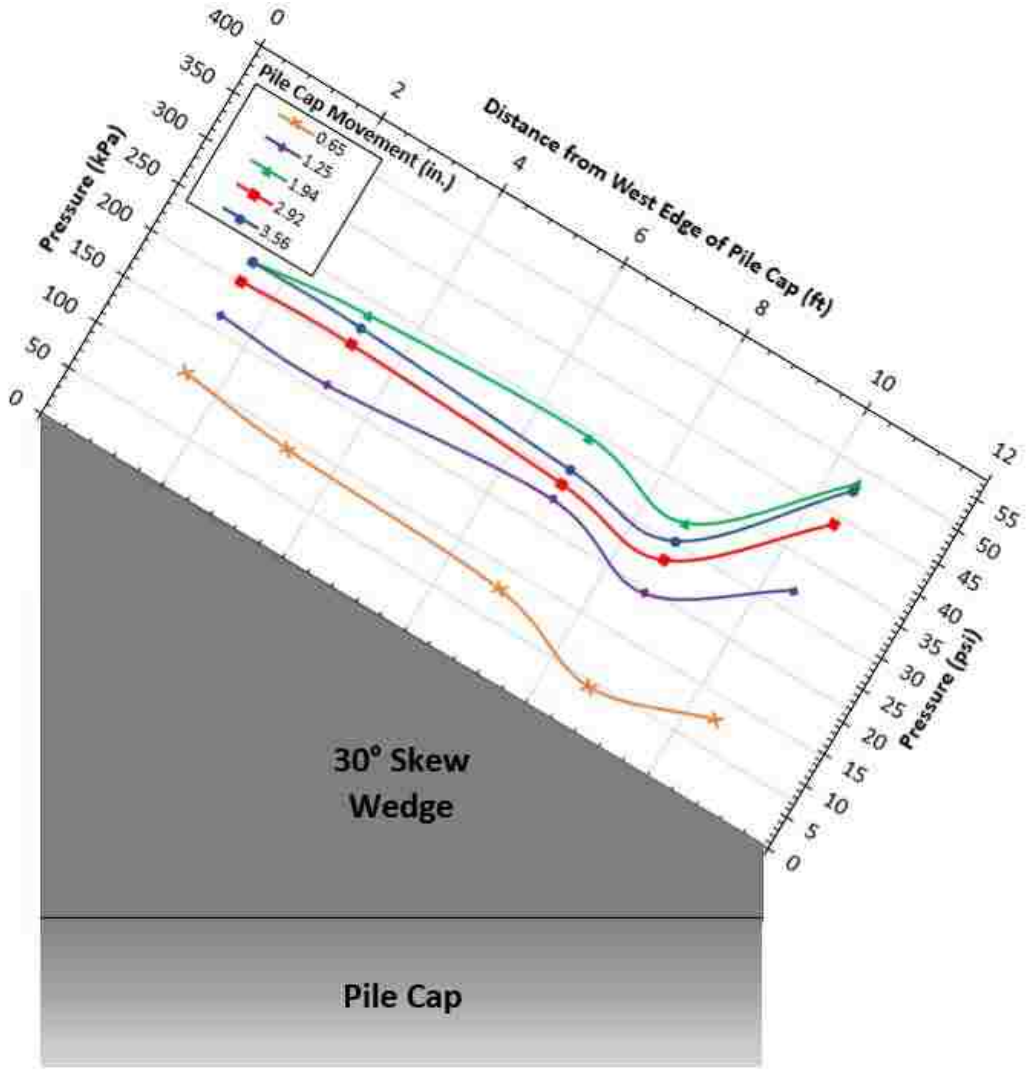

Figure 4-26: Horizontal pressure distribution with pile cap movement neglecting the under-registering pressure plate

Figure 4-27 shows the passive force versus deflection curve as estimated by the pressure cells compared to the passive force measured by the actuators. The shape of the force-deflection curves were very similar, but the passive force estimated by the pressure cells was consistently about 30 to 80 kips lower than the force measured by the actuators. Figure 4-28 shows how neglecting the pressure plate that consistently produced lower pressure measurements and interpolating the pressure from the two adjacent pressure plates improves agreement with the passive force measured by the actuators. However, the passive force estimated by the pressure

cells after neglecting the outlier was still about 10 to 70 kips lower than the force measured by the actuators.

The consistent under-registering of the pressure plates can be explained by the way these plates measure pressure. The plates register compressive strain in the diaphragm as pressure is applied to the pressure plate and the plate compresses slightly. The problem with this mechanism of pressure measurement is that the pressure on the plate also tends to decrease as the plate compresses relative to the surrounding concrete surface which compresses much less. As a result, the backfill soil pressure measured by the plates may be lower than the actual backfill soil pressure. This helps explain why the passive force versus deflection curve as estimated from the pressure cells falls below the curve produced from the load measured by the actuators.

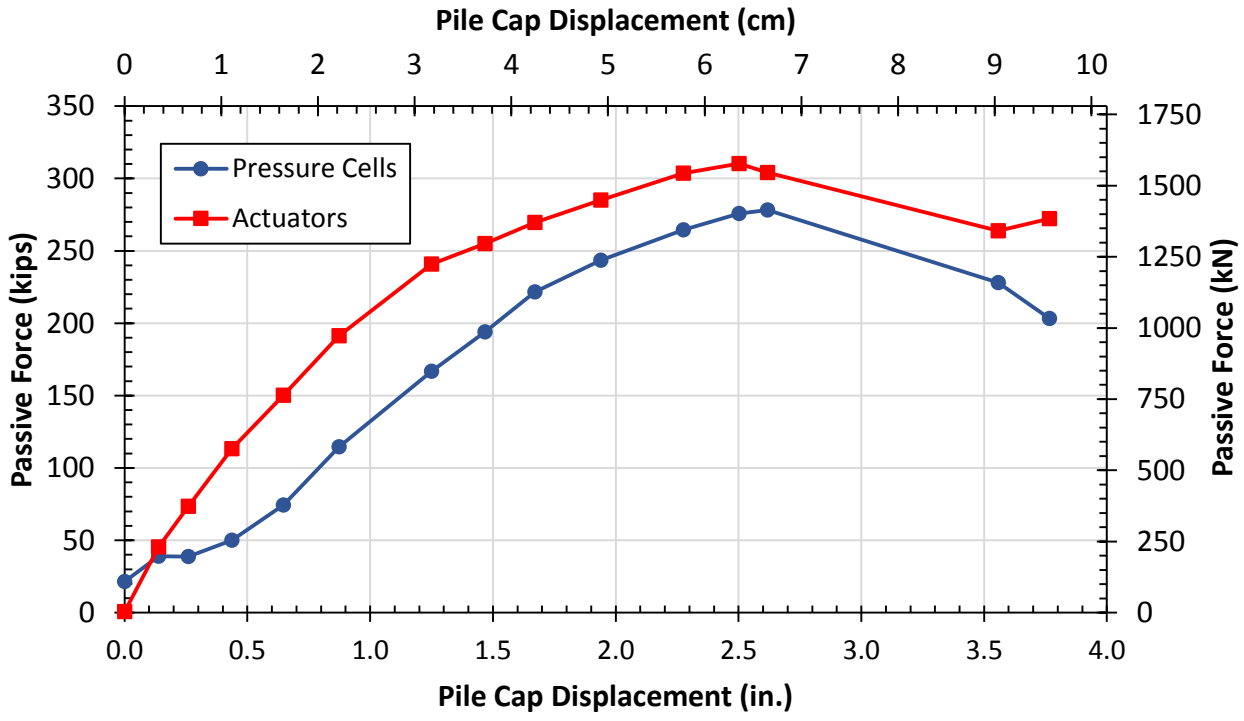

Figure 4-27: Passive force vs. deflection as estimated by the pressure cells and recorded by the actuators for the 30° skew test

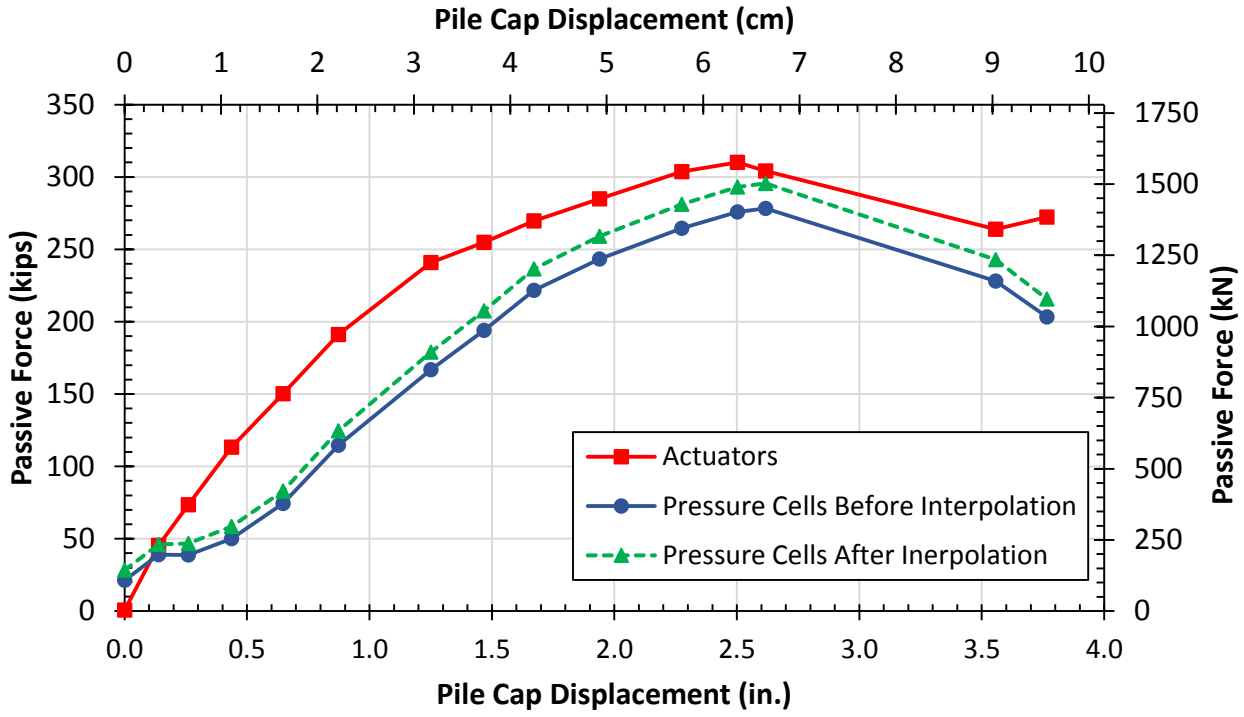

Figure 4-28: Passive force vs. deflection as estimated by the pressure cells (before and after interpolation neglecting the under-registering pressure plate) and recorded by the actuators for the 30° skew test

5 ANALYSIS OF RESULTS

The force-deflection results are analyzed in this section. The PYCAP program developed by Duncan and Mokwa (2001) was used to model the field results. This program uses the Log-Spiral, Rankine, and Coulomb methods to predict the passive resistance of the backfill.

5.1 0° Skew PYCAP Analysis

The PYCAP input values were determined based on the pile cap and soil properties from the 0° skew test. Some of the parameters were left constant while others were adjusted to produce a passive force versus backwall displacement curve that had good agreement with the measured results. The cap height was 5.5 ft and the cap width was 11.75 ft (the pile cap was only 11 ft wide, but there was 4-5 inches of space between the pile cap and the side walls, creating an effective cap width of 11.75 feet). Based on nuclear density testing, the average moist unit weight of the sand backfill was 115.4 pcf and the assumed Poisson's ratio was 0.25. The movement required to fully mobilize passive pressures was taken as 5% of the wall height.

The parameters that were adjusted to optimize the curve were soil friction angle, wall friction, initial soil modulus, and cohesion. The best fit curve was produced with a soil friction angle of 43°, a wall to soil friction angle ratio (δ/ϕ) of 0.8, an initial soil modulus of 450 ksf, and a cohesion of 90 psf. The wall friction ratio of 0.8 is in reasonable agreement with values determined by Potyondy (1961), Cole (2003), and Cummins (2009), as shown in Table 5-1.

Table 5-1: Recommended Sand/Concrete Wall Friction Ratios

	Potyondy (1961)	Cole (2003)	Cummins (2009)
Sand/concrete wall friction ratio (δ_{max}/ϕ)	0.76	0.77	0.68 - 0.73

It should also be noted that the friction angle and cohesion used in the analysis are in very good agreement with values obtained from the in-situ direct shear tests performed on the backfill (ϕ = 42.7° and cohesion of 50 psf) describe in Section 3.5.2. These values are also close to those determined by Marsh (2013) in his PYCAP analysis with similar soil. He determined a friction angle of 40°, wall friction to soil friction angle ratio of 0.7, initial soil modulus of 415 ksf, and a cohesion of 85 psf. Figure 5-1 shows a comparison of the measured passive force versus backwall displacement curve from the 0° skew test to the best fit curve produced using PYCAP.

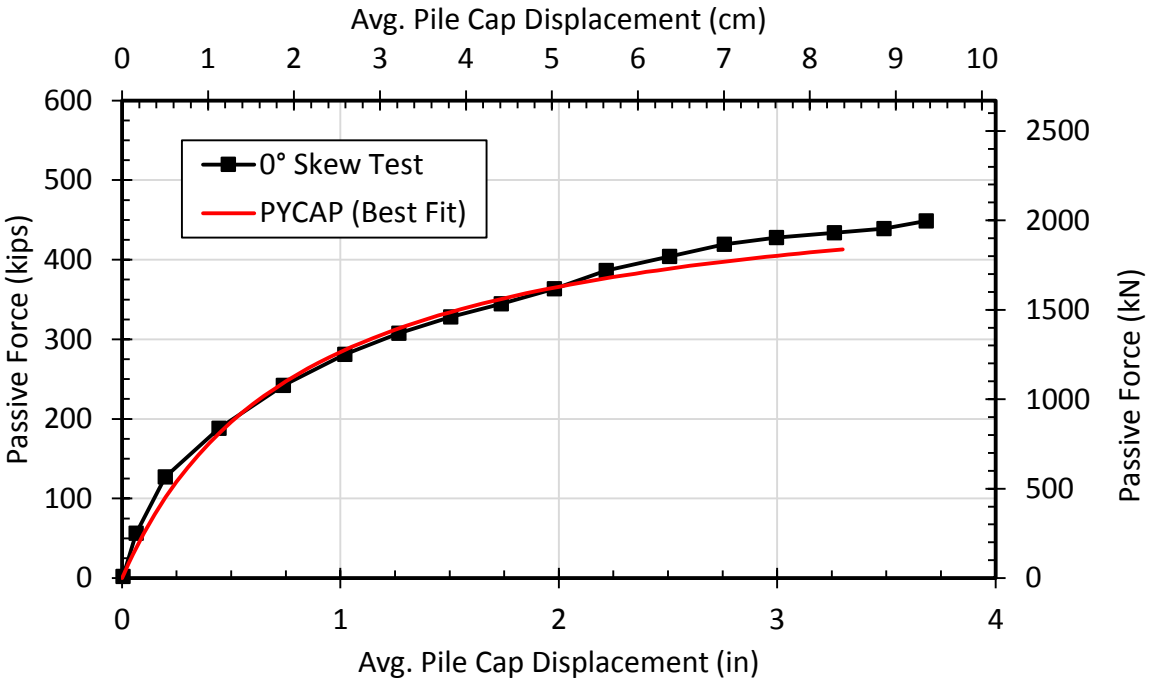

Figure 5-1: Comparison of passive force versus backwall displacement curves from PYCAP analysis and from measured passive resistance for the 0° skew test

To evaluate the influence of various parameters, four separate sensitivity analyses were then performed by adjusting each of the parameters listed above one at a time while holding all other parameters constant. In the first sensitivity analysis, low end and high end soil friction angles of 42° and 44° were used. For the second analysis, low end and high end wall friction to soil friction angle ratios (δ/ϕ) of 0.7 and 0.9 were used. In the third analysis, low end and high end initial soil modulus values of 350 ksf and 550 ksf were used. In the fourth analysis, low end and high end soil cohesion values of 60 psf and 120 psf were used. Table 5-2 shows a summary of the parameters used for the best fit PYCAP curve and for each of the four sensitivity analyses. The results of the sensitivity analyses for soil friction angle, wall friction, initial soil modulus, and cohesion are displayed in Figure 5-2, Figure 5-3, Figure 5-4, and Figure 5-5, respectively. In addition to the four separate sensitivity analyses, PYCAP was also used to generate low and high range passive force versus backwall deflection curves using the low and high range values for all four parameters, as shown in Figure 5-6.

Table 5-2: PYCAP Soil Strength Parameters

Soil Parameter	Low Range	Best Fit	High Range	Units
Cap Width, b	11.75	11.75	11.75	ft
Cap Height, H	5.5	5.5	5.5	ft
Friction Angle, ϕ	42	43	44	Degrees
Cohesion, c	60	90	120	lb/ft^2
Interface Friction Ratio, δ/ϕ	0.7	0.8	0.9	-
Initial Soil Modulus, E	350	450	550	kip/ft^2
Poisson's ratio, ν	0.25	0.25	0.25	-
Soil Unit Weight, γ_m	115.4	115.4	115.4	lb/ft^2

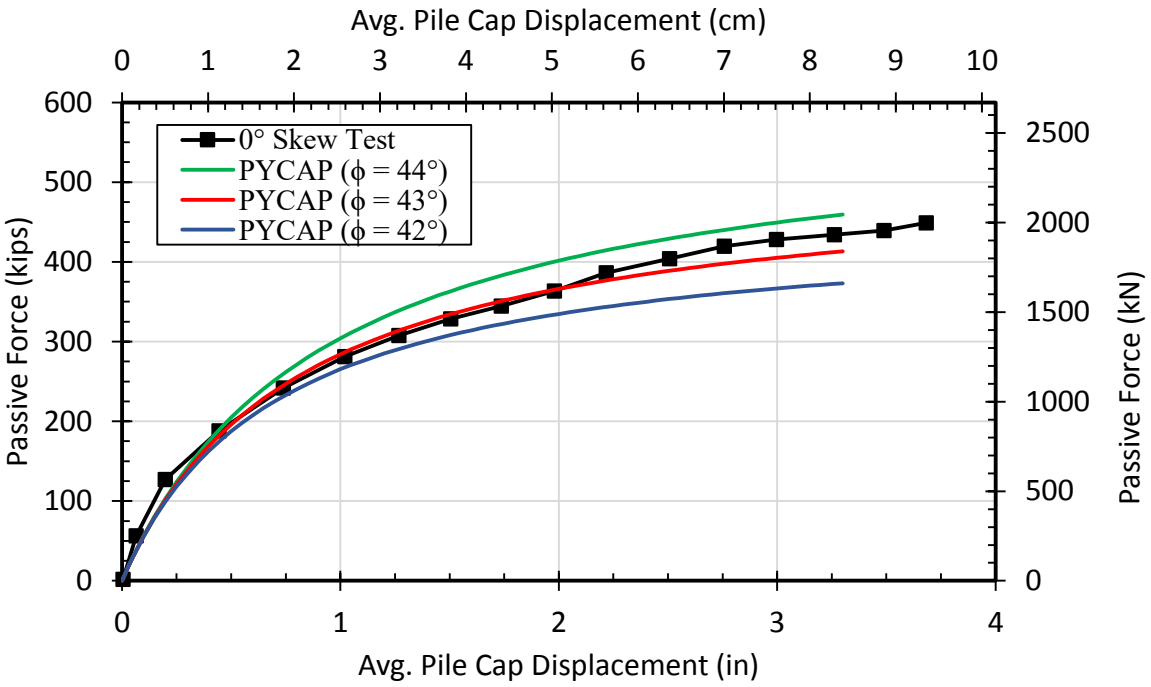

Figure 5-2: PYCAP results from soil friction angle sensitivity analysis in comparison to measured curve

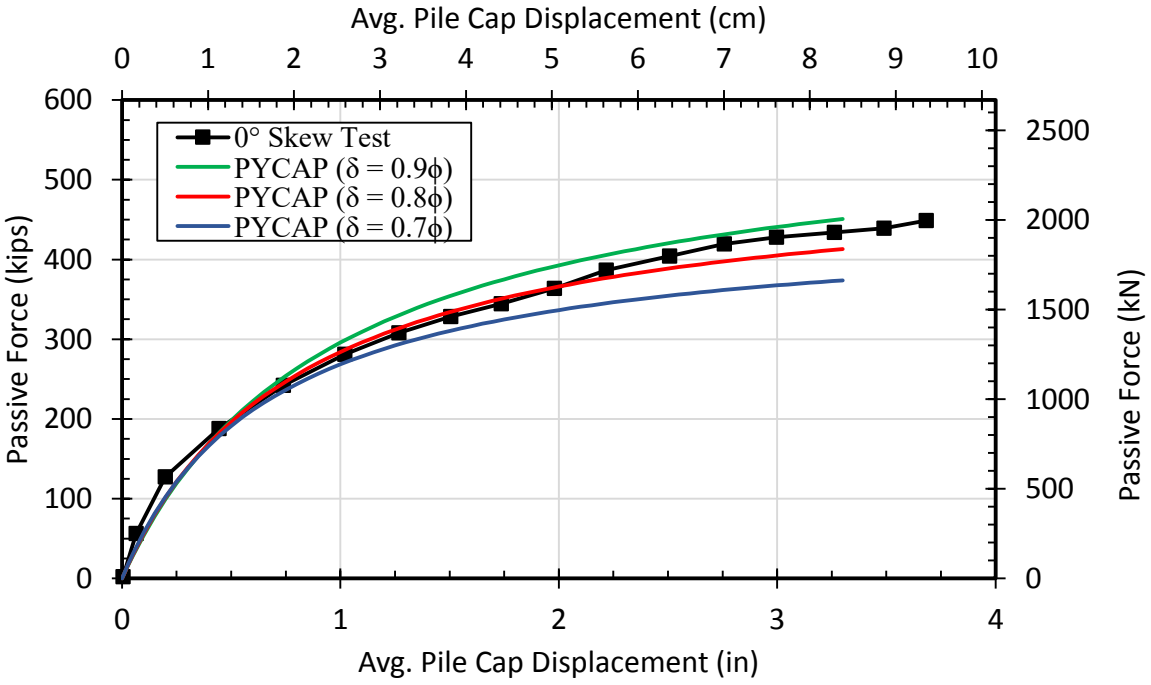

Figure 5-3: PYCAP results from wall friction sensitivity analysis in comparison to measured curve

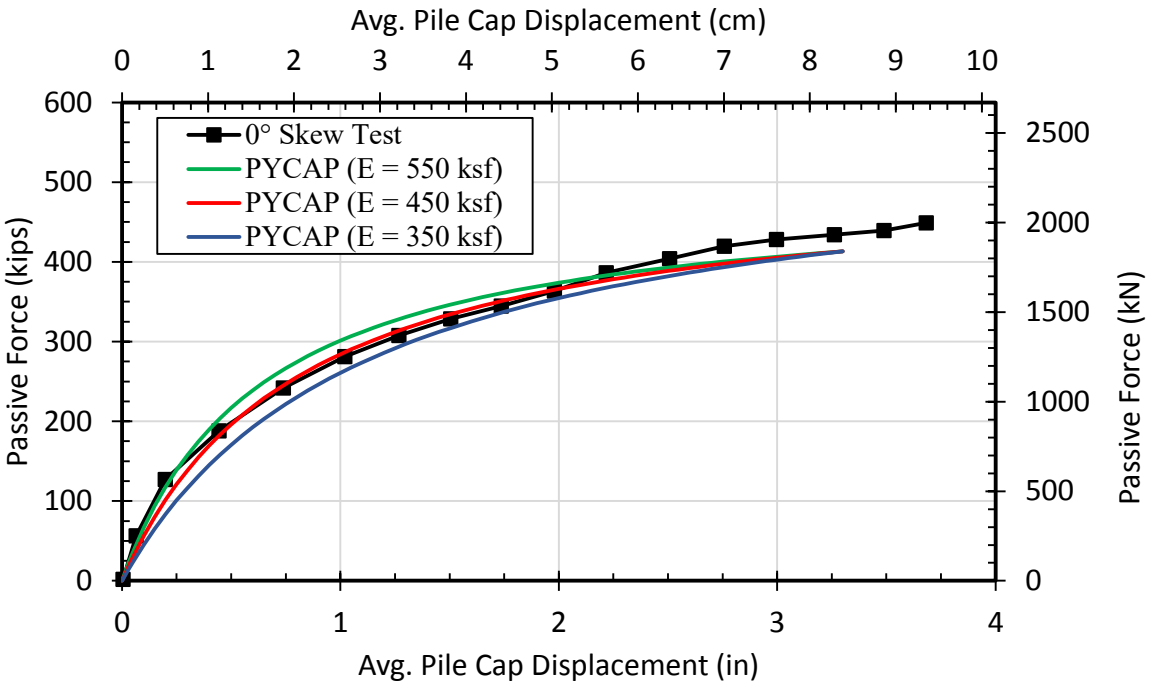

Figure 5-4: PYCAP results from initial soil modulus sensitivity analysis in comparison to measured curve

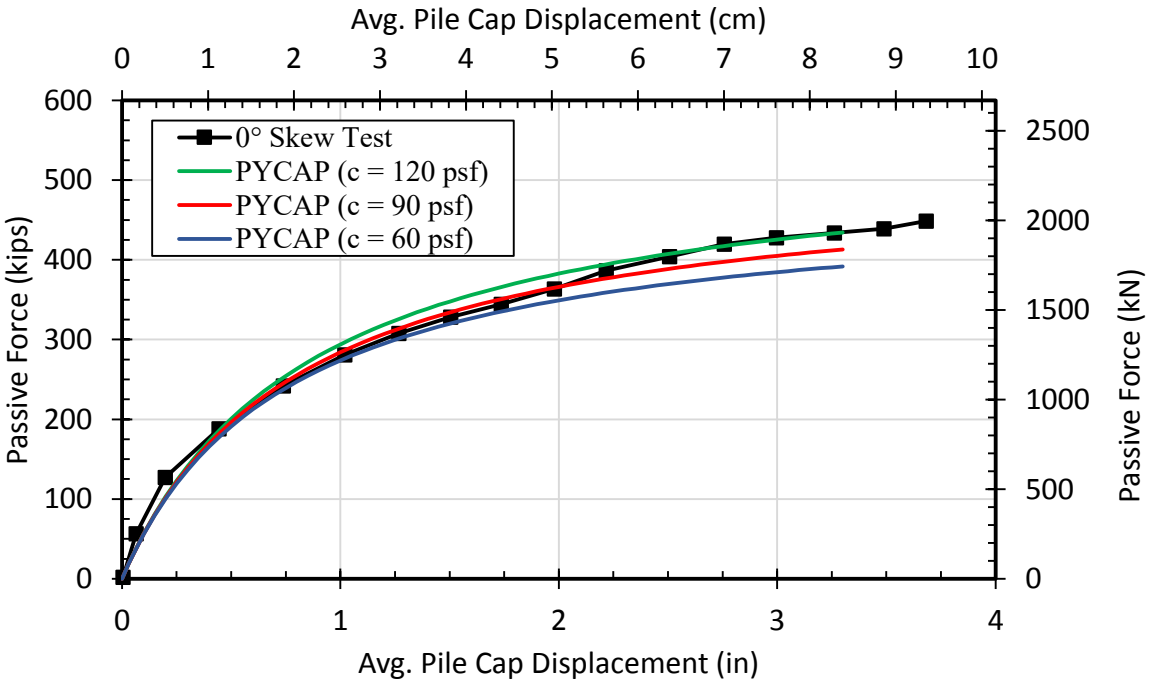

Figure 5-5: PYCAP results from cohesion sensitivity analysis in comparison to measured curve

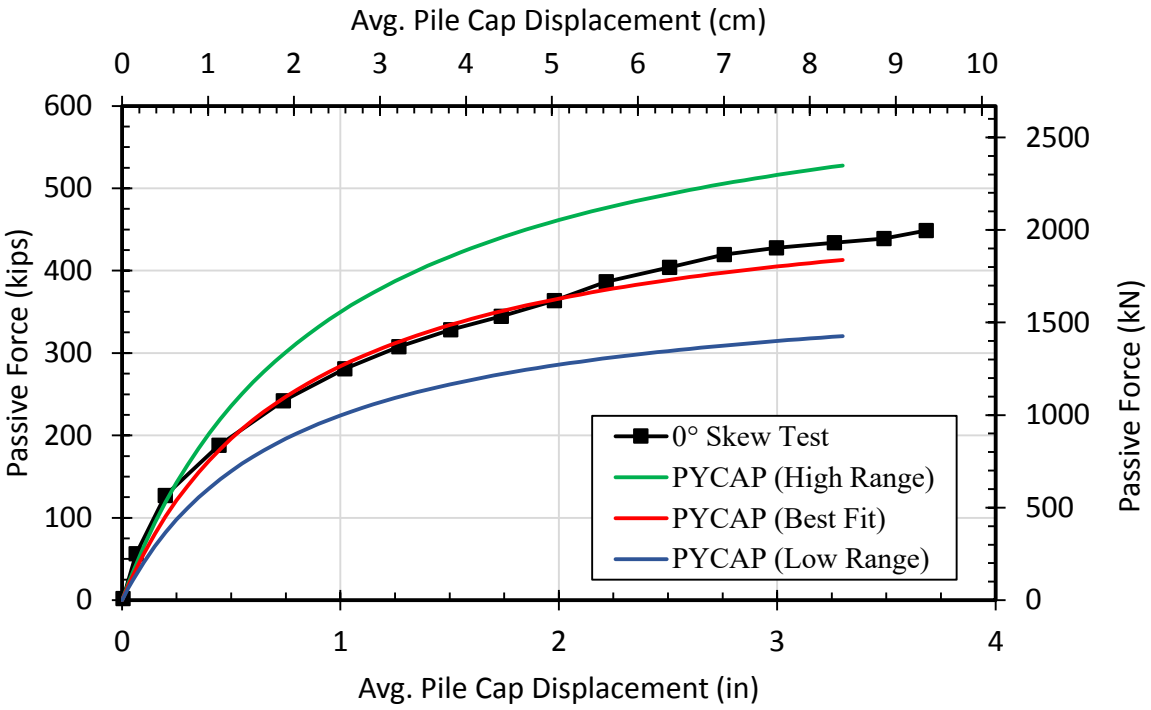

Figure 5-6: Low range and high range PYCAP curves relative to measured curve.

In the soil friction angle sensitivity analysis shown in Figure 5-2, the PYCAP curves for friction angles of 42°, 43°, and 44° remained almost identical at displacements less than 0.5 inches, where the initial soil stiffness has the greatest influence on the curve. For larger displacements, as failure is approached, the higher friction angle produces a higher resistance. A 1° increase in friction angle typically increased the ultimate passive force by about 40 kips. The variation in wall friction used in PYCAP has a similar effect on the resulting passive force curves, as shown in Figure 5-3. The PYCAP curves for wall friction to soil friction angle ratios (δ/ϕ) of 0.6, 0.7, and 0.8 were almost identical up to a displacement of 0.5 inches and then spread out as displacement increased. Increasing the δ/ϕ ratio by 0.10 typically increased the ultimate passive force by about 30 kips.

Increasing the initial soil modulus has a different effect on the passive force curves than increasing the soil and wall friction angles did. The PYCAP curves produced using initial soil

modulus values of 350, 450, and 550 ksf have the greatest variation at low displacements and eventually converge to about the same ultimate passive force at the maximum displacement, as shown in Figure 5-4. Adjusting the cohesion value up or down by about 33% did not have a major impact on the passive force curves. The PYCAP curves produced using cohesion values of 60, 90, and 120 psf stayed pretty constant and only differed by about 20 kips at maximum displacement.

5.2 30° Skew PYCAP Analysis

The best fit PYCAP input parameters determined for the 0° skew test were also used for the 30° skew test. The best fit passive force versus backwall displacement curve produced using PYCAP was then scaled down by the skew reduction factor of 0.69 that was computed from the results of the 0° and 30° skew tests. The curve was also scaled down by a skew reduction factor of 0.51, which was computed from the proposed reduction curve for skewed abutments based on skew angle (Shamshabadi and Rollins, 2014). These two scaled down PYCAP curves are plotted along with the measured passive force versus backwall displacement curve from the 30° skew test in Figure 5-7.

As discussed in Section 3.5 of this report, it was determined that there was an effective skew angle of 21° during the 30° skew test. This effective skew angle is used to compute a skew reduction factor of 0.63 from the proposed reduction curve. The best fit passive force versus backwall displacement curve produced using PYCAP was then scaled down by this reduction factor and plotted along with the curve produced by the original reduction factor of 0.69 and the passive force curve measured from the 30° skew test, as shown in Figure 5-8.

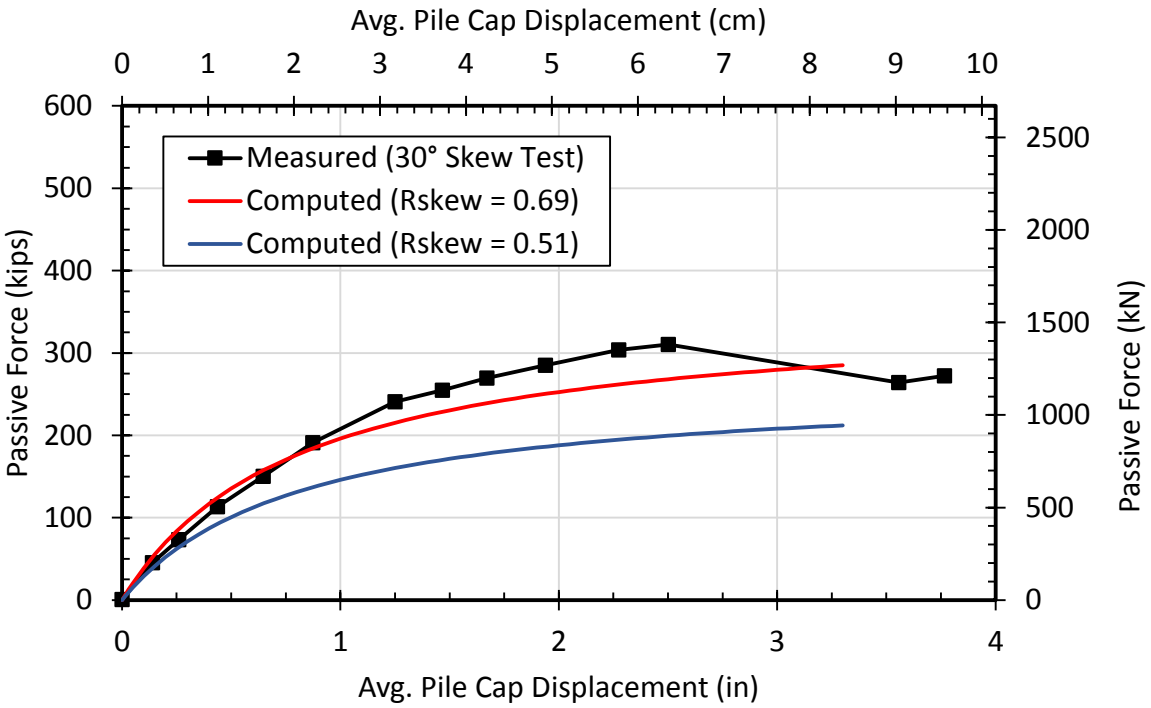

Figure 5-7: Comparison of measured versus computed passive force versus backwall displacement curves for 30° skew

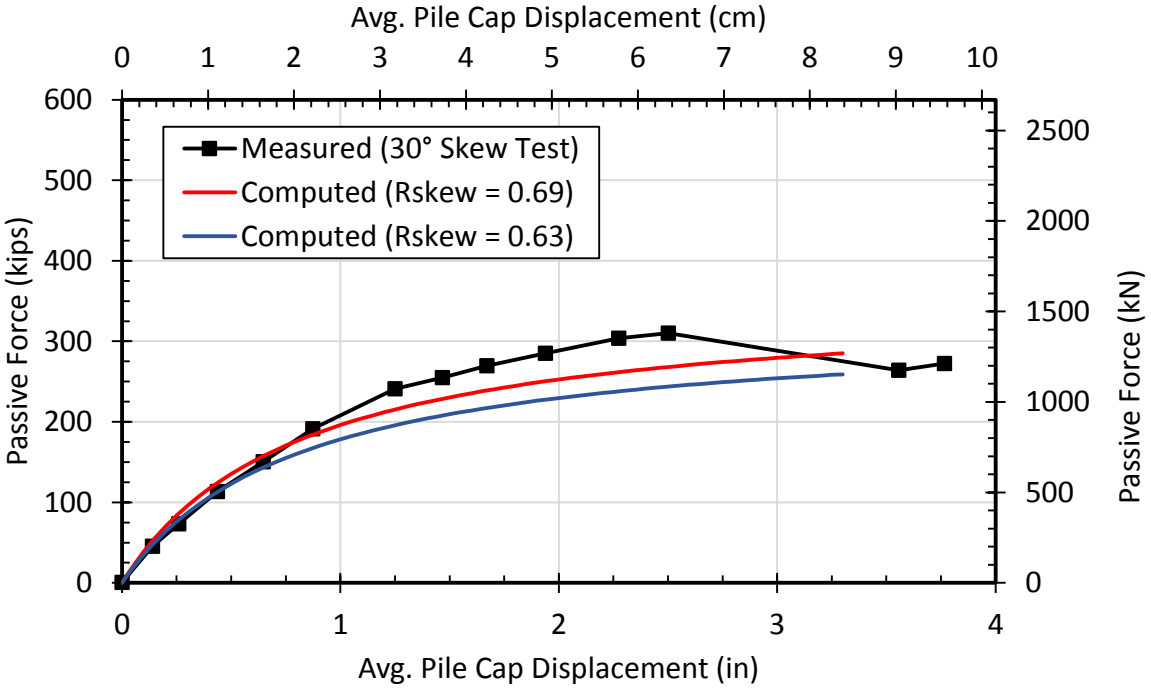

Figure 5-8: Comparison of measured versus computed passive force versus backwall displacement curves assuming an effective skew angle of 21°

There is good agreement between the measured and computed passive force versus backwall displacement curves when using a skew reduction factor of 0.69. When using the recommended reduction factor of 0.51 for an abutment with 30° skew, the computed curve is significantly lower than the measured curve, as seen in Figure 5-7. However, because it was observed that there was an effective skew angle of 21°, a reduction factor of 0.63 should be used in this case. Figure 5-8 shows that there is better agreement when this higher reduction factor is employed. As noted previously, the effective skew angle is only likely to be important for very narrow abutments but relatively insignificant for wide abutments where the friction on the side walls only affects a small portion of the total soil volume.

6 CONCLUSIONS

This thesis presents results from large-scale lateral load tests designed to determine the effect of inclined loading on passive force displacement curves and skew reduction factors. This was accomplished by performing an inclined loading test with a 30° skew angle in addition to a longitudinal loading test with a 0° skew angle. Both tests were performed with a backwall height of 5.5 feet (1.68 m). Based on this work, the following conclusions are drawn:

1. Inclined loading does not have a significant effect on the passive force skew reduction factor. However, the reduction factor computed from the results of these tests was somewhat higher than predicted by the proposed reduction curve developed from previous tests.
2. The friction between the side walls and the back wall reduces the effective skew angle. This might be significant for a one-lane road with a narrow abutment, but for wider abutments the effect would likely be minimal.
3. The inclined loading did not change the amount of movement required to mobilize passive resistance with ultimate passive force developing for displacements equal to 3 to 6% of the wall height.
4. The rotation of the pile cap due to inclined loading produced higher earth pressure on the obtuse side of the skew wedge.
5. The log-spiral method that was successful for predicting passive force-deflection curve for the 0° skew with longitudinal loading was also successful in predicting the

passive force-deflection curve for the 30° skew test with inclined loading after consideration of the skew reduction factor.

6. The best-fit soil stiffness, friction angle, cohesion, and wall friction determined from the PYCAP analysis were close to measured values and similar to that determined from previous analyses.

REFERENCES

Apirakvorapinit, P., Mohammadi, J., and Shen, J. (2012). "Analytical Investigation of Potential Seismic Damage to a Skewed Bridge." *Practice Periodical on Structural Design and Construction*, 17(1), 5-12.

Caltrans, C. D. o. T. (2010). "Seismic Design Criteria, Version 1.6, November 2010." Division of Engineering Services, Office of Structure Design, Sacramento, California.

Canadian Geotechnical Society (1992). "Canadian foundation engineering manual." BiTech, Vancouver, B.C., Canada.

Christensen, D. S. (2006). "Full Scale Static Lateral Load Test of a 9 Pile Group in Sand." *M.S. Thesis*, Department of Civil and Environmental Engineering, Brigham Young University, Provo, UT.

Clough, G. W., and Duncan, J. M. (1991). *Foundation engineering hand-book*, Chapman and Hall, New York.

Cole, R.T. (2003). "Full-scale effects of passive earth pressure on the lateral resistance of pile caps." Doctor of Philosophy Dissertation, Brigham Young University, Department of Civil and Environmental Engineering, Provo, Utah.

Cole, R., and Rollins, K. (2006). "Passive Earth Pressure Mobilization during Cyclic Loading." *Journal of Geotechnical and Geoenvironmental Engineering*, 132(9), 1154-1164.

Coulomb, C. A. (1776). "Essai sur une Application des Règles de Maximis et Minimis a quelques Problèmes de Statique, relatifs a l'Architecture." 3, 38.

Duncan, J. M., and Mokwa, R. L. (2001). "Passive Earth Pressures: Theories and Tests." *Journal of Geotechnical and Geoenvironmental Engineering, ASCE*, 127(3), 248-257.

Elnashai, A. S., Gencturk, B., Kwon, O., Al-Qadi, I. L., Hashash, Y., Roesler, J. R., Kim, S. J., Jeong, S., Dukes, J., and Valdivia, A. (2010). "The Maule (Chile) Earthquake of February 27, 2010: Consequence Assessment and Case Studies." Department of Civil and Environmental Engineering, University of Illinois at Urbana-Champaign, 190.

Franke, B. (2013). "Passive Force on Skewed Abutments with Mechanically Stabilized Earth (MSE) Wingwalls Based on Large-Scalte Tests." *M.S. Thesis*, Department of Civil and Environmental Engineering, Brigham Young University, Provo, UT.

Fredrickson, A. (2015). "Large-Scale Testing of Passive Force Behavior for Skewed Bridge Abutments with Gravel and Geosynthetic Reinforced Soil (GRS) Backfills." *M.S. Thesis*, Department of Civil and Environmental Engineering, Brigham Young University, Provo, UT.

Marsh, A.K. (2013). "Evaluation of Passive Force on Skewed Bridge Abutments with Large-Scale Tests." *M.S. Thesis*, Department of Civil and Environmental Engineering, Brigham Young University, Provo, UT.

Palmer, K.N.. (2013). "Large-Scale Testing of Passive Force Behavior for Skewed Abutments with High Width-Height Ratios." *M.S. Thesis*, Department of Civil and Environmental Engineering, Brigham Young University, Provo, UT.

Potyondy, J. G. (1961). "Skin Friction Between Various Soils and Construction Materials." *Geotechnique, London*, 11(1), 339-353.

Rankine, W. J. M. (1857). "On the Stability of Loose Earth." *Philosophical Transactions of the Royal Society of London*, 147(ArticleType: research-article / Full publication date: 1857 /), 9-27.

Remund, T. (2017). "Large-Scale Testing of Low-Strength Cellular Concrete for Skewed Bridge Abutments." *M.S. Thesis*, Department of Civil and Environmental Engineering, Brigham Young University, Provo, UT.

Rollins, K. M., and Cole, R. T. (2006). "Cyclic Lateral Load Behavior of a Pile Cap and Backfill." *Journal of Geotechnical & Geoenvironmental Engineering*, 11.

Rollins, K. M., Gerber, T. M., and Heiner, L. (2010). "Passive Force-Deflection Behavior for Abutments With MSE Confined Approach Fills." Brigham Young University Department of Civil & Environmental Engineering, Salt Lake City, UT, 83.

Rollins, K. M., and Jessee, S. (2012). "Passive Force-Deflection Curves for Skewed Abutments." *Journal of Bridge Engineering*, ASCE, 17(5).

Sandford, T. C., and Elgaaly, M. (1993). "Skew Effects on Backfill Pressures at Frame Bridge Abutments." *Transportation Research Record: Journal of the Transportation Research Board*, 1-11.

Shamsabadi, A., Kapuskar, M., and Zand, A. (2006). "Three-Dimensional Nonlinear Finite-Element Soil-Abutment Structure Interaction Model for Skewed Bridges." *5th National Seismic Conference On Bridges and Highways*, FHWA, ed.San Francisco, CA, 1-14.

Shamsabadi, A., Rollins, K. M., and Kapuskar, M. (2007). "Nonlinear Soil-Abutment-Bridge Structure Interaction for Seismic Performance-Based Design." *Journal of Geotechnical & Geoenvironmental Engineering*, 133(6), 14p.

Shamsabadi, A. and Rollins, K.M. (2014). “Three-dimensional nonlinear continuum seismic soil-structure interaction analysis of skewed bridge abutments.” Procs., 8th European Conf. on Numerical Methods in Geotechnical Engineering, Delft, the Netherlands, 6 p.

Smith, K. (2014). "Passive Force on Skewed Bridge Abutments with Reinforced Concrete Wingwalls." *M.S. Thesis*, Department of Civil and Environmental Engineering, Brigham Young University, Provo, UT.

Snow, S.(2018) “Numerical Analysis of Passive Force on Skewed Bridge Abutments with Reinforced Concrete Wingwalls” *M.S. Thesis*, Department of Civil and Environmental Engineering, Brigham Young University, Provo, UT. (In Preparation)

Sowers, G. B., and Sowers, G. F. (1961). *Introductory soil mechanics and foundations*, Macmillan, New York.

Strassburg, A. N. (2010). "Influence of Relative Compaction on Passive Resistance of Abutments with Mechanically Stabilized Earth (MSE) Wingwalls." Master of Science, Brigham Young University, Provo, Utah.

Terzaghi, K. (1943). *Theoretical soil mechanics*, J. Wiley & Sons, Inc., New York.

Terzaghi, K., Peck, R. B., and Mesri, G. (1996). *Soil mechanics in engineering practice*, Wiley, New York.

Toro, F., Rubilar, F., Hube, M. A., Santa-Maria, H., and Cabrera, T. (2013). "Statistical Analysis of Underpass Damaged During 2010 Chile Earthquake." *Proc. 7th National Seismic Conference of Bridges and Highways (7NSC)*Oakland, CA.